AD-A048 630 FLORIDA UNIV GAINESVILLE DEPT OF MATERIALS SCIENCE --ETC F/G 6/5
AN INVESTIGATION OF BONDING MECHANISMS AT THE INTERFACE OF A PR--ETC(U)
SEP 74 L L HENCH, H A PASCHALL, W C ALLEN DADA17-70-C-0001

UNCLASSIFIED NL

1 OF 2
AD A048630

Report No. 5

An Investigation of Bonding Mechanisms at the Interface of a Prosthetic Material

L. L. Hench, Department of Materials Science
and Engineering, University of Florida
and
H. A. Paschall, College of Medicine, J. Hillis
Miller Health Center, and Chief of Orthopaedics
Veterans Administration Hospital
and
W. C. Allen, College of Medicine
J. Hillis Miller Health Center
and
G. Piotrowski, College of Medicine, J. Hillis
Miller Health Center, and Department of
Mechanical Engineering, University of Florida

September, 1974

Supported by

U. S. Army Medical Research and Development Command
Washington, D. C. 20314

Contract No. DADA 17-70-C-0001
University of Florida
Gainesville, Florida 32611

(9) AD

Report No. 5 (Annual)
1 Sep 73 - 31 Aug 74

(6) **An Investigation of Bonding Mechanisms at the Interface of a Prosthetic Material.**

(10) Larry L. Hench, Department of Materials Science and Engineering, University of Florida

and

Homer A. Paschall, College of Medicine, J. Hillis Miller Health Center, and Chief of Orthopaedics Veterans Administration Hospital

and

William C. Allen, College of Medicine J. Hillis Miller Health Center

and

George G. Piotrowski, College of Medicine, J. Hillis Miller Health Center, and Department of Mechanical Engineering, University of Florida

(11) Sep [redacted] 74

(12) 134 p.

Supported by

U. S. Army Medical Research and Development Command
Washington, D. C. 20314

(15) Contract No. DADA 17-70-C-0001
University of Florida
Gainesville, Florida 32611

SUMMARY

This research program has had two primary objectives since its inception: (1) to achieve a direct chemical bond between orthopaedic devices and bone using surface active glass and glass-ceramic materials or coatings, and (2) to develop a scientific understanding of the interfacial reactions occurring between materials and bone. This report summarizes progress toward realizing these objectives by reviewing accomplishments of the past five years and presenting a series of new findings.

The influence of phosphorus, boron and fluorine additions on the surface chemical reactivity of a soda-lime-silica glass has been investigated. Several techniques, including infrared reflection spectroscopy, ion solution analysis, scanning electron microscopy, energy dispersive x-ray analysis, x-ray diffraction, Auger electron spectroscopy and ion beam milling, have been employed to develop insight into the morphological and chemical changes which occur on glass surfaces corroded in a simulated physiologic environment.

The resulting corrosion layers and the influence of phosphorus, boron and fluorine on their compositions and rates of formation are defined. Surface ion concentration profiles determined with Auger spectroscopy and ion beam milling detail the structural alterations produced by aqueous attack. A mechanism is postulated which explains the sequence of events leading to the formation of the multiple-layer corrosion structures.

Having defined the surface chemical behavior of the glasses in an in-vitro environment, an effort is made to relate these observations to the response elicited when identical glasses are implanted in laboratory animals. Stable interfacial fixation results when specific surface chemistry conditions are satisfied.

The in-vivo results demonstrated that the four compositions implanted all exhibited direct attachment to bone. There was a wide variation in the appearance of the tissue near the implant. Only the interface of the glass containing 6 wt.% P_2O_5 exhibited a healthy zone of ossification characterized by numerous osteocytes in close proximity to the glass, a layer of unmineralized osteoid, and a layer of osteoblasts actively engaged in laying down new osteoid. The other glasses exhibited a low density of viable osteocytes and an absence of an active osteoid front.

Based upon the in-vivo observations, a theory is proposed that an ideal implant material must have a dynamic surface chemistry that induces histological changes at the implant surface which would normally occur if the implant were not present.

Development of a mechanically suitable resorbable bone plate for the bioglass-ceramics has proven to be difficult. A long series of in-vitro and in-vivo fabrication and design experiments have been conducted to produce plates which will not fracture during implantation. As a result of these studies several successful implantations have been performed. Stable fixation was maintained for relatively short periods of time (4-9 days) followed by failure of the implants. The failures have been attributed to static fatigue which has necessitated further studies to optimize the mechanical strength of the bioglass-ceramic implants.

FOREWORD

The program undertaken in the contract is an interdisciplinary effort of the Departments of Materials Science and Engineering and Mechanical Engineering, College of Engineering, University of Florida; the Departments of Orthopaedics and Anatomy, College of Medicine, University of Florida; and the Department of Orthopaedics, Veterans Administration Hospital, Gainesville, Florida.

In conducting the research described in this report, the investigators adhered to the "Guide for Laboratory Animal Facilities and Care," as promulgated by the Committee on the Guide for Laboratory Animal Resources, National Academy of Sciences-National Research Council.

TABLE OF CONTENTS

LIST OF FIGURES

LIST OF FIGURES (continued)

LIST OF FIGURES (continued)

LIST OF FIGURES (continued)

LIST OF FIGURES (continued)

LIST OF FIGURES (continued)

LIST OF TABLES

I. INTRODUCTION AND OBJECTIVES

There are two primary objectives in this program. 1) To achieve a direct chemical bond between a ceramic material and bone. Accomplishment of this objective will enable the development of a wide range of orthopaedic prosthetic devices which will not loosen with time and require removal from the patient; and 2) to develop a scientific understanding of the interfacial reactions occurring between materials and bone. Accomplishment of this objective will enable the engineer and physician to collaboratively design a materials system to satisfy a specific combination of mechanical and physiological requirements in medical applications.

Previous progress in achieving these objectives has been discussed in Reports No. 1, 2, 3 and 4 prepared for this contract in August 1970, August 1971, August 1972, and August 1973, respectively.

II. PROJECT OVERVIEW

In order to meet the above objectives, glass and glass-ceramic materials have been developed which promote the formation of a direct chemical bond at the interface of the material and bone. The direct bond is obtained without the use of a porous structure in the glass-ceramics, thereby retaining the intrinsic strength of these materials and also enabling the glass-ceramics to be used as coatings on high strength metals. As discussed in Reports No. 1, 2, 3 and 4, promotion of the chemical bonding is accomplished by incorporating into the glass-ceramic structures soluble sodium, calcium and phosphate ions in ratios which can influence the precipitation of hydroxyapatite in bone. Variable rates of ion release have been achieved by varying (1) the Ca/P ratio, (2) the percentage of network formers in the glass, (3) the type of network former (SiO_2 or B_2O_3), and (4) F^- additions.

Previous in-vitro studies have been conducted to establish parameters controlling the bonding of the glass-ceramic materials with bone. These studies have demonstrated that the phosphate containing glass-ceramic surface enhances surface crystallization of hydroxyapatite. Studies presented in Report No. 4 showed what appeared to be a hydroxyapatite-like layer forming on top of a silica-rich layer, due to the reaction of bioglass with an aqueous medium in-vitro. The role of a soluble SiO_2 gel layer at the implant interface may be critical for bonding in light of recent studies showing SiO_2 present as an osteogenic precursor. Certain protein

macromolecules also bond to the bioglass-ceramic surface in a dense, randomly distributed conformation in contrast to a highly oriented distribution on quartz surfaces and a complete lack of bonding on other mineral and ceramic surfaces.

Continued study of the surface chemical behavior of bioglasses during the past year has provided a detailed analysis of the sequence of reactions which lead to the formation of the corrosion films. The degree of selective attack of the silicate network and the resulting corrosion layers are influenced by the quantity of phosphate in the glass, with the addition of phosphate producing a double layered corrosion film which is more effective in protecting the bulk glass from aqueous attack. Detailed concentration profiles of corroded bioglass surfaces have been obtained with Auger Electron Spectroscopy and ion beam milling which confirm the existence of the silica-rich gel and the calcium phosphate gel. The crystalline product which grows from the initially amorphous calcium phosphate film has been identified as hydroxyapatite which contains a considerable quantity of CO_2 within its structure.

Implantation of duplicate bioglass-ceramic samples in rat femurs has been used to evaluate the formation of the chemical bond at a living interface. Tetracycline tracers, microradiography, scanning electron microscopy, light microscopy and transmission electron microscopy all show evidence of new bone growth contiguous with the bioglass and bioglass-ceramic implant surface. A histological sequence shows that mature bone appears at points on the active glass-ceramic surface at four weeks. After twelve weeks a complete mature laminar interface has been established. Transmission electron micrographs show an amorphous gel-like layer immediately adjacent to the implant surface, with highly elongated hydroxyapatite crystals bridging the gap between the implant and the mature bone which has formed around the implant. These hydroxyapatite crystals apparently form after osteoblasts have laid down collagen fibers on this silica gel layer.

In-vivo studies conducted during the past year support the contention that a silica-rich gel on the glass surface serves as the induction site for ossification. Four bioglasses including a soda-lime-silica glass and three compositions produced by adding 3, 6 and 12 wt.% P_2O_5 to the ternary glass exhibited direct attachment to bone at three weeks. As the ternary glass only forms a silica-rich surface, even when phosphates are present in solution, and the glass-bone interface appears very similar for all four compositions, it seems likely that the silica-rich layer is serving as the site for osteoblasts to lay down the organic intercellular substance of bone. The calcium phosphate layer which develops as phosphorus is added to the bioglass composition may serve as a source of ions to be incorporated into the mineralization

process. However, an excess of calcium and phosphate ions lead to cell death and ectopic calcification.

Bioglass-ceramics of low reactivity exhibit very slow mineralization at the materials interface when implanted in regions of low metabolic activity. Transmission electron microscopy shows bone mineral development in a transition layer next to the implant simultaneous with homogeneous mineralization in the newly forming bone in the repair site. The transition layer mineralization incorporates ion released from the implant surface and firmly bonds the newly formed bone to the implant,establishing that interfacial chemical variables are the critical factors in ultrastructural compatibility of bone and implants.

The results of the in-vitro and in-vivo studies have been used to develop prosthetic devices made from the bioglass-ceramics and from high-strength metals flame sprayed with bioglass coatings. The mechanical strength of the interfacial bond developed between a glass-ceramic bone splint with a reactive surface and a rat femur was measured. Interfacial strength began to develop as early as six weeks. After 28 weeks sufficient strength was established that the bone failed under a torsional stress of 513 kg/cm^2 with the glass-ceramic interface remaining intact. Statistical evaluation of segmental bone replacement in monkeys show development of a strong interfacial bond. Computer programs to evaluate stresses actually applied at the implant interface are used in the interpretation of the mechanical test data.

Partial hip prostheses for stumptail monkeys were designed using biomechanics factors. The 316L surgical stainless steel prostheses flame spray coated with bioglass showed stable fixation in the intermedullary canal without the use of screws or other mechanical means of fixation. Functional use of the hip was retained. Histological evaluation after one year showed complete protection of neighboring tissues from metal corrosion products.

The most recent application in this project has centered around an effort to utilize bioglass and bioglass-ceramic materials as resorbable bone plates for fixation of fractured limbs. A plate was designed for application to a fractured dog femur. Initially, problems were encountered as a result of plate failure during the implantation procedure. Revision of the plate design alleviated the problem and several successful operations have been performed.

The plates have remained stable for a maximum of nine days with fracture occurring as early as three days post-operation. The problem has been attributed to static fatigue of the plates, which has necessitated a temporary halt in plate manufacture. A concentrated effort to optimize the

strength of the plates by varying the fabrication process is underway.

Implantation of bioglass-ceramics in soft tissues (rat muscle) shows interfacial phagacytosis by macrophage cells at a rate proportional to the solubility of the implant. This behavior indicates the chemical specificity involved in the biocompatibility of an implant. Although release of Na, Si, Ca and P ions from the bioglass-ceramic surfaces, and accompanying creation of an alkaline pH, elicits the interfacial mineralization required for compatibility with bone, such an environment is foreign to soft tissue requirements and rejection occurs. The rejection occurs by digestion of the implant by cells differentiated to achieve that end.

III. SUMMARY OF MAJOR ACCOMPLISHMENTS, 1969-74

1. Nonporous glass and glass-ceramic materials have been developed which will directly bond to bone by means of a chemical bond. The strength of the bond is sufficient that implants in rat femurs cannot be forcibly extracted. The bonding strength is sufficient that the interfacial attachment of the ceramic to the bone will withstand the impact force of a milling machine cutting bar and diamond microtome.

2. Low viscosity, biocompatible glasses with a variable rate of release of surface ions and change of surface pH have been developed. This series of glasses involved the partial replacement of the SiO_2 network forming oxide with B_2O_3 network formers. The Na_2O-B_2O_3 ions in the glass complex to form a tetrahedral structural unit akin to that of the SiO_2 units. However, the viscosity of the glass is greatly reduced, thus making it possible to flame spray or enamel the bioglass. Both in-vitro and in-vivo evaluations establish the equivalent behavior of this new line of bioglasses to that of the 45S5 composition originally developed in this program.

3. In-vitro evaluation of the surface chemical response of bioglasses to a simulated physiologic environment has been accomplished. A corrosion layer or layers are formed as a result of aqueous attack of the glass structure. If phosphorus is absent from the bioglass composition, sodium and calcium are selectively leached, producing a silica-rich gel layer. The addition of phosphorus to the glass composition does not interfere with the development of a silica-rich gel layer initially. However, a second film composed of an amorphous calcium phosphate develops at the silica gel-water interface and with time crystallizes to form an apatite structure. Increasing the phosphorus content of the glass composition accelerates the formation of the calcium phosphate film.

Partial substitution of B_2O_3 for SiO_2 accelerates the initial dissolution process. The addition of fluorine to the glass composition significantly enhances the resistance of the glass to aqueous attack, probably by substituting for hydroxyl ions in the apatite structure.

4. Composition profiles of the corrosion layers formed on a series of bioglasses with increasing phosphorus content have been measured employing Auger Electron Spectroscopy and ion beam milling. The profiles provide detailed compositional maps which confirm the existence of the calcium phosphate gel-silica gel-bulk glass structure at the bioglass surface after reaction.

5. Confirmation and extension of our earlier bone-bioglass-ceramic interface reaction mechanism studies have been achieved by comparing 45S5, $45B_5S5$ and 45S5F bioglass-ceramics implanted in the cancellous bone of the tibial cortex of young rats. All of the implants grew with the newly forming bone away from the epiphyseal plate.

6. Ultrastructural studies of the bone-ceramic interface have led to a new theory of the formation of the bond, which is through the production of an amorphous ion surface gel on the bioglass. An amorphous gel-like layer has been noted on the surface of the implant, extending over a distance of 800 to 1,000 angstroms. This layer may be equivalent to the substance comprising the "cement line" in mature bone. Osteoblasts lay down collagen fibers onto this bonding layer and mineralization then occurs in an ectopic manner. The resulting, highly elongated, crystals bridge the space between the implant surface and the mature bone.

7. Implantation of a series of bioglasses with variable phosphorus content has given support to the concept of the soluble silica-rich gel serving as an induction site for osteogenesis. In addition, there is an optimum phosphorus level in the bulk composition which leads to a situation where a sufficient but not excessive supply of calcium and phosphate ions is available for incorporation into the mineralization process.

8. It has been shown that sufficient strength is developed at the interface of a bioglass-ceramic segmental bone replacement that a rat femur will fracture in the bone in torsion rather than at the materials-bone interface.

9. Biomechanical evaluation of femoral segmental replacements in primates has shown that the bond developed between the 45S5 glass implants in bone was strong enough to cause the fracture developed in a torsional test to pass through the implant as well as the surrounding bone and the interface. This demonstrates that the bond strength is quite

substantial. This type of bond strength has not been found in stainless steel implants flame sprayed with the 45S5F composition.

10. Implants of the glass-ceramics of the 45S5F composition in the vastus lateralis muscle of the right hind leg of rats showed a fibrous tissue response with the tissues firmly adhering to the implant surface. The reactions to the implants can be interpreted to show early synovial cell type formation about the implant. It can be demonstrated that this cell layer is involved in phagocytosis of the implant.

11. Comparison of other glass-ceramic compositions, 45S5 and $45B_5S5$, in rat muscle showed that the more surface-reactive implant materials induced a more marked foreign body type reaction with multinucleated phagocytic cells attempting to destroy the implant. This general behavior is in marked contrast to that observed for the implant responses on bone. In bone, the more reactive glass surfaces induced osteoblastic formation and development of a chemical bone.

12. Long-term studies (>10,000 hours) of the solubility and pH-time dependence of the various bioglass and bioglass-ceramic compositions show a controlled release rate of Ca, Na, Si and P ions from the implant surfaces. The ion losses in buffered solutions provide the physical-chemical correlation required to interpret the soft tissue and hard tissue in-vivo responses. Fluorine additions decrease the ion release rate and thereby evoke a slower mineralization. Boron oxide additions accelerate the interfacial reactions. Thus, the bioglass and bioglass-ceramics can be designed to match specific metabolic activities.

13. In-vitro solubility studies on flame sprayed $45B_5S5$ and 45S5F bioglass-ceramics have shown that the relative solubilities of these two materials in the flame sprayed state is the same as in the bulk materials.

14. Fatigue studies of flame sprayed specimens show that stress and life are inversely related in a manner quite similar to that shown by ferrous materials. Specimens tested while submerged in distilled water exhibit a lower fatigue life than specimens tested dry. The wet specimens, however, exhibited much smaller cracks once failure began than the dry specimens.

15. In-vitro solubility studies show that crystallization does not significantly affect the rate of surface ion release from the bioglass-ceramics. Implants of identical specimens in rat cortices also show interfacial bonding of bone to the implant irrespective of degree of crystallinity. This correlation shows for the first time that it is interfacial chemical variables that control ultrastructural compatibility of

implants with bone rather than crystallographic or microstructural features of the implants.

16. Physiological dosages of parathyroid extract given to rats for 72 hours prior to sacrifice have not evoked an osteoclastic resorption at the interface of the bioglass-ceramic materials.

17. A partial hip prosthesis combining high strength mechanical behavior and controlled biocompatibility has been achieved on an exploratory scale by flame spray coating the 45S5F bioglass on 316L surgical stainless steel monkey hip prostheses. The hip prostheses have been evaluated in primate after a one-year implantation and show stable fixation in the intramedullary canal without the use of screws, cement, or any other means of mechanical fixation.

18. Histological analyses of the tissue reactions at the interface of the 45S5F flame sprayed monkey hip prostheses shows the absence of migration of metal particles into the tissue surrounding the implant with the bioglass coating. In contrast, the tissues around a surgical stainless steel screw of the same metal composition, without the bioglass coating, have been examined after an equivalent implantation time and show massive migration of metallic deposits into the tissues.

19. In-vitro studies have shown that the crystal structure of the glass-ceramic will promote direct chemical bonding of hydroxyapatite crystals at the interface. These results suggest a mechanistic explanation for the direct bonding achieved in the in-vivo studies. They also suggest means of directly controlling bonding and interfacial reactions desired in specific medical applications.

20. Precipitation of polypeptides on the surfaces of glass-ceramics and various other minerals have shown that the compatibility of proteins is a function of crystal structure and orientation of the crystalline materials surface and is a function of glass composition.

21. The bioglasses and bioglass-ceramics developed in this program bond with certain charged protein groups.

22. Techniques to evaluate the nature of interfacial bonding between ceramics and bone have been successfully developed. These techniques include transmission electron microscopy, scanning electron microscopy, microradiography, tetracycline tracers and optical microscopy.

23. Methods for evaluating the specitif ions released at the surface of the bioglasses and bioglass-ceramics and the structural changes in the implant surfaces have been developed. These include atomic absorption analysis, atomic emission

analysis, colorimetry, infrared reflection spectroscopy, scanning electron microscopy. Auger spectroscopy has been recently used to understand the exact chemical nature of the interfacial surface of the implant materials. Ion-milling of the surface followed by segmental Auger spectroscopy reveal the detailed sequence of Na, Si, Ca and P ions release from the implant surface and build-up of surface gel layers.

24. An effort to enamel 316L surgical stainless steel, in collaboration with Ferro Corporation, met with only limited success because of diffusion of transition metal ions in the bioglass enamel.

25. Human and chick fibroblastic tissue cultures exposed to glass-ceramic compositions (45S5F, $45B_5S5$ and 45S5) were fed and maintained under physiological conditions for periods of two and three weeks on bioglass substrates. During that time the cells were observed to attach to all of the bioglass-ceramic compositions and in some instances to multiply normally. A desensitization of the bioglass surface involving equilibration to solutions of tissue culture media is required to achieve maximum tissue culture compatibility. This equilibration procedure is now used for all in-vivo prostheses prior to implantation.

26. A systems analysis of the various activities in the research program has been completed and has been used to establish budget and personnel allocations as well as the time sequencing required for the interacting functions of the research.

27. A simple method for attaching strain gages to bone for the measurement of mechanical properties during mechanical loading has been accomplished. Evaluation of bone plates has been achieved using this method.

28. A set of computer programs has been developed which allows the computation of torsional and bending stresses in arbitrary multiply-connected cross sections. The programs are user oriented, and allow a quite flexible input data structure. The program has been tested using certain configurations for which analytical stress distributions are available and has demonstrated accuracy to within five percent of the calculated value.

29. Application of the protein-mineral epitaxial results obtained in this program has been made to the problem of urolithiasis. The interfacial interactions between the inorganic substances and organic matrix in the formation of urinary stones is akin to the type of interfacial interactions being examined in detail in this contract. Consequently, application of these results to other medical problems appears to be possible and our research has provided guidance on these matters wherever it seems justified.

30. In studies of the torsional strength of paired bones from three groups of animals it has been shown that there is no significant left-right bias in the measured strength, and that the standard deviation of the percent difference side-to-side strength is typically about 0.10.

IV. CUMULATIVE LIST OF PUBLICATIONS RESULTING FROM THE CONTRACT

1. L.L. Hench, R.J. Splinter, W.C. Allen and T.K. Greenlee, Jr., J. Biomed. Res. Symposium, No. 2, Interscience, New York, 1972, pp. 117-143.

2. C.A. Beckham, T.K. Greenlee, Jr., and A.R. Crebo, J. Calcified Tissue Res., 8 [2] (1971).

3. G. Piotrowski and G.A. Wilcox, "The STRESS Program: A Computer Program for the Analysis of Stresses in Long Bones," J. Biomech., 4, 497-506 (1971).

4. T.K. Greenlee, Jr., C.A. Beckham, A.R. Crebo and J.C. Malmborg, J. Biomed. Mat. Res., 6, 244 (1972).

5. L.L. Hench and H.A. Paschall, "Direct Chemical Bond of Bioactive Glass-Ceramic Materials to Bone and Muscle," published in Symposium on Materials and Design Considerations for the Attachment of Prostheses to the Musculo-Skeletal System, Clemson University, April 1972.

6. B.A. Hartwig and L.L. Hench, "The Epitaxy of Poly-L-Alanine on L-Quartz and a Glass-Ceramic," J. Biomed. Mat. Res., 6 [5], 413-424 (1972).

7. L.L. Hench, "A Systems Approach to the Development, Application and Economics of Biomaterials," submitted to Biomaterials, Medical Devices and Artificial Organs, T.F. Yen, ed., Marcel Dekker, New York.

8. L.L. Hench, "Factors in Protein-Mineral Epitaxy," in Urolithiasis: Physical Aspects, B. Finlayson, L.L. Hench and L.H. Smith, eds., National Academy of Sciences, Washington, D.C. (1972), pp. 203.

9. L.L. Hench, T.K. Greenlee, Jr., W.C. Allen and G. Piotrowski, "An Investigation of Bonding Mechanisms at the Interface of a Prosthetic Material," Reports #1, #2, #3 and #4, U.S. Army Medical Research and Development Command, Contract No. DADA17-70-C-0001 (1970, 1971, 1972 and 1973).

10. L.L. Hench and H.A. Paschall, "Histo-Chemical Responses at a Bio-Materials Interface," to be published in J. Biomed. Mat. Res. Symposium Prostheses and Tissue: The Interface Problem.

11. L.L. Hench, "Ceramics, Glasses and Composites in Medicine," Medical Instrumentation, 7 [2], 136-144 (1973).

12. L.L. Hench, "Factors Affecting the Physiological Interface with Ceramics," to be published in Surfaces and Interfaces of Glass and Ceramics, W.C. LaCourse, ed., Plenum Press, 1974.

13. A.E. Clark, L.L. Hench and H.A. Paschall, "The Influence of Surface Chemistry on Implant Interface Histology: A Theoretical Basis for Implant Materials Selection," 6th Annual Biomaterials Symposium, Clemson, S.C., 1974.

14. G. Piotrowski, L.L. Hench, W.C. Allen and G.J. Miller, "Mechanical Studies of the Bone Bioglass Interfacial Bond," 6th Annual Biomaterials Symposium, Clemson, S.C., 1974.

15. C.G. Pantano, Jr., A.E. Clark and L.L. Hench, "Multilayer Corrosion Films on Bioglass Surfaces," J. Amer. Cer. Soc., 57 [9], 412-413 (Sept., 1974).

16. L.L. Hench, H.A. Paschall, W.C. Allen and G. Piotrowski, "Interfacial Behavior of Ceramic Implants," AAMI Biomaterials Symposium, NBS Publication (in press).

17. L.L. Hench, "Biomedical Applications and Glass Corrosion," Proceedings of Xth International Glass Congress, Kyoto, Japan, July 1974.

18. L.L. Hench and E.C. Ethridge, "Biomaterials--The Interfacial Problem," in Advances in Biomedical Engineering, Academic Press (in press).

19. L.L. Hench, "Prosthetic Implant Materials," in Advances in Materials Science, Annual Reviews, Inc. (in press).

V. REVIEW OF PROGRESS

A detailed description of the progress made in this program during the 1973-74 contract year will be presented in the form of four papers and one review note. These papers and note comprise the remainder of this report and follow on succeeding pages.

A. A Comparison of Bioglass Implant Behavior With Other Orthopedic Biomaterials, by A. E. Clark and L. L. Hench

Introduction

Orthopedic prosthetic devices are employed for fixation, stabilization, and replacement of damaged or diseased bone. A wide variety of implant configurations are in use today. These include plates, nails, screws and pins for fixation, and weight-bearing devices such as hip, femoral, and total knee prostheses.

Historically, metals have played the predominant role as prosthetic devices. As early as 1775 AD, evidence in the literature documents the use of iron wire to suture fractured bone segments together [1]. Since that time numerous metals ranging from gold, silver, aluminum, zinc, lead, copper, nickel, high carbon steel, low carbon steel, cobalt chromium molybdenum alloy, copper aluminum alloy, magnesium, iron, titanium, and titanium-aluminum-vanadium alloy have been investigated as candidates for prosthetic devices [2-7]. As might be expected, a wide range of responses is elicited by the various metals and alloys. These responses range from gross corrosion of the metal and bone necrosis adjacent to the implant, to situations in which the presence of the implant in a physiological environment is well tolerated and bone formation occurs in close proximity to the implant. As the investigation of metallic implants has progressed, a series of requirements for an ideal implant material has evolved. Included in this list are: (a) high corrosion resistance, (b) suitable mechanical properties for the application, (c) excellent wear and abrasion resistance where required, (d) good tissue compatibility, (e) structural homogeneity and soundness, (f) non-thrombogenicity, and (g) reasonable cost [8].

Metal devices predominantly in use in this country fall into three categories: Type 316, 316L and 317 stainless steels (wrought); cobalt-chromium based alloys (cast and wrought); and titanium (unalloyed, wrought). These materials all exhibit superior corrosion resistance in the physiological environment of the body. However, it has been demonstrated that there is an absence of adherence between implants made from these materials and bone, because there is always a fibrous capsule or sheath surrounding the implant and isolating it from tissue [9,10].

The thickness of the fibrous capsule is an indication of the degree of tissue acceptability; i.e., the thinner the capsule the better the acceptability. The development of the fibrous tissue is due to either corrosion of the implant or mechanical irritation produced by movement of the implant [11,12].

The lack of direct attachment of living tissue to metallic implants can lead to loosening and motion. The resulting pain can force surgical removal. Sufficient movement can lead to implant failure or bone fracture. As a result of this situation, numerous investigations have been initiated to find a material which will firmly adhere to bone.

One approach has involved the use of porous metallic implants. The concept involves bone ingrowth into a porous surface providing mechanical interlocking. The mechanical load is distributed over a wide area, reducing the chance of bone necrosis due to stress concentrations at localized sites.

Hirschhorn et al. reported deep bone ingrowth into specimens of sintered Ti and Ti-6A-4V alloy with a pore size of 200 μm [13]. Welsh et al. documented bone ingrowth into porous Co-Cr-Mo alloy (Vitallium) coatings on solid Vitallium rods [14].

Galante et al. [15] used titanium fibers which were compacted in dies and vacuum sintered. The resulting pore size was reported to be within an order of magnitude of the fiber diameter. Specimens placed in rabbit and dog femurs revealed bone ingrowth after 12 weeks. In another related study, hip prostheses were evaluated after 3 months to a year in dogs. Deep bone ingrowth and firm stabilization were reported [16]. Pore size was 230 μm.

A process to produce porous metal implants which involves the use of a sacrificial metal with a low vaporization temperature has been developed at Battelle Northwest Laboratories [17]. A composite containing the sacrificial metal and the implant material is formed and machined to the desired size and shape. The implant is heated to vaporize the sacrificial metal and then sintered. Cylindrical plugs made with 304 stainless steel, Ti, and Ti-6Al-4V powders have been implanted into dog femurs for time intervals up to 12 weeks. Bone ingrowth was reported to depths of 2,500 μm [18].

A method for plasma spraying titanium hydride powder on solid titanium specimens has been developed by Hahn and Palich [19]. Implants with a porous surface (pore size 50-75 μm) were implanted into femurs of sheep for 14 and 26 weeks. A significant increase in bond strength was noted when porous specimens were compared with implants with smooth surfaces. Although histological examination of the bone-porous surface was not reported, bone penetration into the pores was postulated on the basis of the differences in bond strength between the porous and non-porous implants.

The use of porous metal surfaces to anchor prosthetic devices to bone seems promising. One of the major points which remains to be shown is the effect of the increase in

surface area associated with a porous surface and the resulting corrosion which would occur over long periods of time.

Another area of interest has centered around the use of inert porous ceramic materials. Due to their highly oxidized state, ceramics are inert materials capable of resisting degradation in severe environments [20]. In addition, ions incorporated into most ceramics (Na, K, Mg, Ca) are normally found in the body. Thus, release of these ions from a ceramic implant would not present as serious a problem as release of foreign or toxic elements.

One of the first attempts involved the use of a slip cast mixture of alumina, silica, calcium carbonate and magnesium carbonate. The resulting porous material (average pore size 17 μm) was strengthened by vacuum impregnating with an inert epoxy [21]. Openings at the surface were obtained by dissolving the epoxy to a depth of 50-70 mils with methylene chloride. The composite material was called Cerosium and exhibited mechanical properties similar to bone. Evaluation of this material revealed little bone ingrowth into the pores. This was attributed to a small pore size. In addition, a reduction in the strength values of Cerosium which had been implanted was related to epoxy degradation by body fluids [22].

The use of porous calcium aluminate has been investigated by Klawitter and Hulbert [23]. Calcium carbonate and alumina were mixed with water, pressed into pellets, dried, and fired. An interconnected pore structure was produced by the breakdown of the calcium carbonate and the subsequent release of CO_2. Pore size was controlled by varying the particle size of the calcium carbonate. In-vivo studies revealed that a minimum interconnection pore size of 100 μm was necessary for mineralized bone growth. In addition, there was a lack of inflammatory responses due to the calcium aluminate implants. The one unusual response was the presence of a layer of osteoid (∿50 μm thick) separating mineralized bone from the ceramic composite. The authors speculated that a local alkaline pH change produced by hydration of the surface of the ceramic composite inhibited mineralization within 50 μm of the ceramic. Although there was a lack of inflammatory response elicited, the porous ceramic cannot be considered completely inert, because of the hydration and resulting effect on bone mineralization.

Hulbert et al. [24] have reviewed the in-vivo behavior of numerous porous ceramic materials and found no adverse tissue response and mineralized bone ingrowth into several materials.

Preliminary investigations have been conducted employing dense aluminum oxide (Al_2O_3) as a prosthetic device [25].

The development of a fibrous sheath separating bone and ceramic was noted as the major drawback.

Graves et al. have recently reported on the development of a resorbable ceramic implant [26]. The concept of a resorbable ceramic material has several attractive features. The initial pore size can be restricted to values less than optimum for bone penetration. This will result in an increase in the initial strength of the ceramic. As resorption proceeds, enlargement of the pore structure will stimulate bone ingrowth. The drop in strength associated with the increase in pore size will be compensated for by the presence of the new bone. The stress concentration at the implant-bone interface of permanent devices is not a problem as the material is completely resorbed with time. There is the potential for influencing ossification through the release of specific ions incorporated into the ceramic [26].

Calcium aluminate ceramics with additions of phosphorus pentoxide were implanted into femurs of mature Rhesus monkeys. The results pointed to an enhancement of bone formation at the ceramic-tissue interface as well as within the ceramic as the P_2O_5 concentration was increased [26].

A completely unique approach to the problem of permanent fixation has been initiated by L. L. Hench et al. [27-30]. The concept involves the use of surface reactive bioglasses to achieve intimate bonding between an implant and bone tissue. In-vivo results, obtained at an early stage in the program, in the form of transmission electron micrographs, demonstrated glass-ceramic implants intimately bonded to bone at 6 weeks with no indication of an inflammatory response to the implant [31]. It was suggested that some chemical characteristics of the implant may have enhanced ossification at the glass-bone interface.

The purpose of this text is to describe a systematic study of a series of glasses (referred to as bioglasses) with the intent of developing an understanding of their chemical surface behavior. New surface sensitive techniques such as Auger Electron Spectroscopy and Infrared Reflection Spectroscopy along with several other tools have been employed to examine the response of bioglasses to an aqueous environment maintained at physiologic temperature and pH. An effort is then made to relate the observed in-vitro reactions to a series of in-vivo responses. It is the authors' opinion that such an approach has been lacking in many previous investigations of candidate biomaterials and, hopefully, will serve as a model for future studies.

References

1. Icart: J. de Med.; Chir. et Phar. de Roux, 44, 170 (1775).

2. A.A. Zierold, Arch. Surg., 9, 365-412 (1924).

3. F.P. Bowden, J.B.P. Williamson and P.G. Laing, J. Bone and Joint Surgery, 37-B, 676-690 (1955).

4. A.B. Ferguson, P.G. Laing and E.S. Hodge, J. Bone and Joint Surgery, 42-A, 77-90 (1960).

5. J. Cohen, J. Materials, 1 [2], 354-365 (June 1966).

6. H.D. Greene and D.A. Jones, J. Materials, 1 [2], 345-353 (June 1966).

7. G.H. Hille, J. Materials, 1 [2], 373-383 (June 1966).

8. S. Weisman, Biomechanical and Human Factors Symposium 1967, The American Society of Mechanical Engineers.

9. P.G. Laing, A.B. Ferguson and E.S. Hodge, J. Biomed. Mat. Res., 1 [1], 135-150 (March 1967).

10. D.H. Collins, J. Path. and Bacteriol., 65, 100-121 (1953).

11. N.K. Wood, E.J. Kaminski and R.J. Oglesby, J. Biomed. Mat. Res., 4 [1], 1-12 (March 1970).

12. J.T. Scales, Proceedings Royal Society Medicine, 63, 1111 (1970).

13. J.S. Hirschhorn, A.A. McBeath and M.R. Dustoor, Biomedical Material Symposium No. 2, Bioceramics-Engineering in Medicine, Interscience Publishers, 1972, p. 49.

14. R.P. Welsh, R.M. Pilliar and I. Macnab, J. Bone and Joint Surgery, 53A [5], 963 (July 1971).

15. J. Galante, W. Rostoker, R. Lueck and R.D. Ray, J. Bone and Joint Surgery, 53A [1], 101 (January 1971).

16. E. Lembert, J. Galante and W. Rostoker, Clinical Orthop. and Related Research, No. 87 (September 1972), p. 303.

17. "Voids Help Attach Metal to Bone," Indus. Research, December 1971, p. 25.

18. J.L. Nilles and M. Lapitsky, J. Biomed. Mat. Res. Symp., No. 4, John Wiley and Sons, New York, 1973, pp. 63-84.

19. H. Hahn and W. Palich, J. Biomed. Mat. Res., 4, 571 (1970).

20. W.W. Kriegel and H. Palmour, eds., Ceramics in Severe Environments, Plenum Press, New York, 1971.

21. L. Smith, Archives of Surgery, 87, 653 (October 1963).

22. R.P. Welsh and I. Macnab, Bioceramics-Engineering in Medicine, Interscience Publishers, 1972, p. 231.

23. J.J. Klawitter and S.F. Hulbert, Biomedical Materials Symposium No. 2, Bioceramics-Engineering in Medicine, Interscience Publishers, 1972, p. 161.

24. S.F. Hulbert, F.W. Cooke, J.J. Klawitter, R.B. Leonard, B.W. Saver, D.D. Moyle and H.B. Skinner, J. Biomed. Res. Symp., No. 4, 1973, pp. 1-33.

25. P. Griss, G. Heimke, H. von Andrean-Werburg, B. Krempien, S. Reipa, H.J. Lauterbach and H.J. Hartung, J. Biomed. Mat. Res. Symp., No. 6 (in press).

26. G.A. Graves, F.R. Noyes and A.R. Villaneuva, J. Biomed. Mat. Res. Symp., No. 6 (in press).

27. L.L. Hench, T.K. Greenlee, Jr., and W.C. Allen, Annual Report #1, U.S. Army Med. R and D Command, Contract No. DATA-17-70-C-0001 (1970).

28. L.L. Hench, T.K. Greenlee, Jr., and W.C. Allen, Annual Report #2, U.S. Army Med. R and D Command, Contract No. DADA-17-70-C-0001 (1971).

29. L.L. Hench, H.A. Paschall, W.C. Allen and G. Piotrowski, Annual Report #3, U.S. Army Med. R and D Command, Contract No. DADA-17-70-C-0001 (1972).

30. L.L. Hench, H.A. Paschall, W.C. Allen and G. Piotrowski, Annual Report #4, U.S. Army Med. R and D Command, Contract No. DADA-17-70-C-0001 (1973).

31. L.L. Hench, R.J. Splinter, W.C. Allen and T.K. Greenlee, Jr., J. Biomed. Mat. Res. Symp., No. 2, Interscience Publishers, New York, 1972, pp. 117-143.

B. The Influence of P^{+5}, B^{+3} and F^{-1} on the Corrosion Behavior of an Invert Soda-Lime-Silica Glass, by A. E. Clark and L. L. Hench

Abstract

The influence of phosphorus, boron and fluorine additions on the surface chemical reactivity of a soda-lime-silica glass has been investigated. Several techniques including infrared reflection spectroscopy, ion solution analysis, scanning electron microscopy, energy dispersive x-ray analysis and x-ray diffraction have been employed to develop insight into the morphological and chemical changes which occur on glass surfaces corroded in a simulated physiologic environment.

The results show that the glasses investigated develop a corrosion layer or layers in response to attack by an aqueous solution buffered at a pH of 7.4 and maintained at 37°C. Sodium and calcium are preferentially leached from the soda-lime-silica glass, producing a silica-rich film which serves as a buffer zone protecting the remaining bulk glass from aqueous attack. As phosphorus is added to the glass composition a second film is generated at the silica-rich film-water interface. The second film is an amorphous calcium phosphate compound which crystallizes to an apatite structure with time. Increasing the phosphorus content of the glass reduces the time required for the calcium phosphate film to form. Partial substitution of B_2O_3 for SiO_2 leads to weakening of the silicate network and acceleration of the initial dissolution process. Fluorine additions significantly enhance the resistance of the glass to aqueous attack, probably by substituting for hydroxyl ions in the apatite structure of the corrosion film.

Introduction

The corrosion of silicate based glasses can occur by either selective leaching or complete dissolution, but usually involves a combination of the two. In general, the process leads to the formation of a thin film or gel on the exposed glass surface with the composition of the gel being significantly different from that of the uncorroded glass.

The composition and profile of the gel layer are usually a direct measure of the durability of the glass. Studies on binary soda-silica and lithia-silica glasses have established that the corrosion resistance is maximized when the reactions at the glass surface lead to the formation of a thin gel with a high surface silica concentration [1].

A series of invert silica glasses are under investigation for use as prosthetic devices [2-5], and it has been demonstrated that it is possible to achieve bonding between glass and living bone in the body [6]. The biological acceptability of a soda-lime-silica glass is significantly affected by the presence of small amounts of phosphorus, boron, or fluorine [7-10].

The mechanism by which the bond is developed is essentially a controlled corrosion of the glass which produces a surface composition that is compatible with bone. The results of this study have shown that the corrosion behavior of the bioglasses is directly related to the effects of additions of phosphorus, boron, and fluorine on the composition and profile of the resulting gel.

Four nondestructive techniques, infrared reflection spectroscopy (IRRS), ion concentration analysis of the corrosion solution, scanning electron microscopy coupled with energy dispersive x-ray analysis and x-ray diffraction, are employed to characterize the corrosion gels. IRRS provides a direct measure of the surface silica concentration [11], while two parameters calculated from the solution data provide a measure of the total amount of silica available for gel formation [12]. The parameter α is a measure of the extent of selective dissolution and varies in magnitude from 0 to 1. When α approaches 0, selective leaching predominates. As α approaches 1, total dissolution is the controlling proress. The second parameter, ε, referred to as excess silica, is a measure of the amount of silica available for gel formation and is calculated from α and the concentration of SiO_2 in solution. (For a detailed discussion see Ref. 12.)

Six glasses were chosen for study. This series of compositions provides information as to the influence of phosphorus on the corrosion behavior of the ternary soda-lime-silica glass (see comp. 1, Table 1) as well as the influence of boron and fluorine on the behavior of glass number 3. Glass number 3, which contains 6% P_2O_5, is the most compatible with bone. Boron and fluorine were added to facilitate flame spraying onto metal substrates as they both reduce the melting temperature of the glass [13].

Experimental Procedures

The glasses were prepared from reagent grade sodium carbonate, reagent grade calcium carbonate, reagent grade phosphorus pentoxide, reagent grade boric anhydride, and 5 μm silica. Premixed batches were melted in platinum crucibles in a temperature range of 1250 to 1350°C for 24 hours. Samples were cast in a steel mold and annealed at 450°C for 4 to 6 hours.

Table 1

Bioglass Compositions
for Surface Chemistry Analyses

Weight %	Weight %	Weight %
1. 45S-0% P_2O_5	3. 45S-6% P_2O_5	5. 45B_5S5
45% SiO_2	45% SiO_2	40% SiO_2
24.5% CaO	24.5% CaO	5% B_2O_5
30.5% Na_2O	24.5% Na_2O	24.5% CaO
	6% P_2O_5	24.5% Na_2O
2. 45S-3% P_2O_5		6% P_2O_5
45% SiO_2	4. 45S-12% P_2O_5	
24.5% CaO	45% SiO_2	6. 45S5F
27.5% Na_2O	24.5% CaO	43% SiO_2
3% P_2O_5	18.5% Na_2O	12% CaO
	12% P_2O_5	16% CaF_2
		23% Na_2O
		6% P_2O_5

Bulk samples of each composition were prepared by wet grinding with 180, 320, and 600-grit silicon carbide paper. After a final dry grinding with 600-grit silicon carbide paper, samples were immersed in 200 ml of aqueous solution buffered at a pH of 7.4. Buffering was accomplished with a physiological buffer (trishydroxymethyl aminomethane) [14]. Stock solutions of .2 M tris (hydroxymethyl) aminomethane and .2 M HCl were mixed with distilled and deionized water to produce a pH of 7.4. Temperature was maintained at 37°C and the duration of exposure was varied from .1 to 1,500 hours. All sample solutions were maintained in a static state. A Coleman Metrion IV pH meter with ±0.05 pH accuracy was used to monitor change in pH.

Each sample was subjected to infrared reflection analysis immediately upon removal from the corrosion solution and compared with the spectrum of an uncorroded sample. The IR radiation reflected from the glass surface is measured over a spectrum of wavenumbers from 1,400 to 250 cm^{-1}. The peaks produced are characteristic of the vibrations of specific ionic bonds in the glass structure [15]. By comparing the reflectance spectra of corroded versus uncorroded glasses and also the spectra of glasses of varying composition, information about the type of structural change as well as the rates of changes can be obtained [11]. All measurements were taken on a Perkin-Elmer 467 Grating Infrared Spectrophotometer equipped with a specular reflectance accessory.

Solution analysis was performed employing atomic emission spectroscopy and colorimetric techniques. Figure 1 is a schematic block diagram of the atomic emission spectrophotometer employed for these analyses. Samples of buffered aqueous solutions in which glass specimens had been immersed for specific periods of time are introduced into the flame through the nebulizer burner system. An atom vapor which consists of atoms in the ground state and thermally excited states is produced in the flame. As atoms in the thermally excited states return to the ground state, they emit radiation with a wavelength characteristic of the type of atom involved. This characteristic radiation, which is isolated in the monochromator and intensified in the photomultiplier module, can be related to the concentration of the atoms in the original sample solution.

The normal procedure consisted of running undiluted samples and comparing the results with a series of premixed standards with concentrations ranging from 10, 25, 50, 100, 150 and 200 ppm of the ionic species being analyzed. Based on these results, the unknown samples were diluted into a range of 1-10 ppm. Premixed standards of 1, 2, 4, 6, 8 and 10 ppm were analyzed and a plot of intensity versus concentration (ppm) was obtained. The diluted samples were run along with the second series of standards. Plotting the intensities of the unknown samples on the predetermined standard curve enabled one to obtain an accurate measurements of the unknown ionic concentration. This method was employed to determine calcium and sodium released into solution.

The colorimetric procedure involves the use of a Hach Direct Reading Colorimeter which relates the intensity of light at a specific wavelength passing through a sample solution to the concentration of a particular ion in the solution.

The colorimetric molybdosilicate method and heteropoly blue method were used for silica determination [16]. In both of these procedures ammonium molybdate is added to the unknown solution, and reacts with any silica present to form molybdosilicate acid which has a yellow color. The intensity of the yellow color is proportional to the concentration of silica in solution. In the heteropoly blue method, the yellow molybdosilicate acid is reduced with aminonaptholsulfonic acid to heteropoly blue. The resulting blue color is more intense than the yellow and provides a more sensitive measurement of the amount of silica [17]. The molybdosilicate method has a range of 0-150 ppm, whereas the heteropoly blue method has a range of 0-3 ppm. Normal procedure involved measurement of undiluted samples with the molybdosilicate method, followed by dilution and a second measurement with the heteropoly blue method. In both tests oxalic acid was used to eliminate interference from phosphate groups.

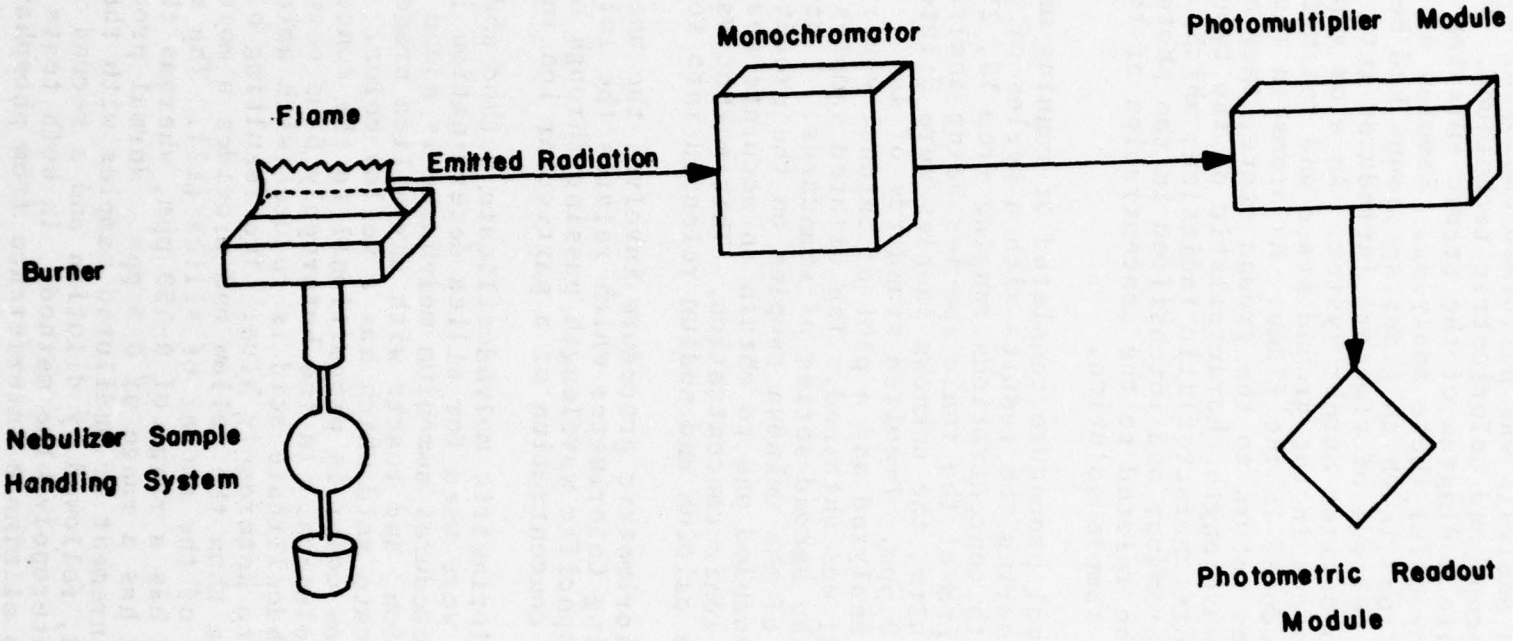

Figure 1. Schematic block diagram of the atomic emission spectrophotometer employed for solution analyses.

The Phos Ver III method [16] was employed for total phosphate determination. This method has a range of 0-3 ppm. Dilutions were made until two successive dilutions yielded the same results.

Several samples of each composition were examined with a Cambridge Scanning Electron Microscope equipped with an Ortec Energy Dispersive X-ray Analysis System. In this system a lithium drifted silicon detector is used to separate radiation according to its energy. X-rays, produced as a result of the primary electron beam striking the sample surface, excite electrons of the silicon atoms. Each of the excited electrons absorbs 3.8 eV of energy. Since numerous electrons are excited by a single x-ray, the total charge generated produces a current which is proportional to the energy of the x-ray. The current is then stored in a multichannel analyzer according to its amplitude, until a sufficient number of x-rays have been counted [18].

X-ray diffraction patterns of selected samples were utilized to identify the corrosion films which formed on the glass surfaces. A Phillips Vertical Diffractometer with a graphite diffracted beam monochromator was employed. CuKα radiation was used, with tube settings of 40 kV and 15 milliamps. Pulse height selection was utilized to reduce background noise.

Data Analysis

Sanders and Hench have presented the following equation for the calculation of α for binary silicate glasses:

$$(1)\quad \alpha = \frac{\text{moles of } SiO_2 \text{ in solution}}{\text{moles } R_2O \text{ in solution}} \Big/ \frac{\text{moles } SiO_2 \text{ in glass}}{\text{moles } R_2O \text{ in glass}}$$

$$(2)\quad = \frac{\text{PPM } SiO_2}{1/2 \text{ PPM } R^+} \cdot \frac{\text{MW } R^+}{\text{MW } SiO_2} \cdot \frac{Pm}{1-Pm}$$

where Pm = mole fraction R_2O in glass, MW = molecular weight, PPM SiO_2 = concentration of SiO_2 in solution, and PPM R^+ = concentration of R^+ in solution [12].

Extension of the relation to a ternary soda-lime-silica glass leads to the following modification of equation (2).

$$(3)\quad \alpha = \frac{\dfrac{\text{PPM } SiO_2}{\text{MW } SiO_2}}{\dfrac{1/2 \text{ PPM } Na^+}{\text{MW Na}} + \dfrac{\text{PPM } Ca^{+2}}{\text{MW Ca}}} \cdot \frac{1-P_{SiO_2}}{P_{SiO_2}}$$

where P_{SiO_2} = mole fraction of SiO_2 in glass and all other symbols are as presented in equation (2). All alpha values presented in this text were calculated from equation (3).

The presence of small amounts of phosphorus, boron, and fluorine in the bioglasses may introduce slight inaccuracies into the absolute magnitudes of the individual alpha values. However, the significant information obtained from the α data is the extent of selective leaching from the silicate network with time and its effect on the resulting corrosion layers which are produced. In this respect, the equation employed for the alpha calculations (3) becomes a sensitive indicator of the influence of the phosphorus, boron, and fluorine additions on the corrosion behavior of the silicate network.

The equation utilized for the calculation of the excess silica (ε) was introduced by Sanders and Hench [12] and is presented in equation (4).

$$(4) \quad \varepsilon = \text{PPM } SiO_2 \left(\frac{1-\alpha}{\alpha}\right)$$

Results

The time dependent behavior of ion release into solution is presented in Figures 2-5 for the four glasses with increasing phosphorus content. The glasses containing 0, 3 and 6 wt.% P_2O_5 exhibit an orderly decrease in the amount of Na, Ca and SiO_2 in solution, whereas the glass containing 12% P_2O_5 reverses the trend with an increase in SiO_2 and Ca released compared with the 6% P_2O_5 glass.

Figure 5 shows the phosphorus solution data for the three glasses with increasing phosphorus content. The behavior of all three compositions is similar in that a linear increase is followed by a drop in the phosphorus level. The glass containing 3% P_2O_5 exhibits an increase in phosphorus released for 100 hours, whereas the glasses containing 6 and 12% P_2O_5 show a drop after 10 hours.

The theoretical parameters α and ε are calculated from the solution data. Figure 6 is a plot of α, the extent of selective leaching, versus time for the four glasses. The glass containing 0% P_2O_5 exhibits a behavior which suggests that selective leaching predominates throughout the entire process. Although the curve initially increases, indicating a tendency towards complete dissolution [12], the maximum α value attained is only 0.37 and this is followed by a leveling off to an α value of 0.28. As the phosphorus content of the glass is increased, the maximum α value achieved increases, with the glass containing 12% P_2O_5 having an α value of 0.6 at 100 hours.

In evaluating the influence of P_2O_5 content on the overall corrosion process, Figure 6 can be divided into three time regimes. During the initial 20 hours of exposure the glasses containing 0, 3 and 6 wt.% P_2O_5 show a fairly consistent

Figure 2. Time dependent release of Na^{+1} ions from bulk bioglass surfaces into aqueous solution at 37°C.

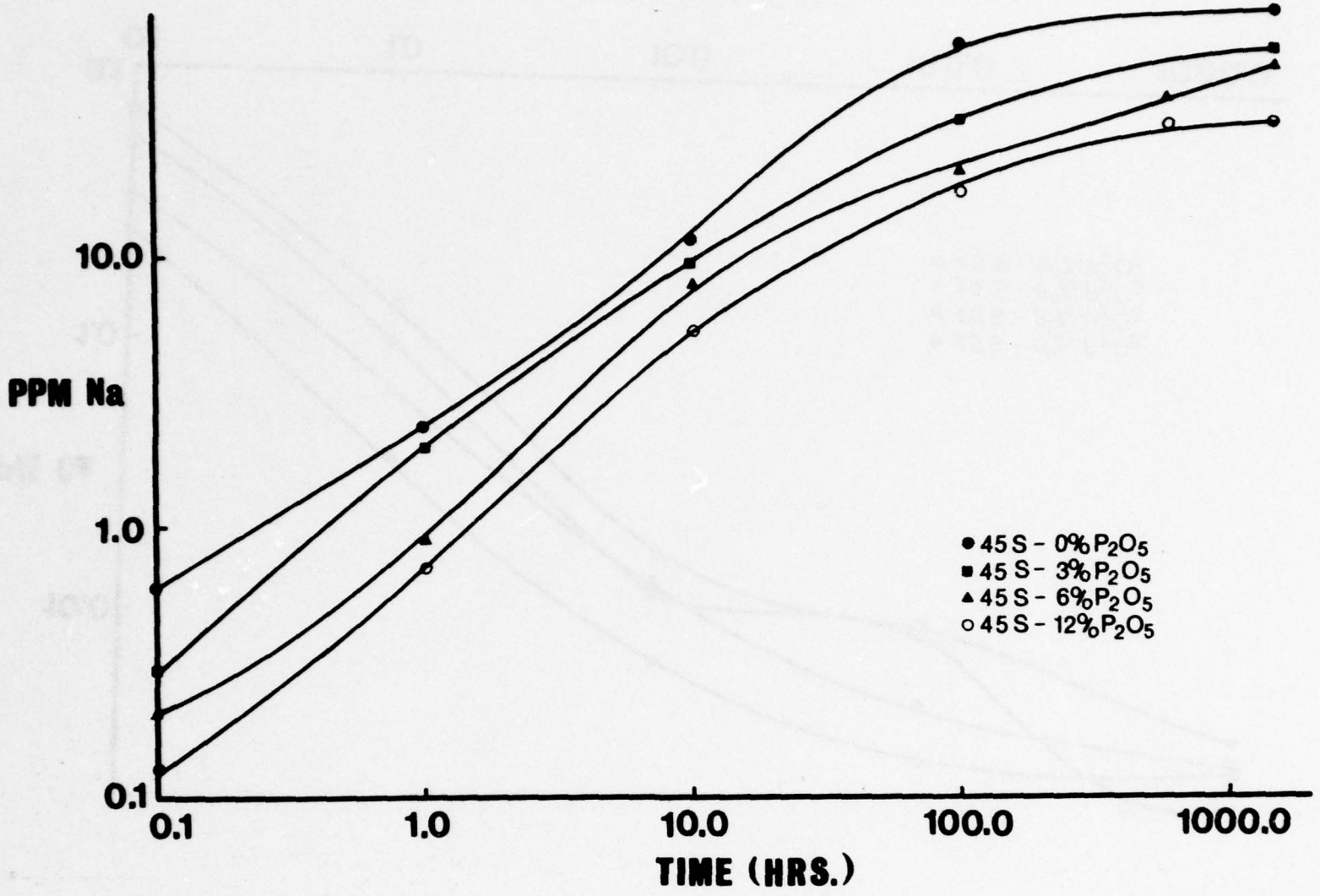

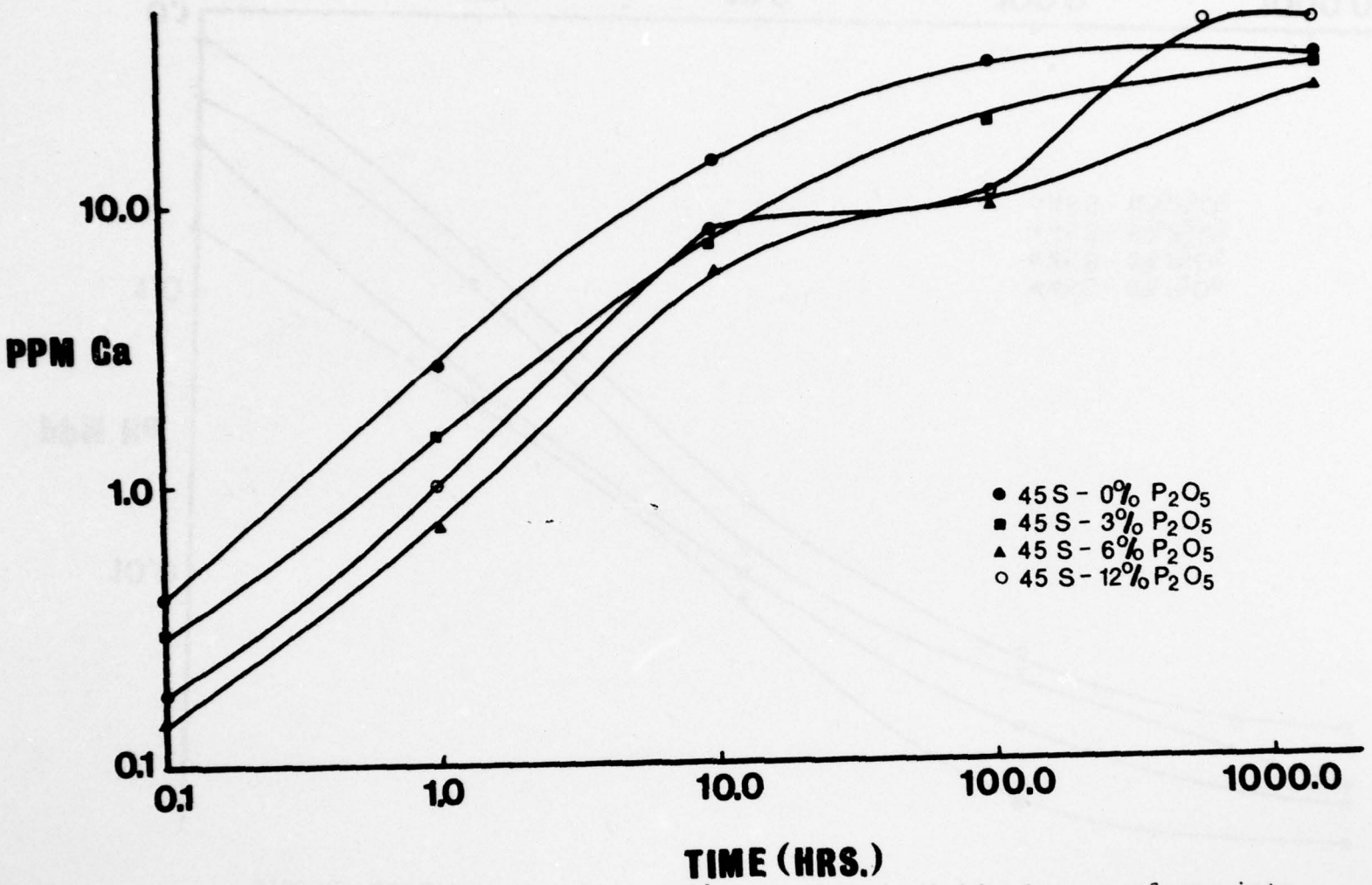

Figure 3. Time dependent release of Ca^{+2} ions from bulk bioglass surfaces into aqueous solution at 37°C.

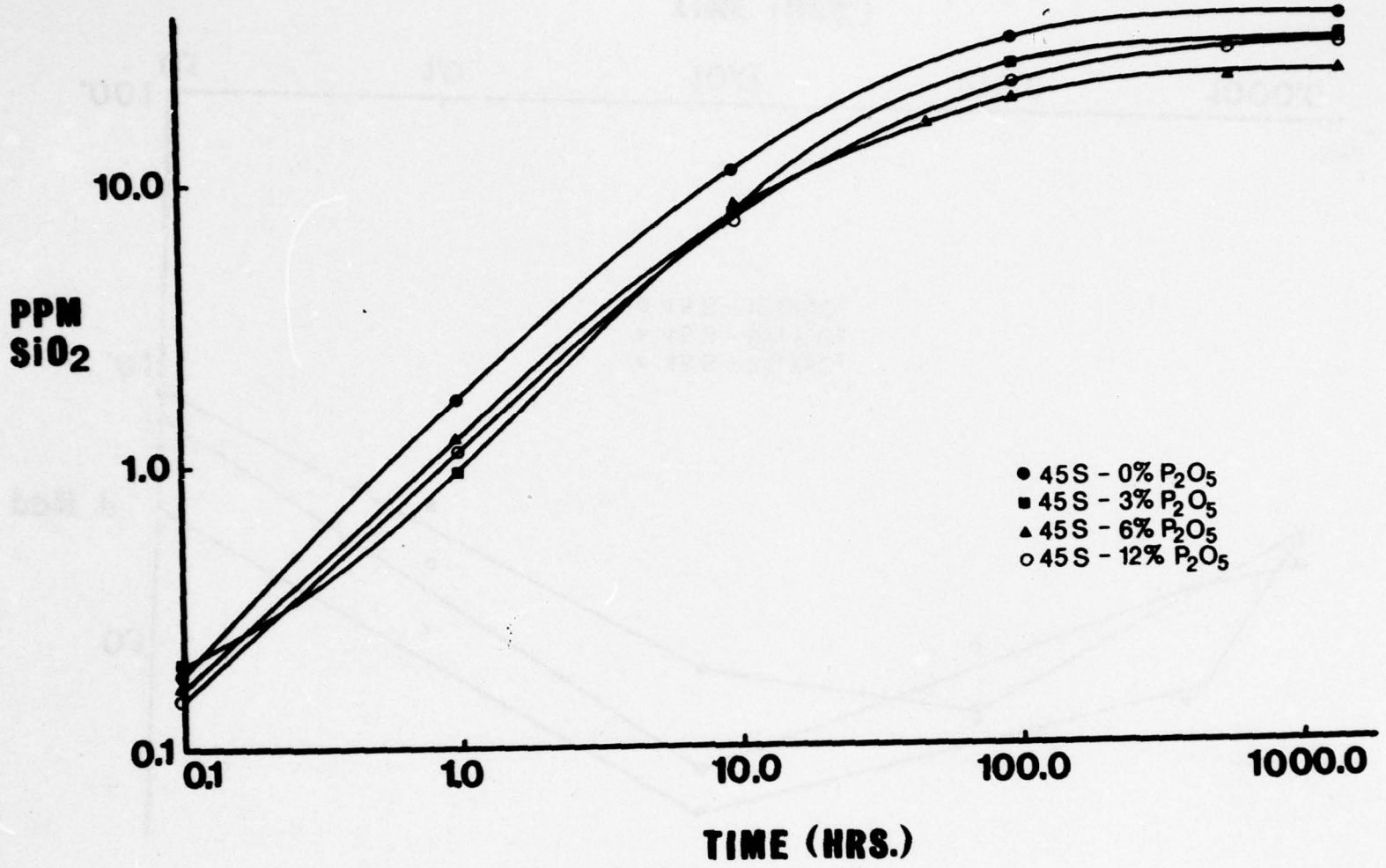

Figure 4. Time dependent release of SiO_2 from bulk bioglass surfaces into aqueous solution at 37°C.

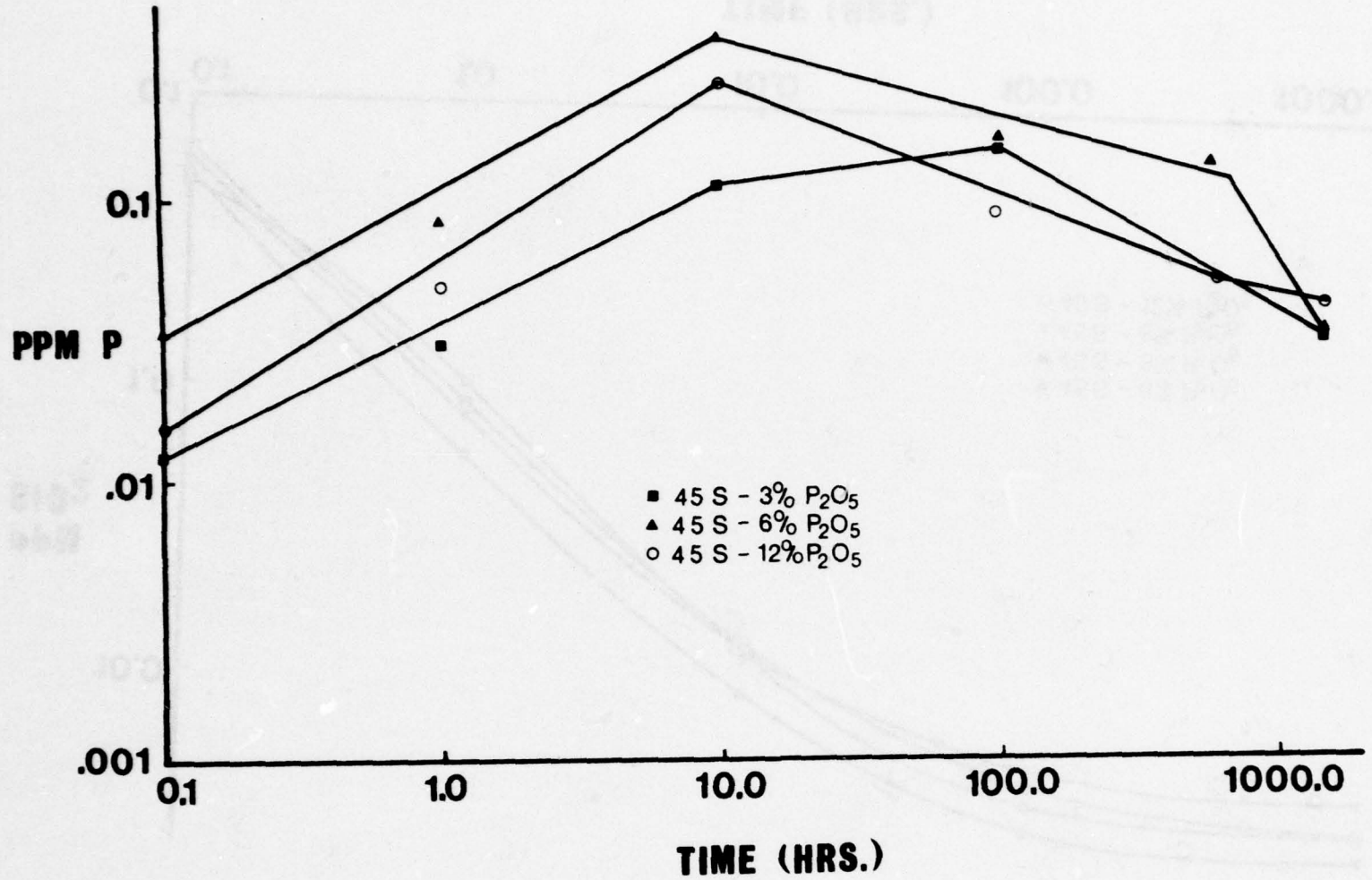

Figure 5. Time dependent release of P^{+5} ions from bulk bioglass surfaces into aqueous solution at 37°C.

Figure 6. Effect of P_2O_5 content of bioglasses on the variation of alpha (α) with corrosion time.

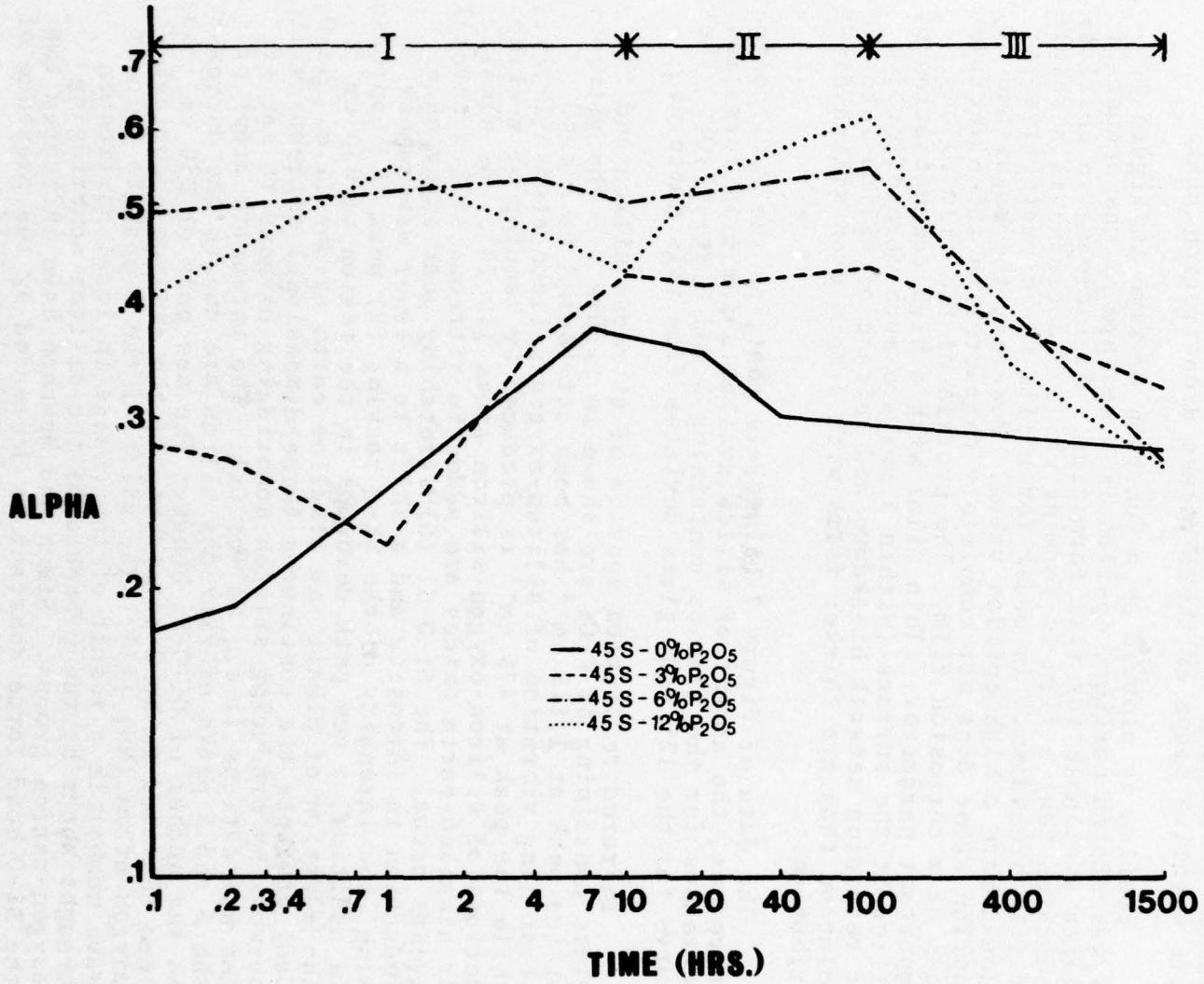

increase in their respective α values. The curve obtained for the glass containing 12% P_2O_5 fluctuates above and below the curve of the 6% P_2O_5 glass. In region II a uniform trend is observed, i.e., as the P_2O_5 content increases the α values increase. At 100 hours this behavior reverses with the glasses containing a larger percentage of P_2O_5 exhibiting a more negative slope as the α values drop (region III).

Epsilon is plotted as a function of time in Figure 7. As was stated earlier, epsilon is a measure of the amount of silica available for film formation. An increase in epsilon indicates that a film is forming while a decrease is a result of film breakdown. In order for a film to be protective it should have a high epsilon value. However, the magnitude of epsilon alone does not completely characterize the effectiveness of a corrosion film. The profile of the film is an important parameter. Thin films with a high concentration of silica at the surface (within 5 μm) are much more effective at retarding network breakdown and release of silica into solution than are thicker films with a more even silica distribution.

The data of Figure 7 illustrate that, as the P_2O_5 content increases, the amount of silica available for film formation decreases for the glasses containing 3 and 6 wt.% P_2O_5. The curve for the 12% P_2O_5 glass deviates from this pattern.

Infrared reflection spectra of vitreous silica and the glass containing 6% P_2O_5 are shown in Figure 8. The vitreous silica peak at 1,115 cm^{-1} has been attributed to a bond stretching vibration of silicon-oxygen-silicon atoms [19,20], while the peak at 475 cm^{-1} is produced by bending or rocking motions of silicon-oxygen-silicon atoms [19,20]. As alkali or alkaline-earth oxides are added to vitreous silica several events occur. The Si-O-Si (S) stretching peak experiences a reduction in intensity and a shift to a lower wavenumber. Also, the intensity of the Si-O rocking (R) peak is suppressed. In addition, a new peak develops in the region of 950 cm^{-1}. The addition of alkali and alkaline earth oxides (i.e., Na_2O, CaO) disrupts the continuous three-dimensional vitreous silica network by producing silicon-nonbridging oxygens to satisfy the new cations (i.e., Na^+ or Ca). The intensity drops of the S and R peaks of vitreous silica are due to the decrease in the number of Si-O-Si bonds. The new peak at 950 cm^{-1} has been ascribed to bond stretching of the silicon-nonbridging oxygen atoms (NS) [11]. The shift of the S peak to a lower wave number is a result of the change in local environment brought about by the presence of the silicon-nonbridging oxygen-cation groups. Simon and McMahon have indicated that the Si-O bond force constant is decreased by the presence of the cationic field of the network modifiers [21].

Figure 7. Effect of P_2O_5 content of bioglasses on the variation of epsilon (ε) with corrosion time.

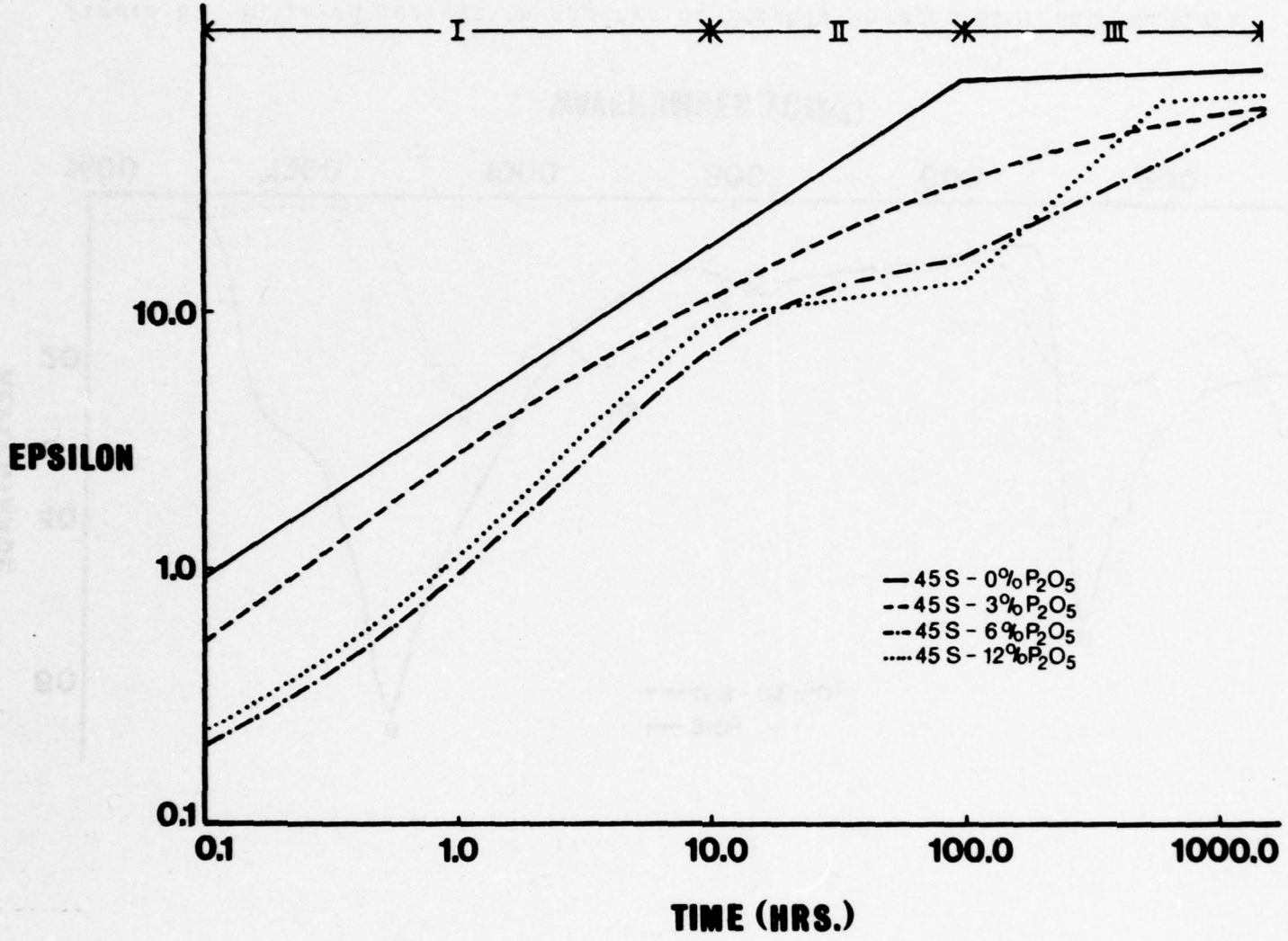

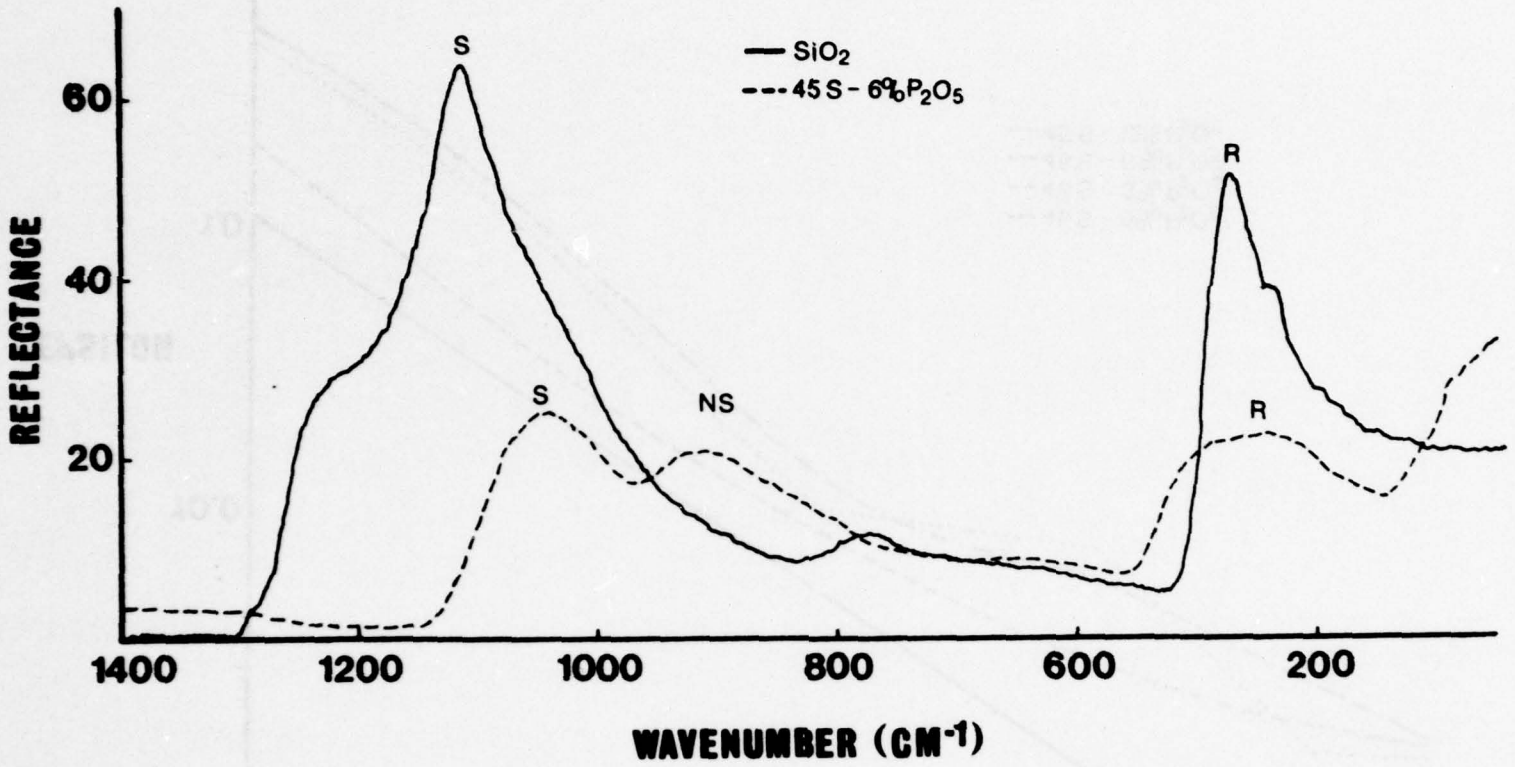

Figure 8. Infrared reflection spectra of freshly abraded SiO_2 and bioglass composition 45S-6% P_2O_5.

Infrared reflection spectra of corroded and uncorroded surfaces from the series of glasses containing P_2O_5 are presented in Figure 9. Comparison of the uncorroded spectra with the short and long corrosion times reveals several interesting facts. The silicon-oxygen-silicon stretching peak (S) at 1,000 cm^{-1} begins to sharpen and shift towards the location of the Si-O-Si stretching peak for pure vitreous SiO_2 (1,115 cm^{-1}) after 15 minutes for the glass containing 0% P_2O_5. Simultaneously there is a considerable drop in the intensity of the silicon-nonbridging oxygen peak (NSX) at 950 cm^{-1}. The silicon-oxygen rocking peak (R) located at 500 cm^{-1} also increases in intensity and sharpness after 15 minutes' corrosion. In addition, there is a shift in location towards the Si-O-Si rocking vibration frequency of pure silica (475 cm^{-1}). These trends continue for a corrosion exposure of 120 minutes with one exception. The intensity of the rocking peak at 475 cm^{-1} is somewhat lower than it was at 15 minutes.

For glasses with higher phosphorus contents, the 15-minute spectra show an increasing preferential attack of the silicon-oxygen-silicon stretching peak (S), and a decreasing preferential attack of the silicon-nonbridging oxygen peak (NSX). The increase in intensity, and location of the shift of the silicon-oxygen rocking peak (R) are also retarded for the higher phosphorus glasses.

At corrosion times varying from 75 to 120 minutes, there is a complete reversal in behavior. For each of the three glasses containing P_2O_5 there is an increase in the intensity of the S peak while the intensity of the NSX peak is significantly reduced. The longer corrosion times for each composition represent the maximum exposure before the glass surface has roughened to the point where the intensity of the spectra is reduced to the extent that reliable data cannot be obtained. The time required before surface roughening dominates is shortened as the P_2O_5 content of the glass increases. Eventually the spectra of the glasses containing P_2O_5 become flat curves with a very low intensity.

However, with sufficient corrosion time a new infrared spectrum develops which is different from that of the glass. Figure 10 contains a series of IR spectra which illustrate the sequence of reactions for the glass containing 6% P_2O_5. This new spectrum (see Figure 10d and e) develops for all three glasses containing P_2O_5, the only variable being the length of corrosion treatment required to produce it. The new spectrum begins to appear in as short a time as 4 hours for the glasses containing 12% P_2O_5, and takes 12 hours to develop for the glass containing 3% P_2O_5.

X-ray spectra taken from the glass containing 6% P_2O_5 with the energy dispersive system of the SEM are shown in

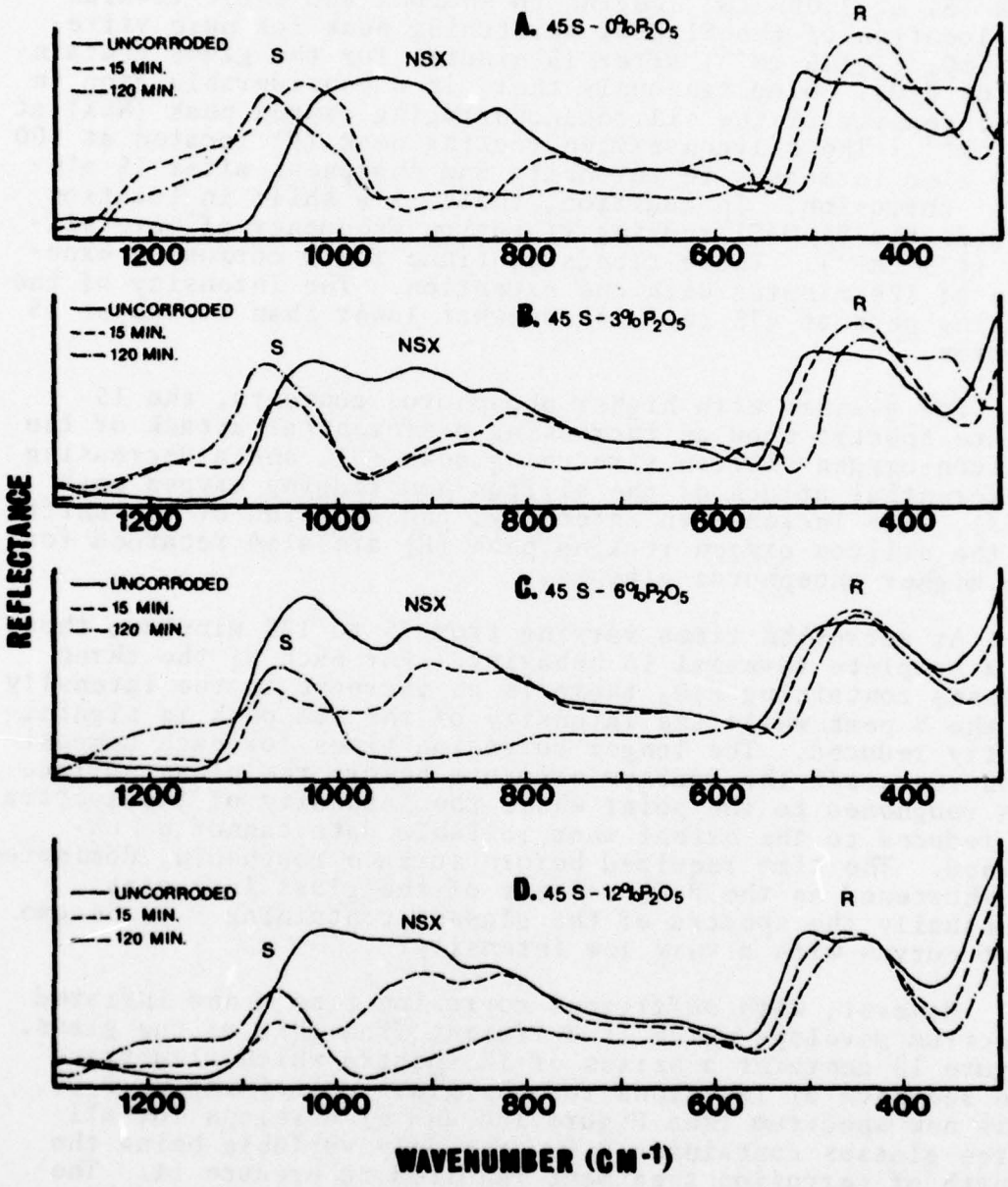

Figure 9. Changes in infrared reflection spectra of four bioglasses with increasing phosphorus content as a function of corrosion time. Solutions were buffered at a pH of 7.4 and maintained at 37°C.

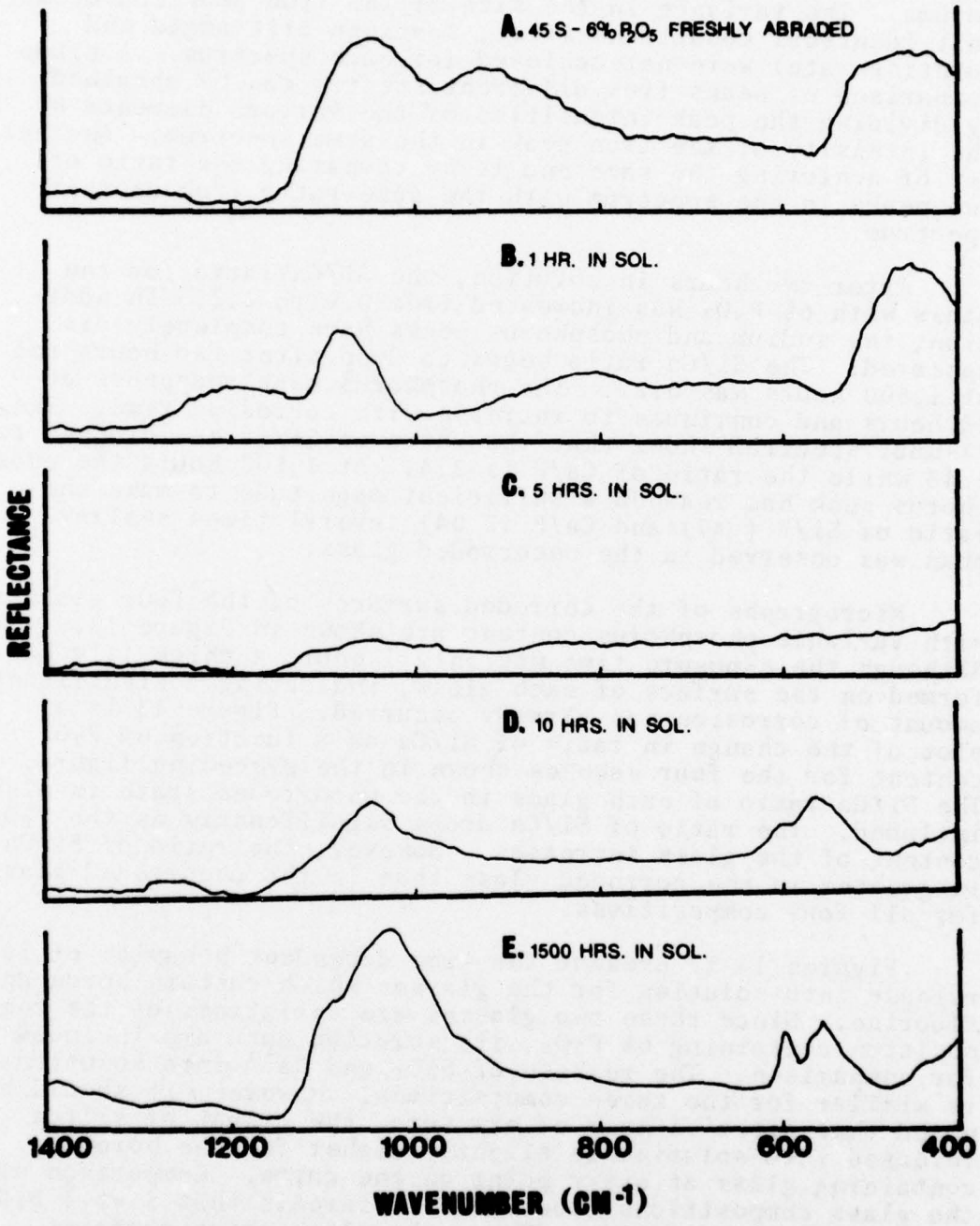

Figure 10. Changes in infrared reflection spectrum of bioglass composition 45S-6% P_2O_5 as a function of corrosion time.

Figure 11. The iron peak seen in each of the spectra is produced by x-rays originating from a pole piece in the SEM column. The variance in the size of the iron peak indicates that identical conditions (i.e., specimen tilt angle and counting rate) were not achieved for each spectrum. A crude comparison of peaks from different spectra can be obtained by dividing the peak intensities of the various elements by the intensity of the iron peak in the same spectrum. Another way of achieving the same end is by comparing the ratio of two peaks in one spectrum with the same ratio from another spectrum.

After two hours in solution, the Si/Ca ratio for the glass with 6% P_2O_5 has increased from 0.9 to 2.2. In addition, the sodium and phosphorus peaks have completely disappeared. The Si/Ca ratio began to drop after two hours and at 1,500 hours was 0.23. The phosphorus peak reappears at 20 hours and continues to increase with corrosion time. The 24-hour spectrum shows that the ratio of Si/Ca has dropped to 1.43 while the ratio of Ca/P is 2.4. At 1,500 hours the phosphorus peak has reached a sufficient magnitude to make the ratio of Si/P (.47) and Ca/P (2.04) several times smaller than was observed in the uncorroded glass.

Micrographs of the corroded surfaces of the four glasses with variable phosphorus content are shown in Figure 12. Although the exposure time was only 1 hour, a thick film has formed on the surface of each glass, indicating a significant amount of corrosion has already occurred. Figure 13 is a plot of the change in ratio of Si/Ca as a function of P_2O_5 content for the four samples shown in the preceding figure. The Si/Ca ratio of each glass in the uncorroded state is also included. The ratio of Si/Ca drops significantly as the P_2O_5 content of the glass increases. However, the ratio of Si/Ca is greater in the corroded glass than in the uncorroded glass for all four compositions.

Figures 14-17 present the time dependent behavior of ion release into solution for the glasses which contain boron and fluorine. Since these two glasses are variations of the composition containing 6% P_2O_5, its solution data are included for comparison. The release of SiO_2 and Na^{+1} into solution is similar for the three compositions. However, it should be noted that after .1 hour of exposure, the amount of silica released into solution is slightly higher for the boron-containing glass at every point on the curve. Comparison of the glass compositions (see Table 1) reveals that 5 wt.% B_2O_3 was substituted for SiO_2. Thus, the glass which contains boron has the least amount of silica in its bulk composition.

There is a significant difference in the behavior of calcium released into solution (Figure 16). At 10 hours there has been more Ca^{+2} released from the glasses containing

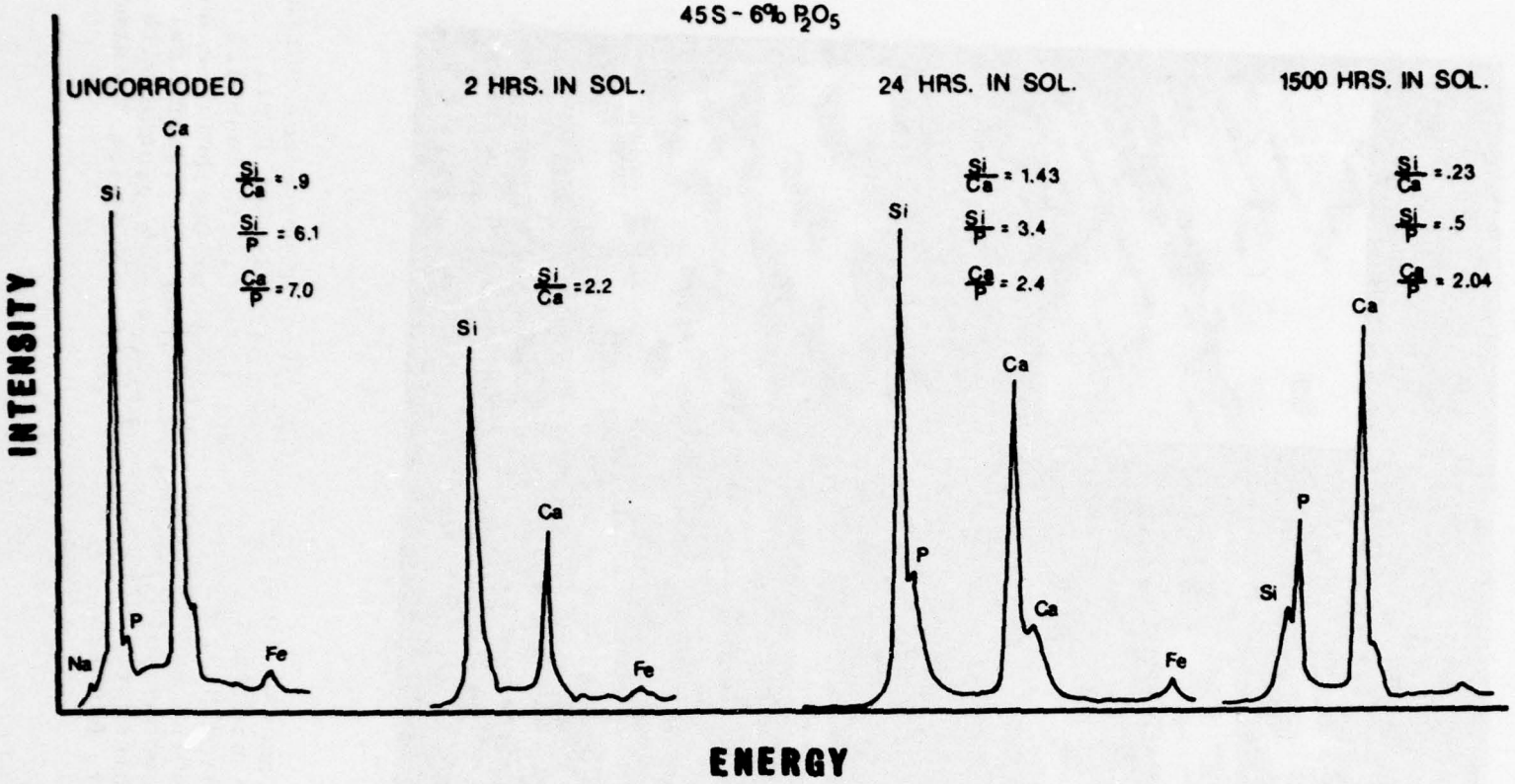

Figure 11. Compositional surface changes of a 45S-6% P_2O_5 bioglass exposed to a buffered aqueous solution (pH = 7.4). Spectra were obtained with an Ortec Energy Dispersive X-ray System on a Cambridge Scanning Electron Microscope.

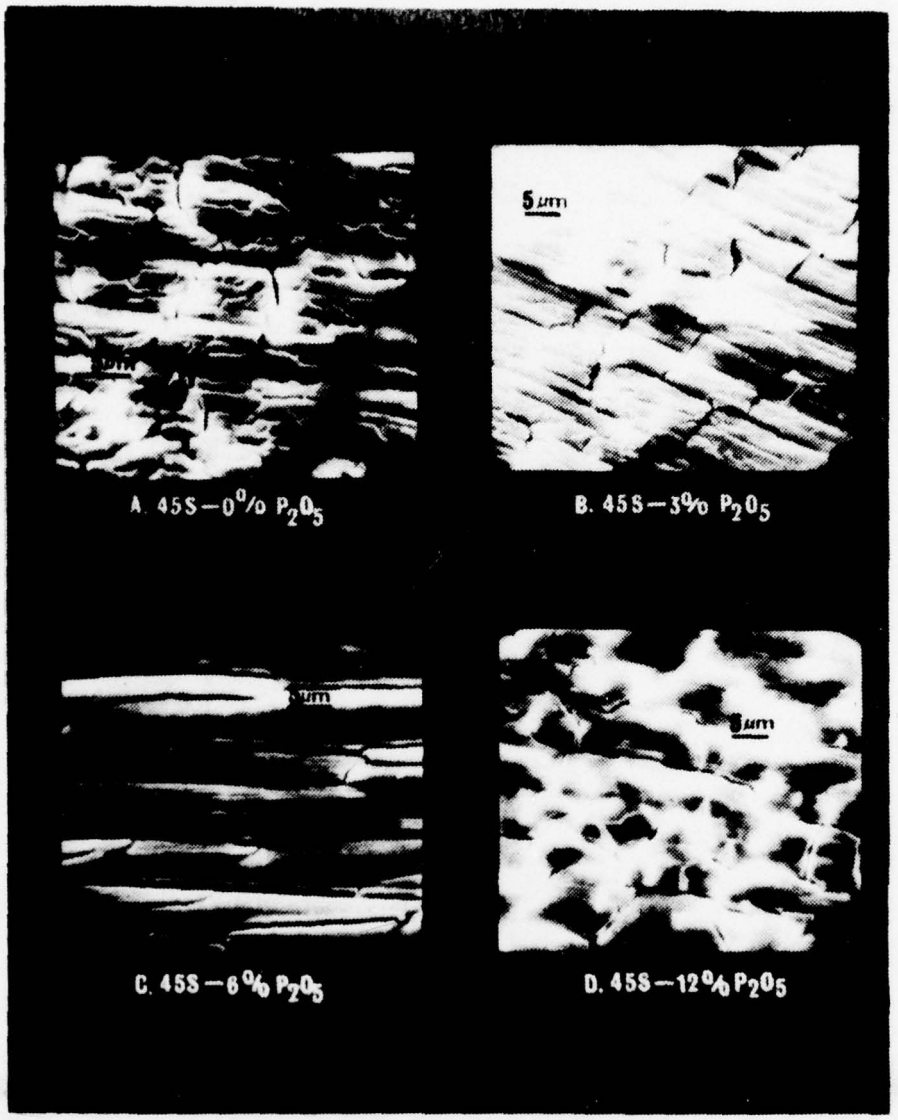

Figure 12. Scanning electron micrographs of corroded surface of bioglass compositions. (A) 45S-0% P_2O_5, (B) 45S-3% P_2O_5, (C) 45S-6% P_2O_5, (D) 45S-12% P_2O_5. Samples were corroded for one hour in an aqueous solution buffered at pH of 7.4 and maintained at 37°C. The surfaces were ground with dry 600 grit SiC prior to the corrosion treatment.

Figure 13. Effect of P_2O_5 content on the ratio of Si/Ca for bioglasses corroded 1 hour in an aqueous solution buffered at pH of 7.4 and maintained at 37°C. Data were obtained with Ortec Energy Dispersive X-ray System on a Cambridge Scanning Electron Microscope.

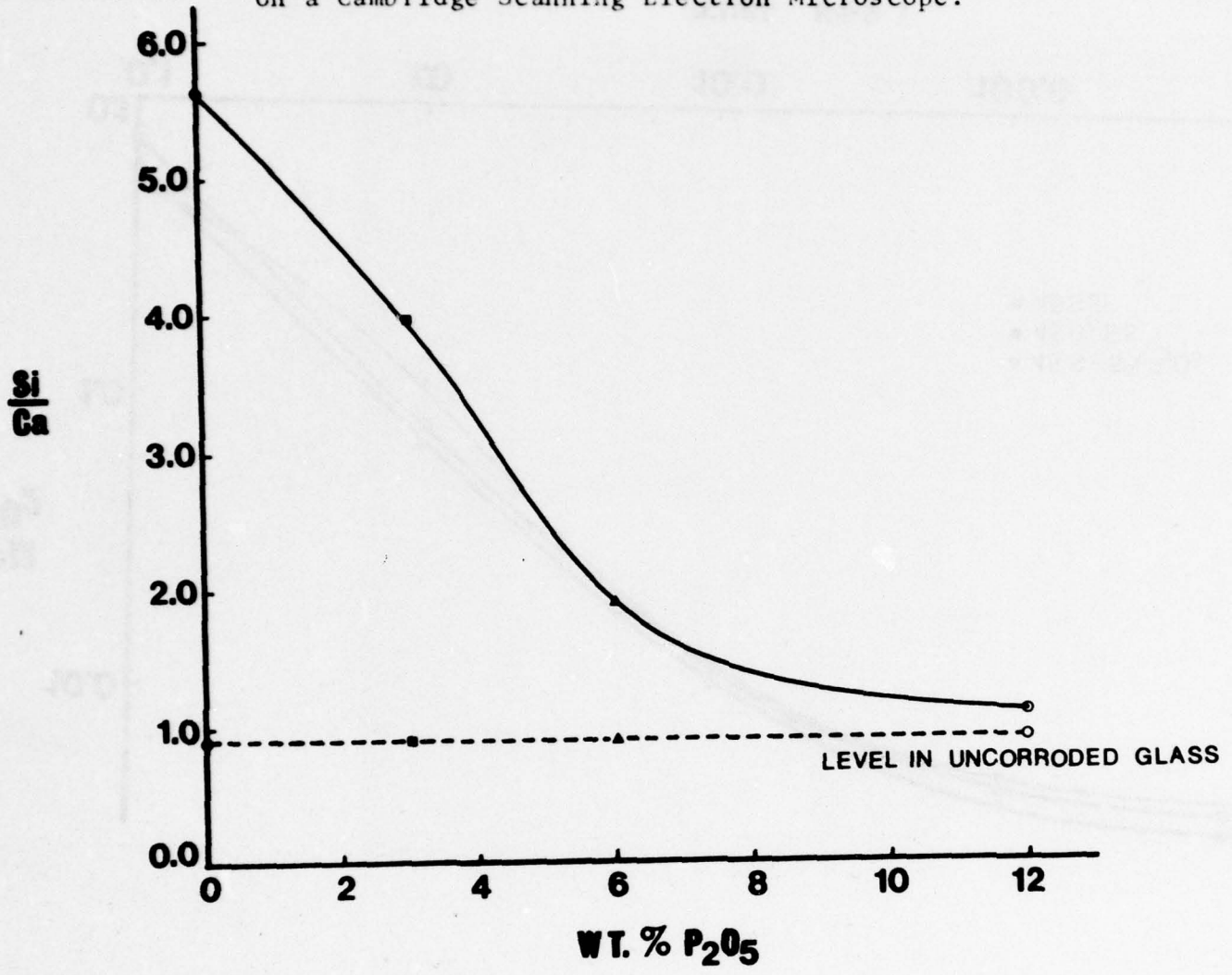

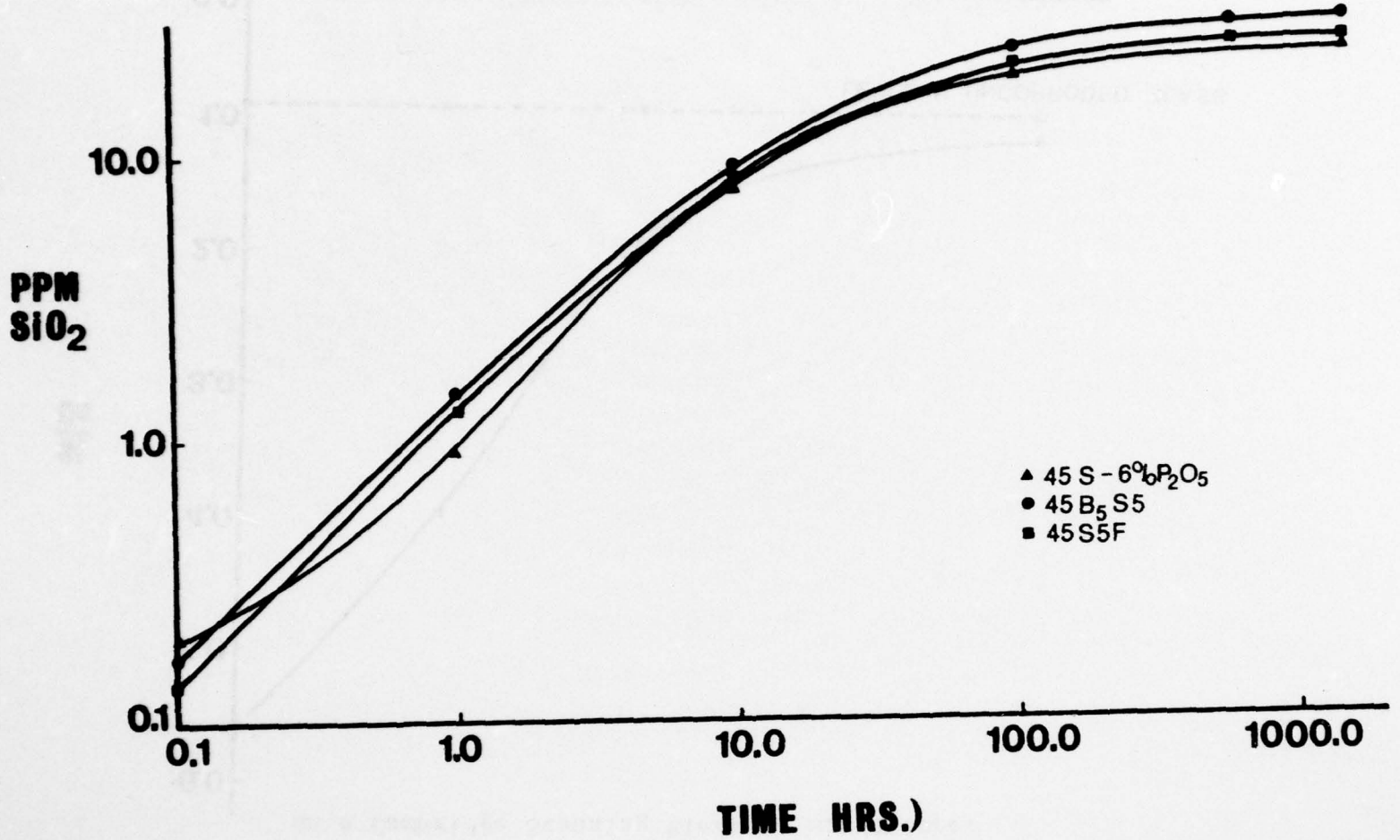

Figure 14. Time dependent release of SiO_2 from bulk bioglass surfaces into aqueous solution at 37°C.

Figure 15. Time dependent release of Na^{+1} ions from bulk bioglass surfaces into aqueous solution at 37°C.

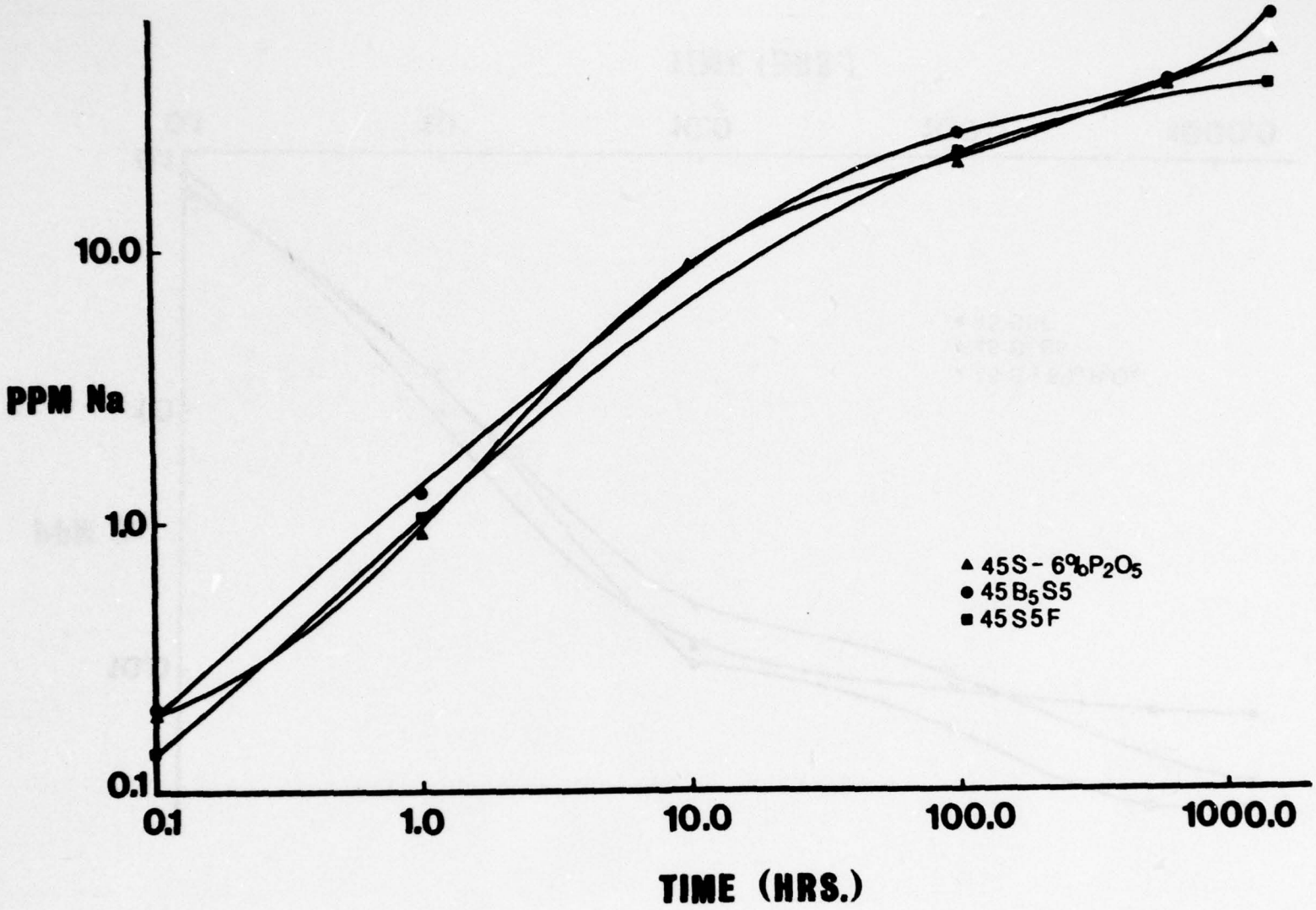

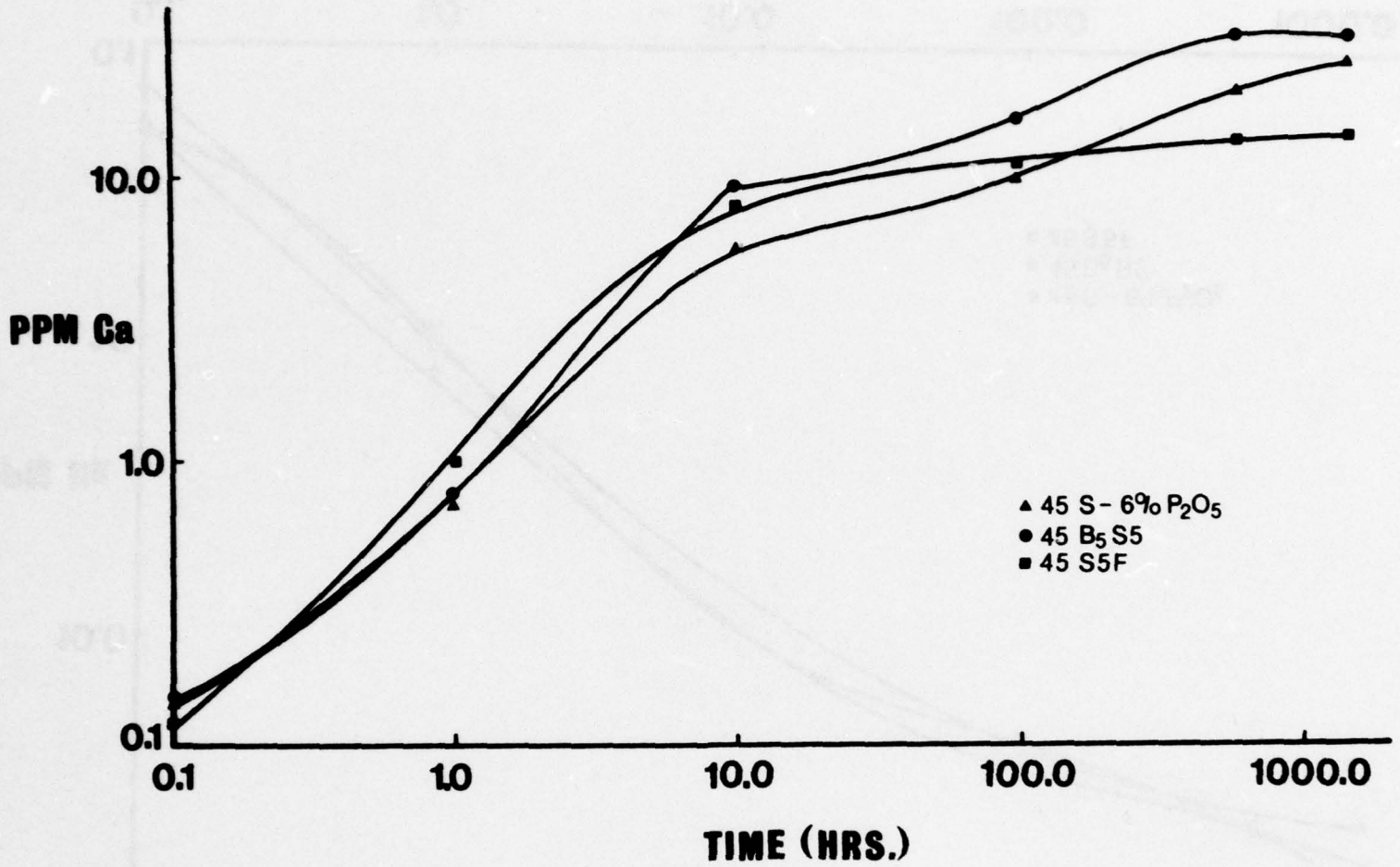

Figure 16. Time dependent release of Ca^{+2} ions from bulk bioglass surfaces into aqueous solution at 37°C.

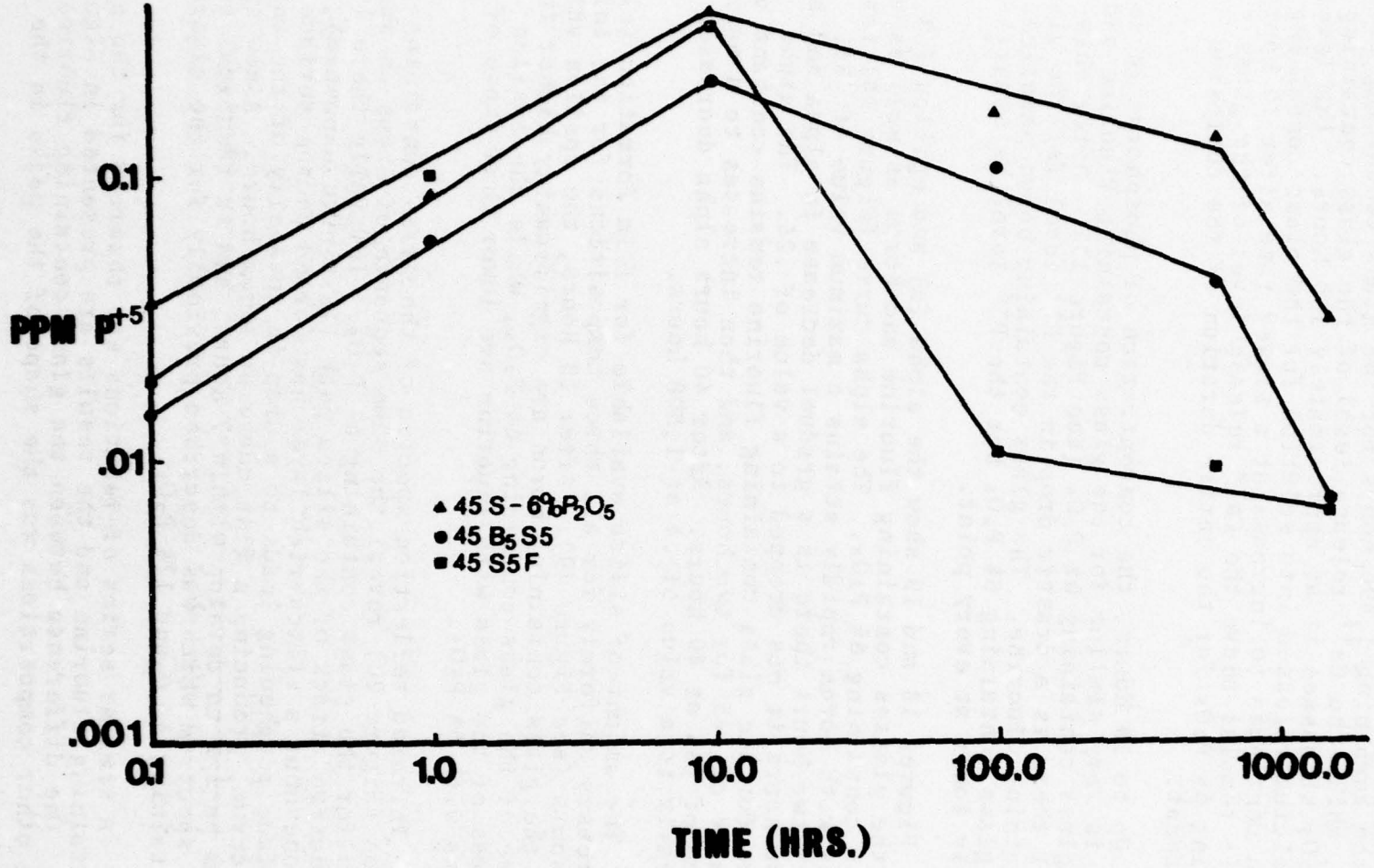

Figure 17. Time dependent release of P^{+5} ions from bulk bioglass surfaces into aqueous solution at 37°C.

boron and fluorine than from the glass containing 6% P_2O_5. The level of calcium released remains fairly constant throughout the remaining 1,490 hours for the glass containing fluorine, while the Ca^{+2} release level of the glass containing 6% P_2O_5 surpasses it at approximately 150 hours. The level of calcium released into solution for the glass containing boron continues to increase at a slower rate after 10 hours, but it remains above the Ca^{+2} release level of the glass containing 6% P_2O_5 for the entire duration of the corrosion treatment.

Up to 10 hours, the concentration of phosphorus in solution is very similar for the glass containing fluorine and the glass containing 6% P_2O_5 (see Figure 17). After this point there is a drastic drop in the P^{+5} level for the glass containing fluorine. The glass containing boron parallels the glass containing 6% P_2O_5 but the P^{+5} level is significantly lower at every point.

Figures 18 and 19 show the alpha (α) and epsilon (ε) data for the glasses containing fluorine and boron as well as the glass containing 6% P_2O_5. The alpha curve (Figure 18) for the glass with boron rapidly attains a maximum value of .58. After two hours there is a gradual decrease in alpha and at 1,500 hours it has dropped to a value of .25. The alpha curve for the glass containing fluorine remains constant at a value of .45 for two hours, and then increases to a maximum value of .56 at 40 hours. After 40 hours alpha decreases linearly to a value of .4 at 1,500 hours.

The amount of silica available for film formation (ε) increases uniformly for all three compositions for the initial 10 hours (see Figure 19). After 10 hours, the epsilon values for the glass containing boron are significantly higher than those of the glass containing 6% P_2O_5, while the epsilon values of the glass with fluorine are lower than those of the glass with 6% P_2O_5.

Infrared reflection spectra of the glass containing boron (Figure 20) reveal the same sequence of steps as was seen for the glass containing 6% P_2O_5. Initially there is selective attack of the silica peak (15-minute exposure), but by one hour a silica-rich layer has formed on the surface. Surface roughening leads to a drop in intensity of the entire spectrum, producing a flat curve at three hours. A new spectrum begins to develop within 7 hours, and is identical to the spectrum which was described previously for the glasses containing 3, 6 and 12% P_2O_5.

A similar series of reactions was observed for the glass containing fluorine and the results are presented in Figure 21. One difference between the glass containing fluorine and all other compositions was the shape of the peaks in the IR

Figure 18. Effect of B^{+3} and F^{-1} additions to the bioglass composition 45S-6% P_2O_5 on the variation of alpha (α) with corrosion time.

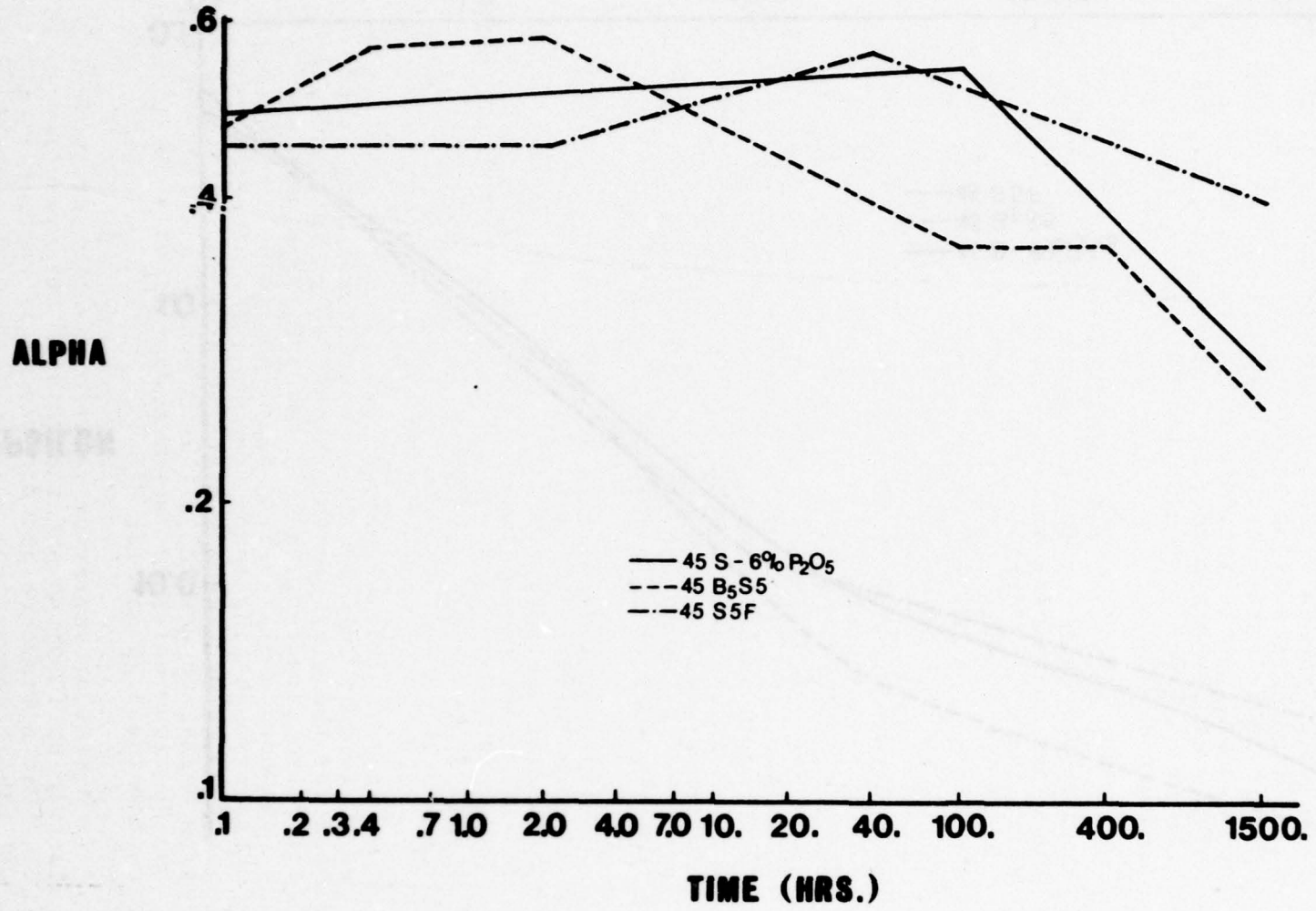

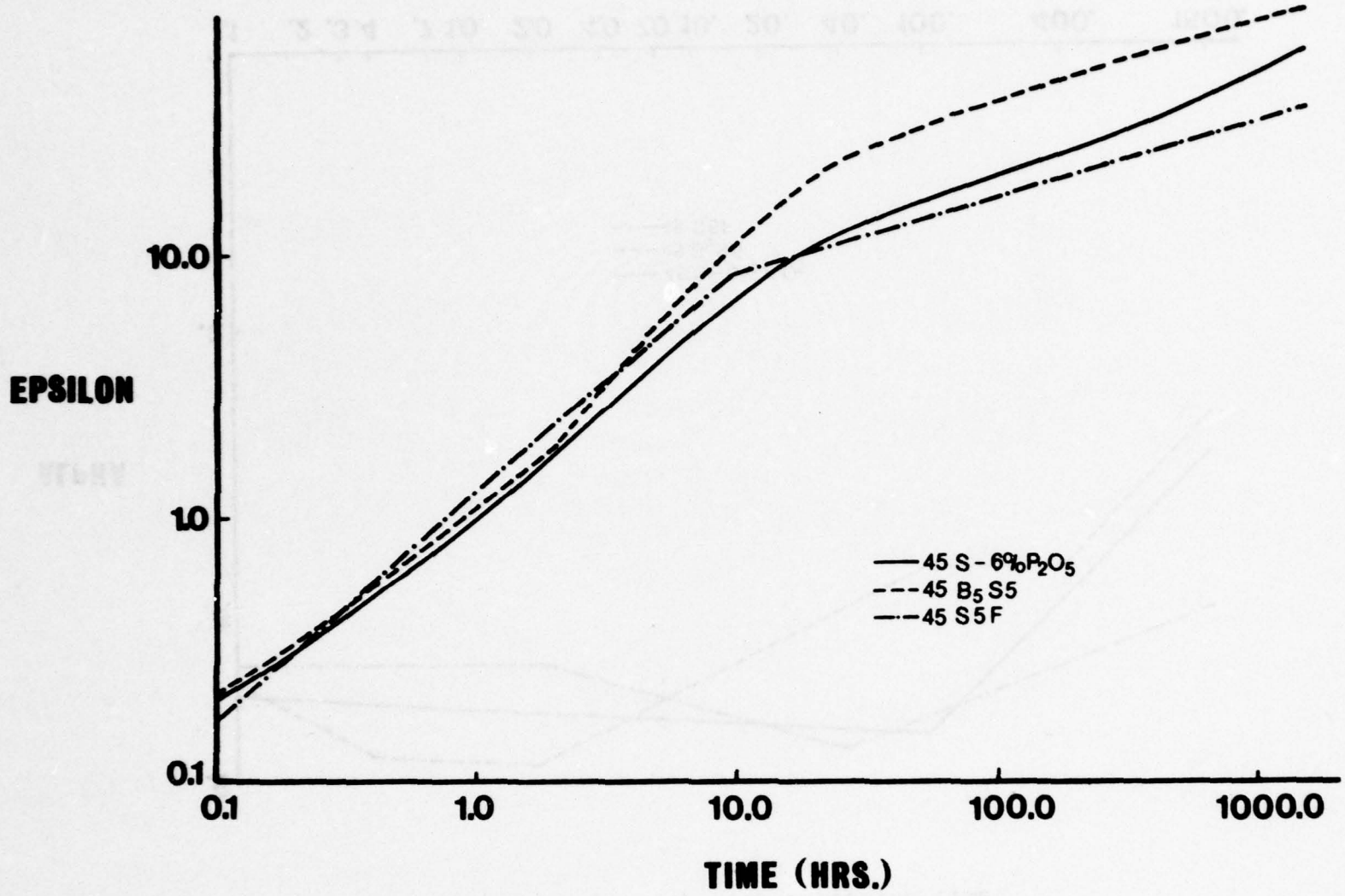

Figure 19. Effect of B^{+3} and F^{-1} additions to the 45S-6% P_2O_5 bioglass on the variation of epsilon (ε) with corrosion time.

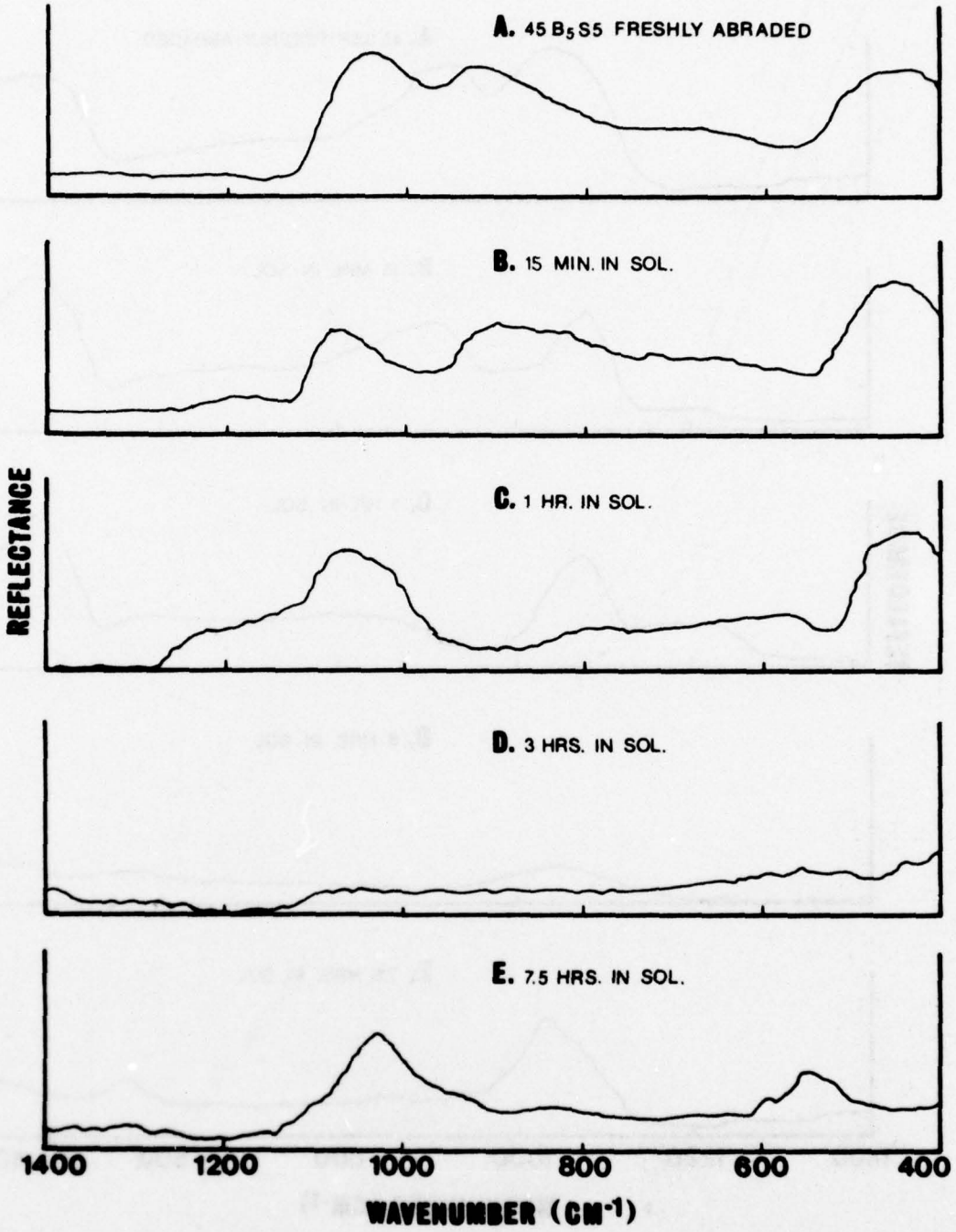

Figure 20. Changes in infrared reflection spectrum of the bioglass 45B_5S5 as a function of corrosion time.

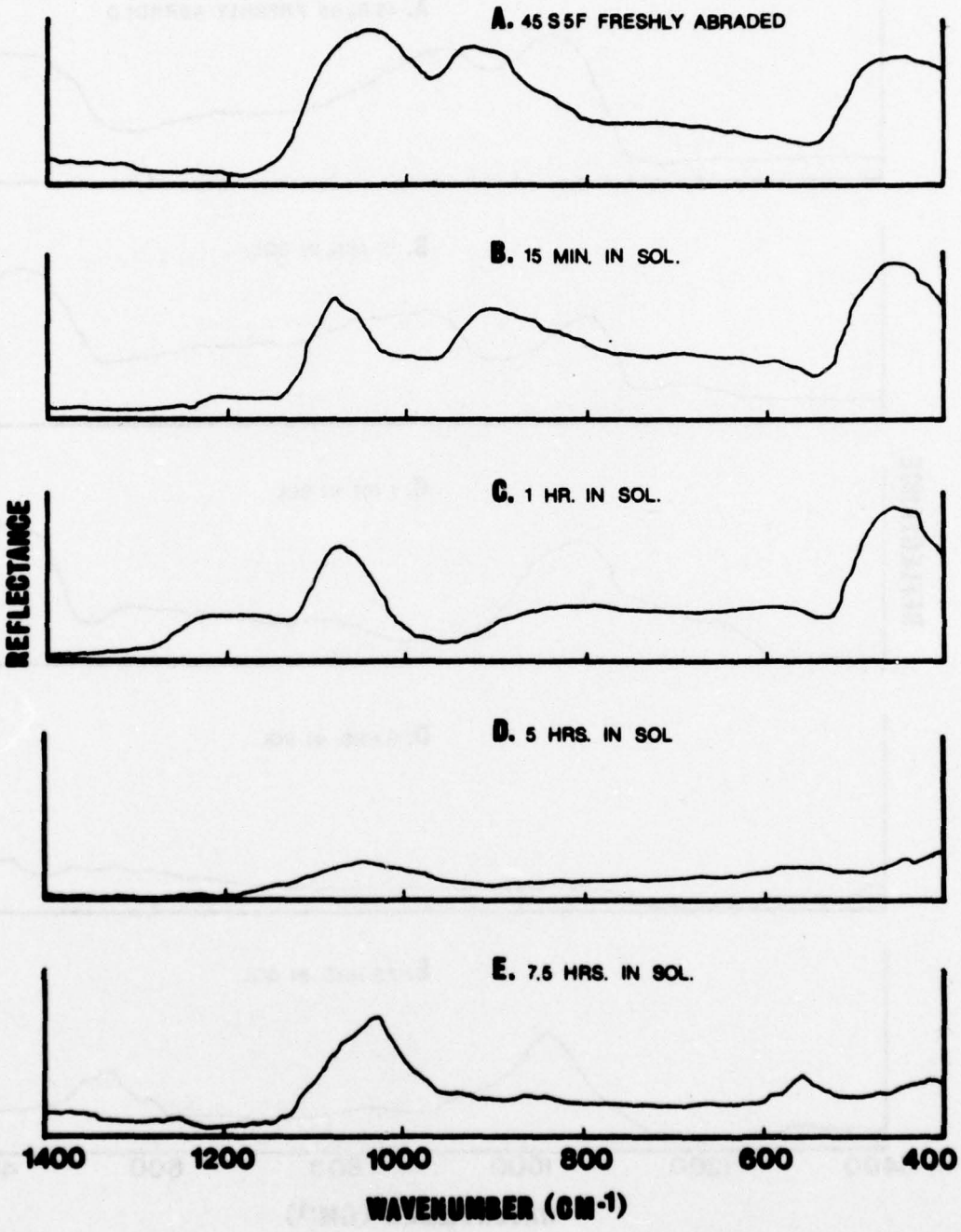

Figure 21. Changes in infrared reflection spectrum of the bioglass 45S5F as a function of corrosion time.

spectrum which developed after the spectrum of the glass disappeared. Figure 22 enables one to compare the IR spectra of the glass containing 6% P_2O_5, the glass containing boron, and the glass containing fluorine, after each had been in solution for 100 hours. There are three peaks in the wavenumber region 500-650 cm^{-1} and the peak at 600 cm^{-1} has the greatest intensity for the glass containing fluorine. The spectra of the other two compositions have only two peaks in this region and the peak at 560 cm^{-1} is dominant. In addition, the main peak at 1,035 cm^{-1} is sharper and more intense for the glass with fluorine than for either of the other two compositions.

Infrared reflection spectra of the glass containing boron (which had been exposed for 1,500 hours) and reagent grade hydroxyapatite are shown in Figure 23. The two spectra are very similar, the main differences being the lack of definition of the shoulder at 1,085 cm^{-1} and the broadness of the peak at 1,035 cm^{-1} for the spectrum of the glass surface.

Figure 24 contains x-ray diffraction curves of the glass containing 6% P_2O_5 which was immersed for 15, 100 and 1,500 hours. This series illustrates the gradual development of an amorphous film into a crystalline product. Figure 25 illustrates the diffraction curve of the glass containing boron which had been in solution for 1,500 hours.

Discussion

The behavior of the glass containing 0% P_2O_5 is easily interpreted since the results all point to the development of a silica-rich film through a corrosion reaction dominated by selective leaching. The evidence in support of this statement is:

(1) The maximum value of α is .37 (see Figure 6) and this occurs at an early stage (10 hours). In order for complete dissolution to occur, α must approach a value of 1 [11].

(2) After reaching its maximum value, α rapidly drops to .3 and remains near this value for over 1,400 hours, indicating no tendency for the film to break down.

(3) Epsilon (Figure 7) increases linearly with time for 100 hours and then levels off. The rapid increase in ε which occurs during the initial 100 hours indicates that a silica-rich film is developing. Any tendency for film breakdown would result in a drop in the ε curve. Clearly, no such tendency is observed throughout the entire 1,500 hours of exposure.

(4) The infrared reflection spectrum in Figure 9a shows immediate selective attack of the silicon-nonbridging oxygen

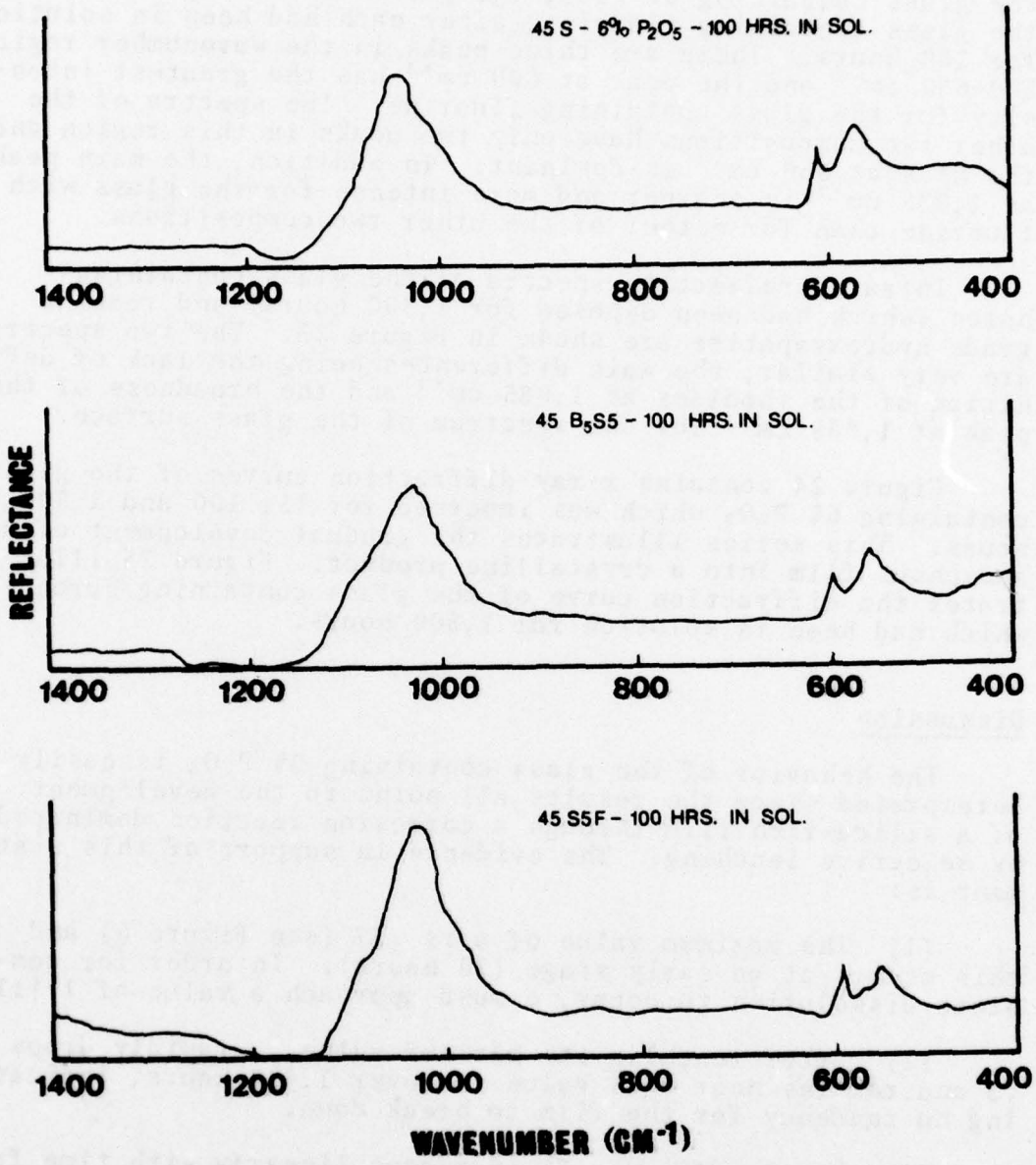

Figure 22. A comparison of the infrared reflection spectra of the bioglasses 45S-6% P_2O_5, 45B_5S5 and 45S5F after a corrosion treatment of 100 hours in an aqueous solution buffered at pH 7.4 and maintained at 37°C.

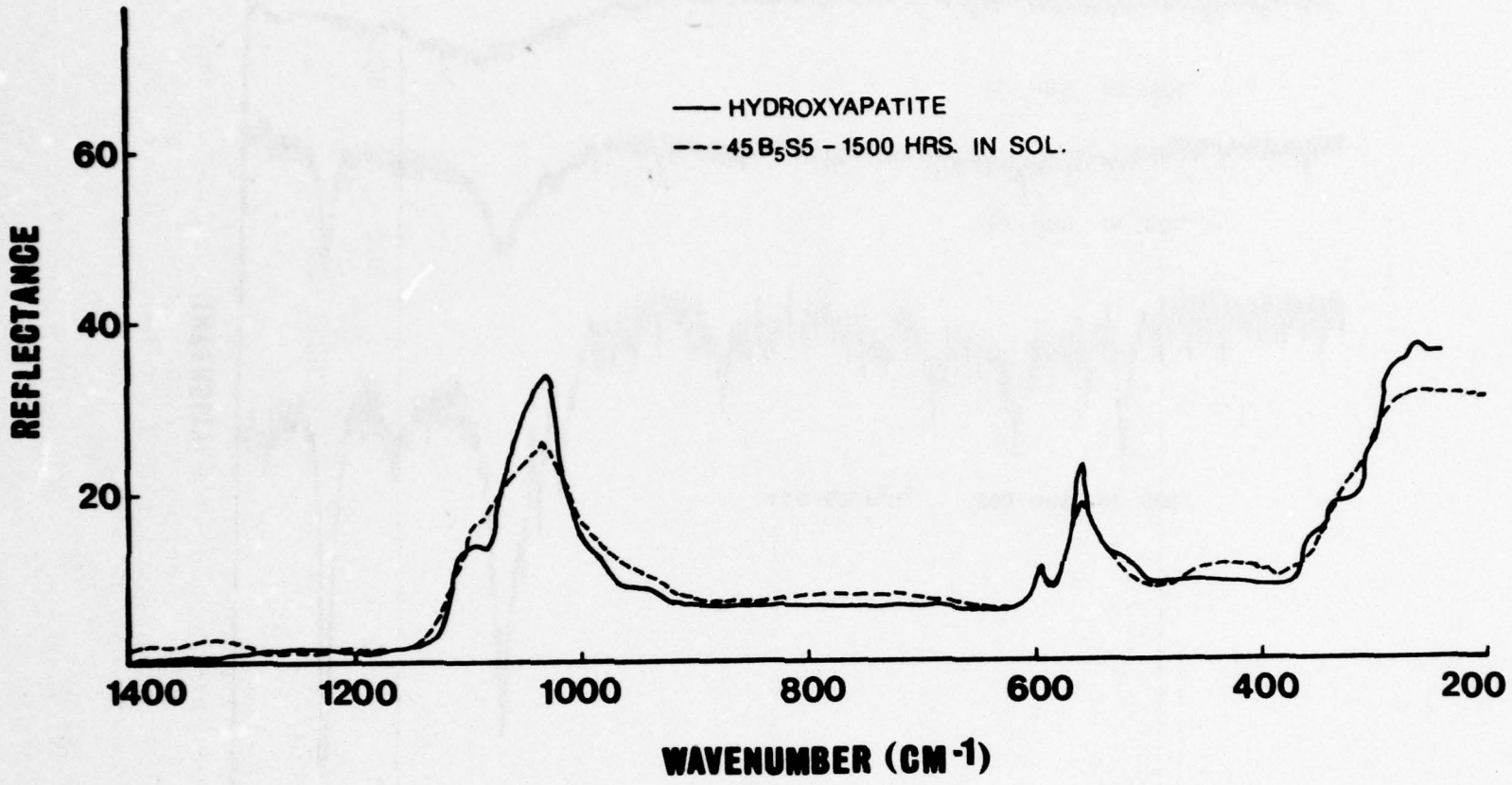

Figure 23. A comparison of the infrared reflection spectra of the bioglass $45B_5S5$ which had been corroded for 1,500 hours in an aqueous solution and reagent grade hydroxyapatite.

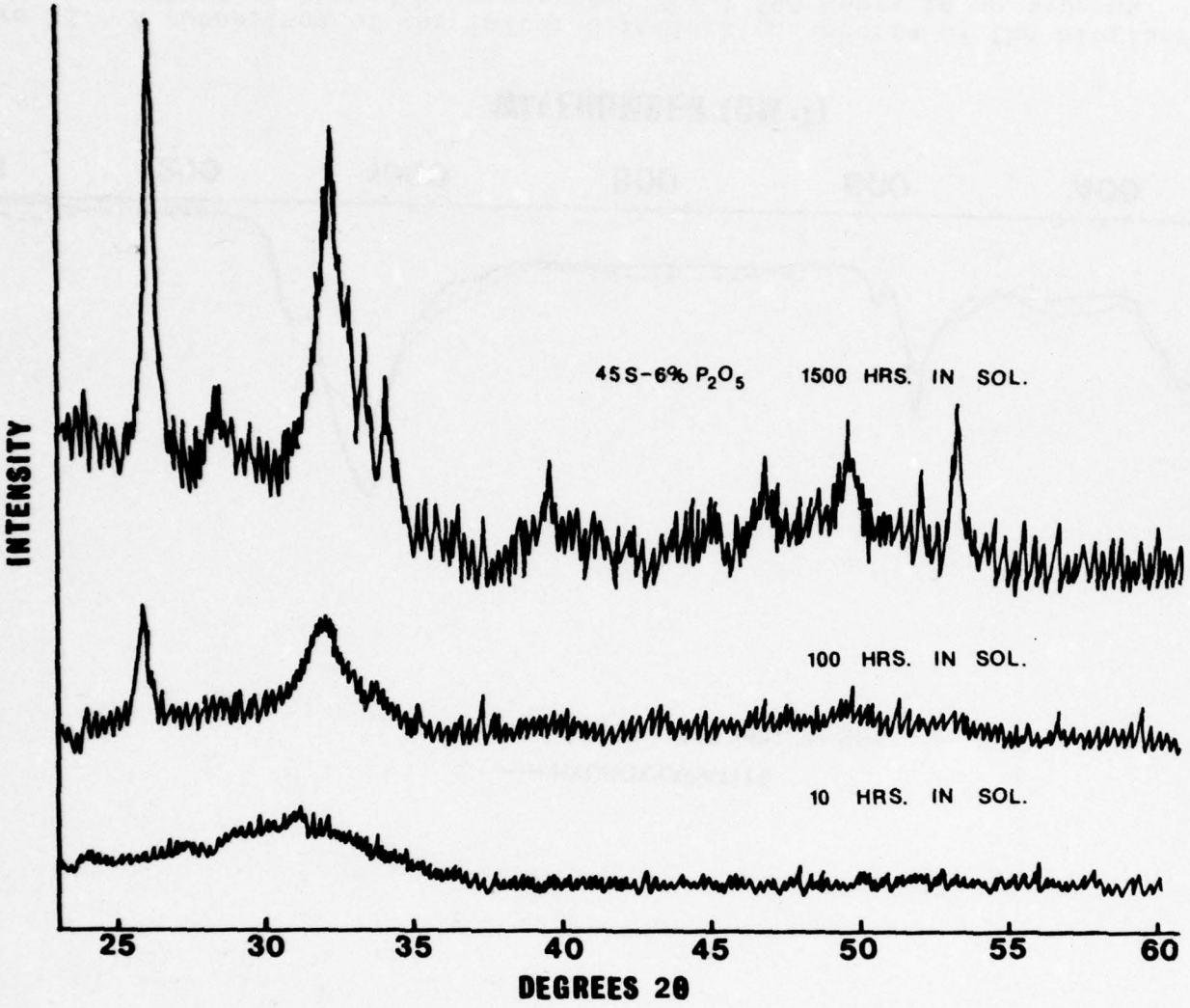

Figure 24. X-ray diffraction analysis of the crystallization of hydroxyapatite on the surface of a 45S-6% P_2O_5 bioglass as a function of corrosion time.

Figure 25. X-ray diffraction spectrum of the crystalline hydroxyapatite film on the surface of a $45B_5S5$ bioglass corroded for 1,500 hours.

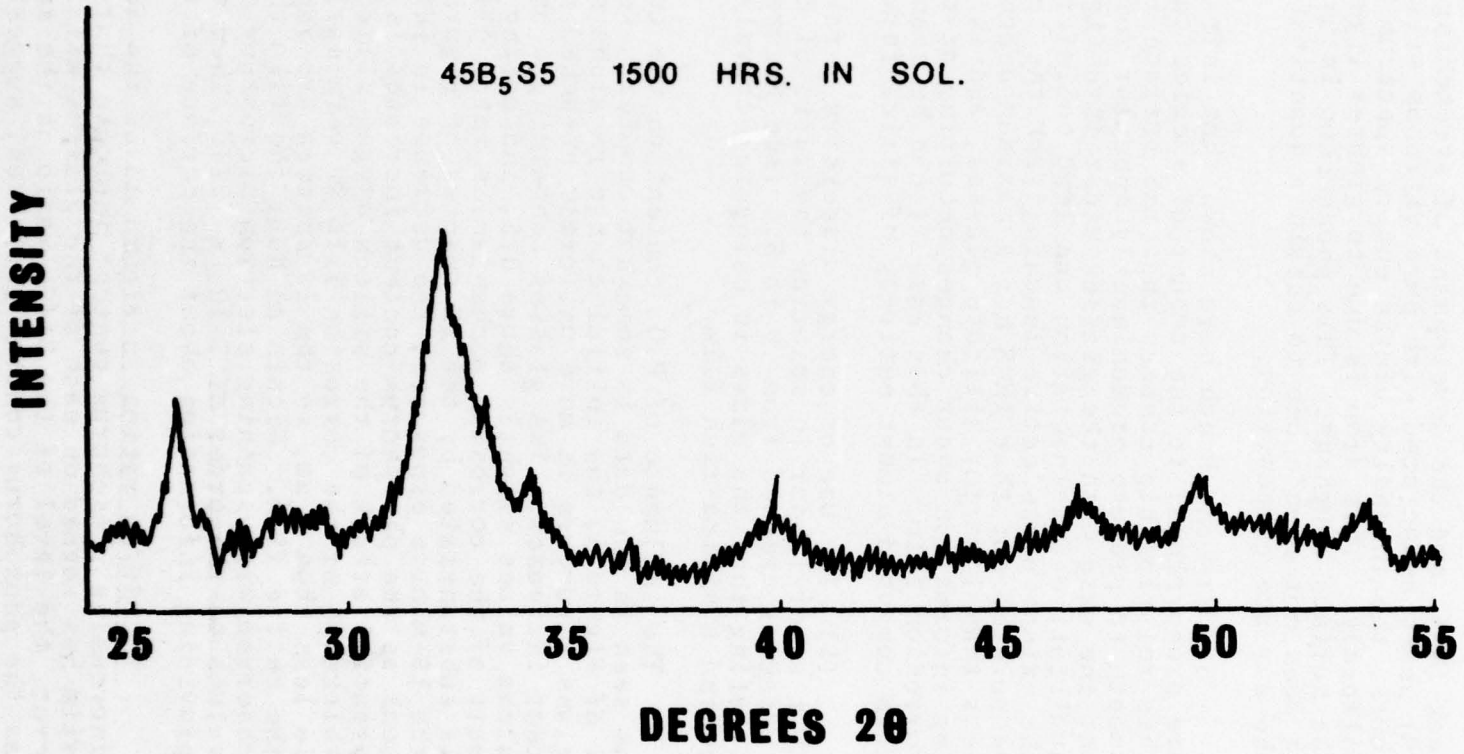

peak (NSX) and the development of stretching (S) and rocking (R) peaks associated with pure vitreous silica. After two hours, the intensity of the entire spectrum begins to drop uniformly. This drop is due to greater light scattering as the surface roughens. This phenomenon is unfortunate because it does not enable one to obtain a quantitative estimate of the surface composition.

Sanders and Hench have shown that infrared reflectances are proportional to the amount of species causing them [11]. This relationship assumes that the surface is sufficiently smooth to produce predominantly specular reflection. This is not the case with the glasses under investigation. However, qualitative interpretation can lead to information concerning the extent of selective leaching from the surface. It should be pointed out that IRRS has a maximum depth penetration of less than 1 μm for silicate glasses, and is therefore providing information about changes occurring at the surface of the corrosion film. In this case it can be seen that a surface film composed almost entirely of silica forms within 2 hours.

(5) The use of energy dispersive x-ray analysis shows that after 1 hour in solution the ratio of Si/Ca on the glass surface increased from .9 to 5.6 (see Figure 13), again demonstrating that the glass is being selectively leached, leaving behind a silica-rich film.

The influence of P_2O_5 content on the corrosion behavior as seen in the data is somewhat complex. Referring to region I of Figure 6, the initial change in alpha suggests that the glass structure is more uniformly attacked as the P_2O_5 content increases. The glasses containing 6 and 12% P_2O_5 have alpha values slightly above 0.5, indicating that a significant part of the corrosion mechanism is total dissolution. This is substantiated by the IR spectra of Figure 9. Referring to the 15-minute exposures, the decrease in intensity of the S peak as the phosphorus content increases is a result of preferential attack of the silicon-oxygen-silicon bonds. The thickness of the corrosion film at very early corrosion times is less than 1 μm, so the IR spectra are representative of the entire film. Within an hour the film thickness has been observed with scanning electron microscopy to increase to values on the order of 5-10 μm [22]. Then the IR spectra are providing information about the surface of the corrosion film.

The Si/Ca ratios in Figure 13 of the four glasses with increasing phosphorus content indicate that a silica-rich film has formed on each of the glasses within one hour. However, the level of the Si/Ca ratio on the surface decreases as the phosphorus content increases, suggesting that the surface is more uniformly attacked as the phosphorus content of the glass increases. The corrosion films in Figure 12 exhibit less surface roughness as the phosphorus content increases,

as would be expected if the glass structure was being uniformly attacked. Examination of the corroded glass surfaces with a scanning electron microscope equipped with an energy dispersive x-ray system leads to the same conclusion derived from solution analysis of the ions leached from the glass structure.

The glass containing 3% P_2O_5 forms a silica-rich layer almost immediately, while the 6 and 12% P_2O_5 glasses show preferential silica attack within the first 15 minutes of exposure. This behavior is reversed within two hours for the glasses containing 6 and 12% P_2O_5 as the intensity of the S peak increases while the intensity of the NSC peak is reduced (see Figure 9). As was discussed earlier, light scattering resulting from surface roughness leads to an intensity drop in an IR spectrum. The fact that the intensity of the S peak increases after the initial drop indicates that a significant amount of silica is present on the surface.

The amount of silica available for film formation (Figure 7) increases uniformly with time in region I for all four compositions. It is during this period that the silica-rich film forms on the glasses. A break occurs in each of the curves in region II. This event corresponds to the formation of a calcium phosphate film for the three glasses containing P_2O_5 and occurs earlier as the P_2O_5 content increases.

Direct evidence for the existence of the calcium phosphate film is presented in Figure 11. The series of spectra show the changes which occur at the surface of the glass containing 6% P_2O_5 when it is exposed to an aqueous environment. A silica-rich film forms within 2 hours as has already been discussed. The phosphorus peak has reappeared in the 24-hour spectrum and the ratio of Si/Ca has dropped. By 1,500 hours the phosphorus peak has continued to grow while the silicon peak has been drastically reduced. Comparison in Figure 11 of the respective ratios of Si/Ca, Si/P, and Ca/P clearly demonstrates the formation of a calcium phosphate rich layer.

The calcium phosphate film is responsible for the infrared reflection spectra which develop after surface roughening causes the spectra of the glasses containing phosphorus to diminish. The new spectrum is very similar for all the glasses containing phosphorus and it develops more rapidly as the phosphorus content increases. Figure 10e illustrates the spectrum for the glass with 6% P_2O_5 which had been immersed for 1,500 hours. The peaks occur in two regions, 1,045 cm^{-1} and 560 cm^{-1}. Levitt et al. have identified fundamental wavenumbers for the phosphate ion of hydroxyapatite in these same regions [23]. In addition, Nakamoto [24] has predicted that the infrared active fundamentals of the PO_4^{-3} ion in aqueous solution are at 1,080 cm^{-1} and 500 cm^{-1}. This evidence, along with the simultaneous buildup of calcium and

phosphorus at the surface, identified from Figure 11, is the basis for specifying the origin of the new spectrum as a calcium phosphate compound.

The details of the calcium phosphate compound film formation are not completely understood. It has been established that after 10 hours, phosphorus which has been leached into solution precipitates back onto the glass surface (see Figure 5) for the compositions containing 6 and 12% P_2O_5. In addition, Ca^{+2} release is retarded during this same time period. Figure 3 shows a leveling off in the amount of Ca^{+2} released after 10 hours and the effect is more pronounced as the P_2O_5 content of the glass increases. The data points in Figure 13 emphasize this concept. The ratio of Si/Ca drops significantly with increasing P_2O_5 content when the four glasses are corroded under identical conditions. The decrease indicates that proportionally less Ca^{+2} is removed as the phosphorus content of the glass increases.

The formation of the calcium phosphate film influences the corrosion behavior of the glasses significantly. Its effect is seen in region III of Figure 6. As the phosphorus content of the glass increases, the α curves descend with increasing negative slopes, indicating selective leaching is the controlling mechanism. The solution data (see Figures 2-4) show that both the silicon and sodium release levels off during region III but that the Ca^{+2} release actually increases after the calcium phosphate film is formed. This could be due to the excessive amount of Ca^{+2} present in the glass compositions as compared to the P_2O_5 content. Once all the phosphorus has been used up in the film formation, the remaining Ca^{+2} goes into solution. However, the film acts as a barrier to further attack of the bulk glass structure.

The relative effectiveness of the films in isolating the bulk glass from the aqueous environment is demonstrated in Figure 26. It can be seen that the time required to override the pH of a buffered solution increases as the P_2O_5 content increases. Since the pH increase results from a sodium-proton exchange between the glass and solution [25], the formation of the calcium phosphate film retards this reaction and the effect is more pronounced as the film formation is accelerated.

Now let us turn our attention to the influence of boron and fluorine additions on the corrosion behavior of the glass containing 6% P_2O_5. There is a pronounced difference in the protectiveness of the calcium phosphate film which forms on these glasses. Figure 27 demonstrates the effect of adding boron or fluorine to the bulk glass on the time required to override the pH of a buffered solution. Obviously, the glass containing fluorine is much more effective than either of the other two glasses in preventing an increase in pH due to a

Figure 26. Influence of P_2O_5 content on the time required to overrive the pH of a buffered aqueous solution.

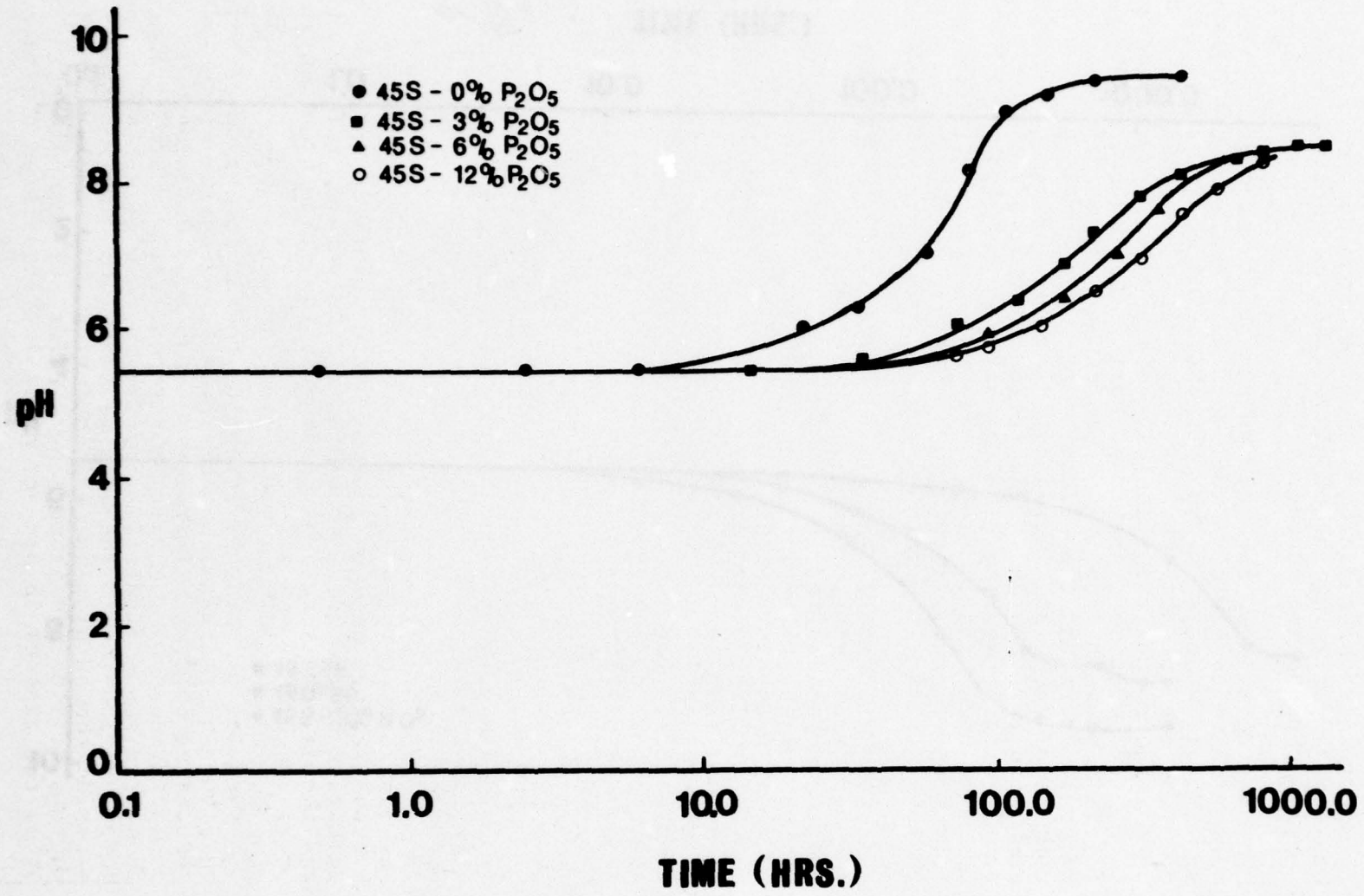

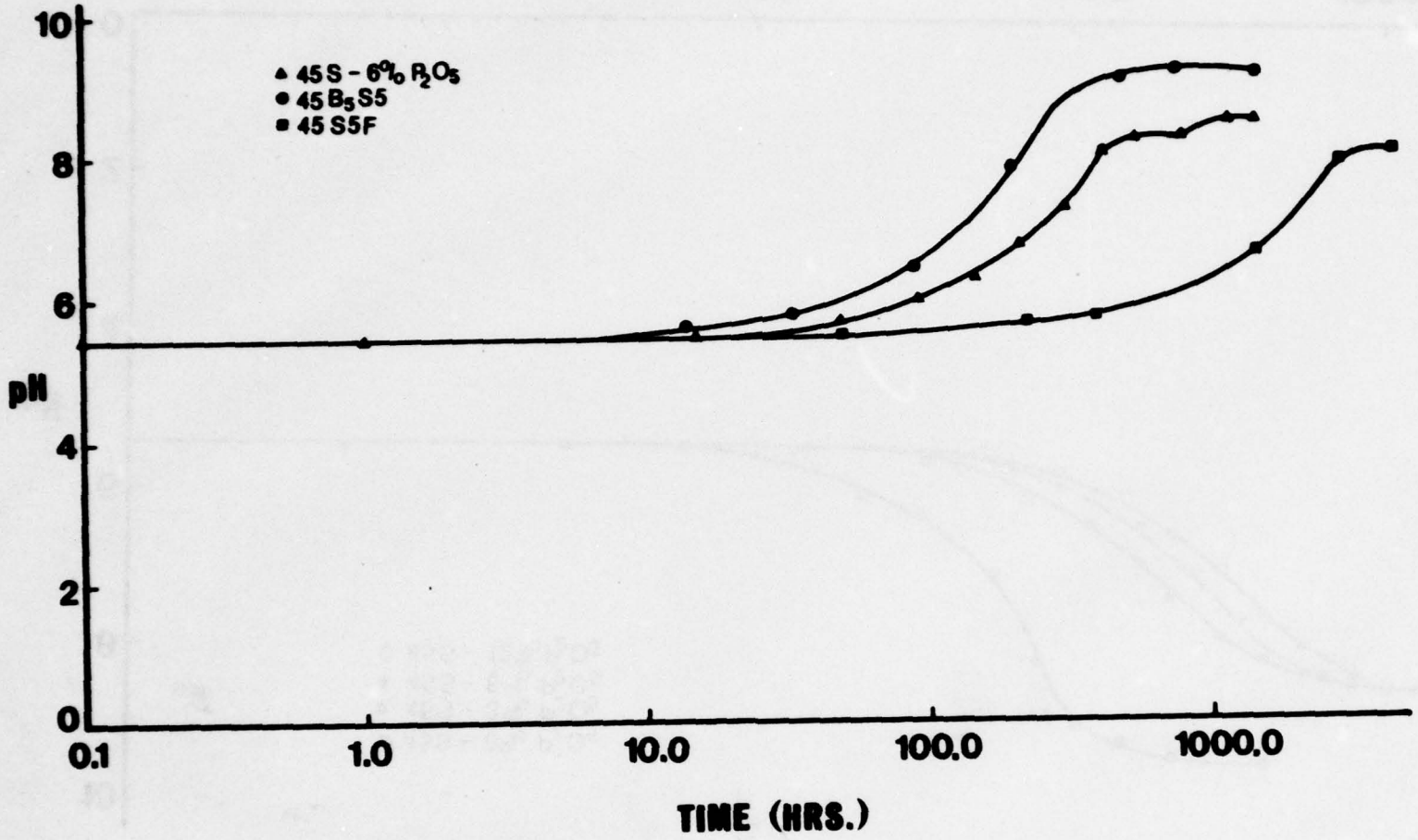

Figure 27. Influence of B^{+5} and F^- additions to the 45S-6% P_2O_5 bioglass on the time required to override the pH of a buffered aqueous solution.

sodium-proton exchange. In fact, the addition of boron actually reduces the reaction time necessary to overcome the buffering capacity of the solution.

The reasons for the drastic difference in behavior are not intuitively obvious. Both the glass with boron and the composition containing fluorine exhibit a behavior similar to that of the glass with 6% P_2O_5. That is, initially there is selective leaching of silica which ceases after approximately 15-30 minutes. Within the next 30 minutes a silica-rich film is established, and finally a calcium phosphate film is produced at the silica-rich film-water interface (see Figures 20 and 21).

The key to the variable corrosion resistance appears to be associated with the calcium phosphate films. Initially, they appear to be amorphous. Figure 24a contains an x-ray diffraction pattern of the surface of the composition containing 6% P_2O_5 which had been in solution for 15 hours. Infrared reflection spectra of this sample showed that a calcium phosphate film was present on the surface. The absence of any diffraction peaks indicates that the film is completely amorphous. However, it is possible that some crystalline material is present but not in sufficient quantity to produce peaks. A diffraction pattern of the same composition after 100 hours in solution shows peaks beginning to appear (Figure 24b). Figure 24c is a diffraction pattern of the glass containing 6% P_2O_5 which had been in solution for 1,500 hours. The d spacings obtained from the film show reasonable agreement with the d spacings of carbonate hydroxyapatite (dahllite). The values are compared in Table 2. There is one discrepancy in the relative intensities and that is for the 3.402 d value. It is the sharpest peak and has the highest intensity for the calcium phosphate film, whereas it has a relative intensity of 70 for dahllite. This effect could be accounted for if growth occurred along a preferential direction. Figure 25 contains a diffraction pattern of the calcium phosphate film on the surface of the glass containing boron which has been in solution for 1,500 hours. Again there is reasonably good agreement between its d spacings and those of dahllite. The relative intensities are also in good agreement.

Referring to Figure 23, the similarity between the infrared reflection spectrum of the reagent grade hydroxyapatite and the spectrum of the glass containing boron which had been in solution for 1,500 hours takes on added significance. Considering the x-ray diffraction patterns, the infrared reflection spectra and the energy dispersive analysis which shows calcium and phosphorus to be the main components on the surface after 1,500 hours in solution (see Figure 11), it would indicate that the crystalline calcium phosphate material which forms contains a considerable amount of hydroxyapatite.

Table 2

d-Spacings Obtained from Corrosion Films on 45S-6% P_2O_5 and $45B_5S5$ Glasses Corroded for 1,500 Hrs. Corresponding d-Spacings of Dahllite Are Included.

Dahllite	45S-6% P_2O_5 1,500 Hrs in Sol.	$45B_5S5$ 1,500 Hrs in Sol.
4.120	--	--
3.402	3.411	3.411
2.768	2.769	2.777
2.687	2.688	2.697
2.607	2.619	2.619
2.232	2.268	2.257
1.931	1.939	1.931
1.834	1.832	1.839
1.721	1.717	1.713

It has been stated by Körber and Tromel [26] that in the system $CaO-P_2O_5$, hydroxyapatite will form at temperatures up to 1050°C if water is not carefully excluded.

It should be pointed out that the most synthetic calcium phosphate precipitates form nonstoichiometric crystal compounds with numerous possible substitutions existing, i.e., sodium for calcium, carbonate for phosphate, fluorine for hydroxyls, water for hydroxyls. McConnell [27] has stated that unless special precautions are taken it is practically impossible to obtain apatite crystals which do not contain carbonate groups. Furthermore, he suggests that carbonate substitution for phosphate groups can produce distortion in the hexagonal apatite structure which can lead to line splitting in diffraction patterns.

It thus seems likely that the calcium phosphate film which forms at the silica-rich film-water interface of the glasses containing phosphorus is indeed hydroxyapatite. However, it almost surely deviates from stoichiometry due to substitution of carbonate, sodium and possibly silicon.

One explanation for the significant difference between the protectiveness of the calcium phosphate film of the glass containing fluorine and all of the other compositions is that the fluorine substitutes for the hydroxyl ions in the apatite structure. It has been reported that if water containing trace amounts of fluorine is brought into contact with hydroxyapatite, fluorapatite will form as an insoluble product [28]. Another source [29] has stated that in aqueous systems

containing trace amounts of fluorine, fluorapatite is the most stable calcium phosphate compound. Referring to Figure 17, it can be seen that there is a drastic drop in the phosphorus level in solution between 10 and 100 hours for the glass containing fluorine. The level of calcium released into solution is also significantly lower after 100 hours for the glass containing fluorine, when compared to the data for all other glasses examined (see Figure 16).

The main influence of boron is an acceleration of the initial attack of the glass network. Figure 14 illustrates that even though the glass containing boron has the least amount of silica in the bulk composition, more silica is released into solution than is released from the glass containing 6% P_2O_5 or the glass with fluorine. This effect is thought to be due to a weakening of the three-dimensional silica network due to the presence of the boron atoms. Boron can exhibit either three-fold or four-fold coordination. It has been reported [30] that at high temperatures, boron present in borosilicate glasses exhibits three-fold coordination which changes to four-fold at lower temperatures. However, during the cooling process there is not sufficient time for complete reordering and some of the boron remains in three-fold coordination. It is the presence of the boron atoms with three-fold coordination which produce weak regions in the glass network. Aqueous solutions attack these areas, releasing substantial amounts of boron and sodium.

A similar type of behavior could account for the observed surface reactions of the glass containing boron. The presence of three-fold coordinated boron atoms lead to an accelerated release of sodium and boron atoms. This would produce a more rapid overriding of a buffered solution which has been observed (see Figure 27). Release of silica would also be accelerated due to the increased basicity of the solution. The data in Figure 18 substantiate this hypothesis. The addition of boron to the glass containing 6% P_2O_5 results in an increase in the initial alpha values, which is a sign that the extent of total dissolution is increasing. It should be noted that this event is only temporary as a silica-rich film is established within 1 hour. The epsilon curve of Figure 19 shows an increase in magnitude of ε for the glass containing boron which is greater than the glass containing 6% P_2O_5, indicating there is more silica available for film formation.

Conclusions

In summary, the following facts have been established:

(1) The glass containing 0% P_2O_5 forms a silica-rich film which protects the glass throughout 1,500 hours of exposure.

(2) The glasses containing phosphorus also form silica-rich films. However, in the case of the glasses containing 6 and 12% phosphorus, the silica-rich film formation is preceded by a short period (15-30 minutes) of selective silica attack.

(3) After the silica-rich film formation, the phosphorus containing glasses form a calcium phosphate film at the silica film-water interface. The rate of formation of the calcium phosphate film is accelerated as the amount of phosphorus in the bulk glass composition is increased.

(4) Although the calcium phosphate film appears to be amorphous initially, it crystallizes with time into an apatite structure.

(5) The calcium phosphate film is more effective than the silica-rich film in isolating the glass from its aqueous environment.

(6) The addition of fluorine to the glass containing 6% P_2O_5 significantly increases the resistance of the glass to aqueous attack.

(7) The addition of boron to the glass containing 6% P_2O_5 accelerates the initial dissolution process in an aqueous solution.

References

1. D.M. Sanders and L.L. Hench, J. Amer. Ceramic Soc., 56 [7], 373-377 (July 1973).

2. L.L. Hench, T.K. Greenlee, Jr., and W.C. Allen, Annual Report #1, U.S. Army Med. R and D Command, Contract No. DADA-17-70-C-0001 (1970).

3. L.L. Hench, T.K. Greenlee, Jr., and W.C. Allen, Annual Report #2, U.S. Army Med. R and D Command, Contract No. DADA-17-70-C-0001 (1971).

4. L.L. Hench, H.A. Paschall, W.C. Allen and G. Piotrowski, Annual Report #3, U.S. Army Med. R and D Command, Contract No. DADA-17-70-C-0001 (1972).

5. L.L. Hench, H.A. Paschall, W.C. Allen and G. Piotrowski, Annual Report #4, U.S. Army Med. R and D Command, Contract No. DADA-17-70-C-0001 (1973).

6. L.L. Hench, R.J. Splinter, W.C. Allen and T.K. Greenlee, Jr., J. Biomed. Mat. Res. Symp., No. 2, Interscience Publishers, New York, 1972, pp. 117-143.

7. T.K. Greenlee, Jr., C.A. Beckham, A.R. Crebo and J.C. Malmorg, J. Biomed. Mat. Res., 6, 244 (1972).

8. C.A. Beckham, T.K. Greenlee, Jr., and A.R. Crebo, J. Calcified Tissue Res., 8, 2 (1971).

9. L.L. Hench and H.A. Paschall, J. Biomed. Mat. Res. Symp., No. 4, John Wiley and Sons, New York, 1973, pp. 25-42.

10. L.L. Hench and H.A. Paschall, "Prostheses and Tissue: The Interface Problem," to be published in J. Biomed. Mat. Res. Symp.

11. D.M. Sanders and L.L. Hench, Applied Spectroscopy, 28 [3], 247-255 (May/June 1974).

12. D.M. Sanders and L.L. Hench, J. Amer. Ceramic Soc., 54 [7], 373-378 (1973).

13. L.L. Hench, Medical Instrumentation, 7 [2], 136-144 (1973).

14. G. Gomori, Methods in Enzymology, Vol. 1, Academic Press, New York, 1955, pp. 138-146.

15. Scott Anderson, J. Amer. Ceramic Soc., 33 [2], 45-51 (February 1950).

16. D.R. Hach, Colorimeter Methods Manual, 7th Ed., October 1971.

17. American Public Health Association, Standard Methods of Waste Water Analysis, American Public Health Association, New York, 1969, p. 258.

18. R.E. Ferrell and G.G. Paulson, Energy Dispersive Analysis of X-ray Spectra Generated in the SEM, ORTEC Manual.

19. R.J. Bell and P. Dean, "The Vitreous State," in Disc. Faraday Soc., Butterworths, London, 1970, p. 50.

20. P.H. Gaskell, "The Vitreous State," in Disc. Faraday Soc., Butterworths, London, 1970, p. 50.

21. I. Simon and H.D. McMahon, J. Chemical Physics, 21 [1], 23-30 (January 1953).

22. A.E. Clark and L.L. Hench, "Effects of P^{+5}, B^{+3}, and F^{-} on the Surface Chemistry of Bioglass," Annual Report #4, U.S. Army Med. R and D Command, Contract No. DADA-17-70-C-0001 (1973), p. 37.

23. S.R. Levitt, K.C. Blakeslee and R.A. Condrate, Sr., Mem. Soc. Roy. Sci. Liege, 20, 121-141 (1970).

24. K. Nakamoto, Infrared Spectra of Inorganic and Coordination Compounds, John Wiley and Sons, Inc., New York, 1963.

25. L. Holland, "Surface Chemistry and Corrosion of Glass," in The Properties of Glass Surfaces, John Wiley and Sons, New York, 1964.

26. F. Körber and G. Tromel, Z. Elektrochem., 38, 578-582 (1932).

27. D. McConnell, Arch. oral Biol., 10, 421-431 (1965).

28. D. McConnell, Science, 136, 241-244 (1962).

29. T.D. Farr, G. Tarbutton and H.T. Lewis, J. Phys. Chem., 66, 318 (1962).

30. N.V. Belov, The Structure of Glass, Acad. Sci. U.S.S.R., Chapman and Hall, Ltd., London, 1953.

C. Auger Spectroscopic Analysis of Bioglass Corrosion Films, by A. E. Clark and L. L. Hench

Abstract

Auger spectroscopy and ion beam milling are used to determine surface ion concentration profiles on a series of bioglass implant materials after exposure to simulated body conditions. Four glasses were examined, a soda-lime-silica glass and three compositions produced by adding 3, 6 and 12 wt.% P_2O_5 to the ternary glass.

The results show an SiO_2-rich film is formed on the surface of all glasses investigated. As P_2O_5 is added to the bulk composition a second film rich in Ca and P forms at the SiO_2-rich film-water interface. The rate of formation of the Ca-P film is accelerated as the P_2O_5 content of the bulk glass increases. Furthermore, when glasses are corroded under identical conditions, the thickness of the Ca-P layer increases as the P_2O_5 content of the bulk composition is increased.

Introduction

Auger electron spectroscopy has been employed to further characterize the corrosion films which form on a series of bioglasses. An investigation by Clark and Hench [1] has established that when exposed to an aqueous environment, a silica-rich film forms on the glasses within two hours. A second film composed primarily of calcium and phosphate is produced at the silica film-water interface. This second film is produced only when phosphorus is contained in the glass composition and the rate of formation is related to the amount of phosphorus in the bulk glass. IRRS, EDXA and X-ray diffraction confirmed that the film crystallized into an apatite structure with time. Auger electron spectroscopy has been utilized to obtain detailed chemical profiles of the corrosion films in hopes of elucidating the mechanism of film formation.

Theory

The technique involves bombarding the sample surface with a beam of monoenergetic electrons. A series of interactions leads to the release of electrons which were contained in the electronic structure of the surface atoms. Figure 1 illustrates such a series of interactions. Impinging electrons from the beam create a vacancy in the K shell. An electron from one L shell then cascades back into the empty slot in the K shell. In the process, sufficient energy

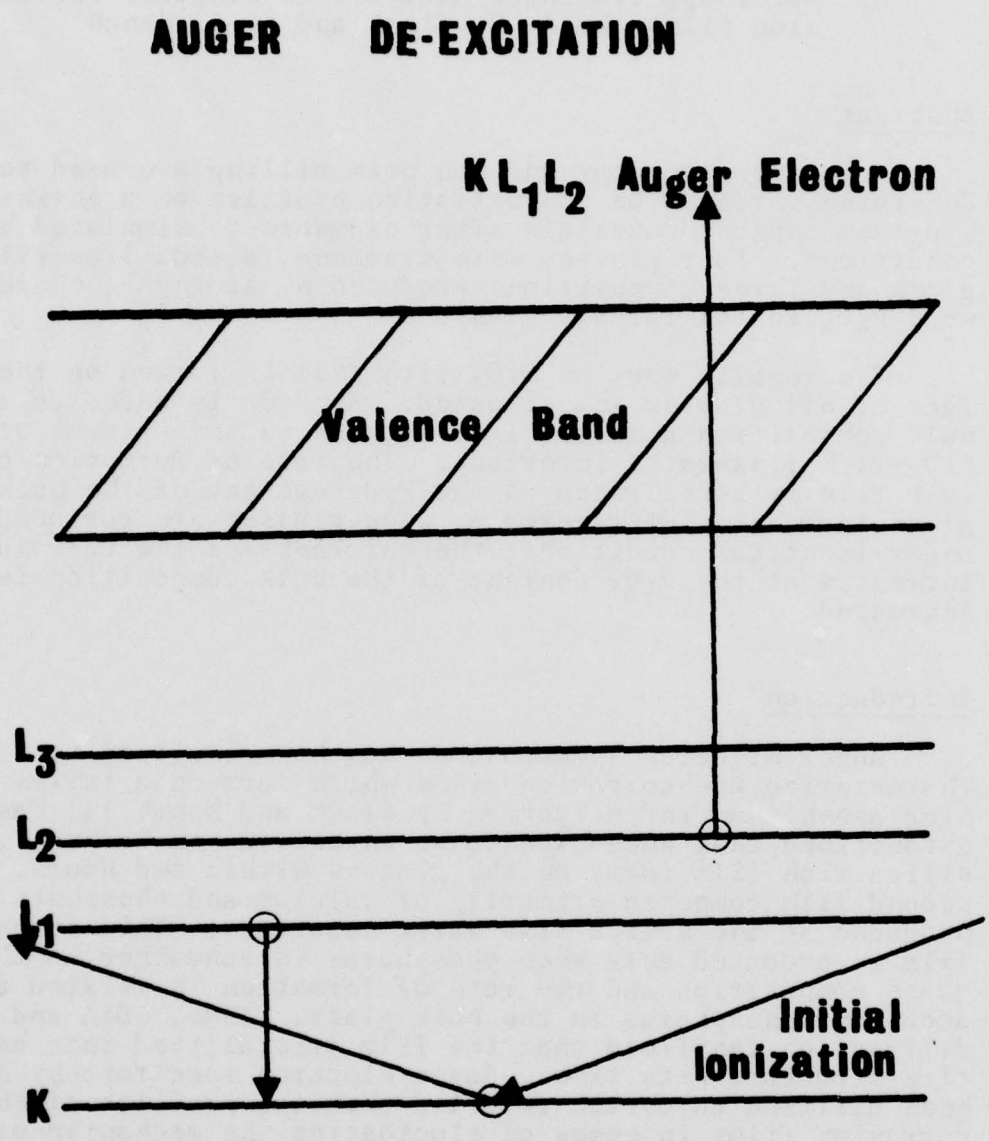

Figure 1. X-ray energy level diagram depicting a KL_1L_2 Auger transition.

is available for the ejection of an electron from another L level. This process is termed an Auger transition and the electron with an energy characteristic of the atom from which it was ejected is called an Auger electron. The Auger electrons produce peaks in the secondary electron energy spectrum and thus by monitoring the energy distribution due to Auger electrons, it is possible to identify the atoms producing them. In actual practice, the derivative of the energy spectrum is taken, which enhances the Auger peaks and suppresses the background present in the secondary electron distribution [2]. Due to a short mean free path, Auger electrons have a maximum escape depth of 50 Å, making this a truly surface sensitive process. In addition to atom identification, it is possible to relate the amplitude of the Auger peaks to the concentration of the atoms producing them.

A complementary process of Argon ion bombardment removes surface atoms a layer at a time. By simultaneously ion milling the surface and measuring Auger spectra it is possible to obtain a chemical profile of the structure.

The raw data directly observed are the changes in peak height with ion milling time. In order to obtain quantitative information about the amount of atoms present at the surface, the differences in Auger transition probabilities for different atoms must be considered. Factors contributing to these differences are the influence of the environment on an atom's electronic structure as well as the distribution of atoms within the volume of material producing the detected Auger electrons.

To overcome this problem, sensitivity factors were determined by a recently developed process [3]. These factors normalize the Auger peaks, enabling one to make a quantitative comparison of one component with respect to another. The sensitivity factors were obtained by analyzing Auger spectra of uncorroded glasses which had been ion milled for long periods of time to expose the bulk structure, and comparing these data to the known glass composition. Modifying the raw data with the sensitivity factors allows one to obtain a measure of relative atomic percent versus ion milling time.

By assuming that the cations are present as specific compounds with oxygen, i.e., SiO_2, CaO, P_2O_5, the relative atomic percent data can be altered to provide a measure of mole percent versus ion milling time. There was usually an excess of oxygen near the surface which was unaccounted for. The extra oxygen atoms are probably associated with hydrogen atoms (which cannot be detected with AES) as water molecules. Although approximations are involved in determining the amount of species present, the observed changes in peak height with ion milling time correspond to an increase or decrease in the amount of species at the surface and are unaffected by the approximations.

Experimental Procedure

The four glass compositions selected for investigation are listed in Table 1. The glasses were prepared from reagent grade sodium carbonate, reagent grade calcium carbonate, reagent grade phosphorus pentoxide, and 5 μm silica. Premixed batches were melted in covered Pt crucibles in a temperature range of 1250 to 1350°C for 24 hours. Samples were cast in a steel mold and annealed at 450°C for 4 to 6 hours.

Table 1

Bioglass Compositions Selected for Auger Spectroscopic Analysis

1.	45S-0% P_2O_5	3.	45S-6% P_2O_5
	45 wt.% SiO_2		45 wt.% SiO_2
	24.5 wt.% CaO		24.5 wt.% CaO
	30.5 wt.% Na_2O		24.5 wt.% Na_2O
2.	45S-3% P_2O_5		6 wt.% P_2O_5
	45 wt.% SiO_2	4.	45S-12% P_2O_5
	24.5 wt.% CaO		45 wt.% SiO_2
	27.5 wt.% Na_2O		24.5 wt.% CaO
	3 wt.% P_2O_5		18.5 wt.% Na_2O
			12 wt.% P_2O_5

Bulk samples of each composition were prepared by wet grinding with 180, 320, and 600-grit silicon carbide paper. After a final dry grinding with 600-grit silicon carbide paper, samples were immersed in 200 ml of aqueous solution buffered at a pH of 7.4 (trishydroxymethyl aminomethane buffer). Temperature was maintained at 37°C, and all sample solutions were maintained in a static state. Samples of each of the four compositions were immersed in buffered aqueous solution for one hour. In addition, samples of the glass containing 6% P_2O_5 were exposed to the buffered aqueous solution for 10, 20, 30, 40, 50 and 60 minutes.

The samples were placed in a stainless steel vacuum chamber maintained at a background pressure of 1×10^{-7} Torr. To prevent destruction of the corrosion films, the beam current was held at a low value (5-10 μa) and was slightly defocused. Previous attempts to obtain spectra with a beam current of 75-100 μa resulted in complete degradation of the films. The beam energy was 3 KV for the series of samples

corroded for one hour and 2 KV for the 10-60 minute exposures of the glass containing 6% P_2O_5. The angle of incidence of the electron beam was kept at 45° to prevent unstable charging on the surface. The energies of the emitted Auger electrons were measured with a cylindrical mirror electron analyzer.

Ion bombardment of the sample surface with 2 KV Argon ions was employed to remove the outermost atoms. As discussed in the previous section, the concurrent use of milling and AES produces a chemical profile of the corrosion films.

Profiles were determined for each of the four compositions corroded for one hour. Two silicon peaks can be seen in the Auger spectra of Figure 2. It was observed that the low energy silicon peak (78 eV) changed shape as the sample was ion milled. The correlation between peak size and atom concentration does not hold if the peak shape varies. As a result, the high energy silicon peak (1,630 eV) was measured for the silicon profiles.

A recording profilometer with a sensitivity of .02 μm was employed to calibrate the ion milling rate. Figure 3 contains the type of plot generated by the profilometer. Using the value obtained and assuming a uniform milling rate, calculations were made to convert ion milling time to depth, yielding an estimate of the corrosion film thickness.

Ion milling was not employed on the series of samples corroded at 10-minute intervals, as only Auger spectra of the surface were taken. An attempt was made to measure a layer as thin as possible. Since the electrons which produce the low energy silicon peak have an escape depth (∿8 Å) about one-fourth that of the high energy peak (∿30 Å), the magnitude of the low energy peak was monitored. The lower beam energy (2 KV) was used for these samples to minimize the thickness of the detected volume and to prevent radiation damage which can lead to splitting of the low energy silicon peak.

Results

Figure 2 shows Auger spectra obtained at three different ion milling times for the glass containing 6% P_2O_5 which was corroded for one hour. The location of the peaks on the abscissa enables one to identify the atoms producing them. As was discussed earlier, changes in peak height are caused by an increase or decrease in the amount of element in the surface layer. These changes are most pronounced for the phosphorus and calcium peaks in Figure 2. Plotting the peak magnitudes versus ion milling time produces a chemical profile as is seen in Figure 4.

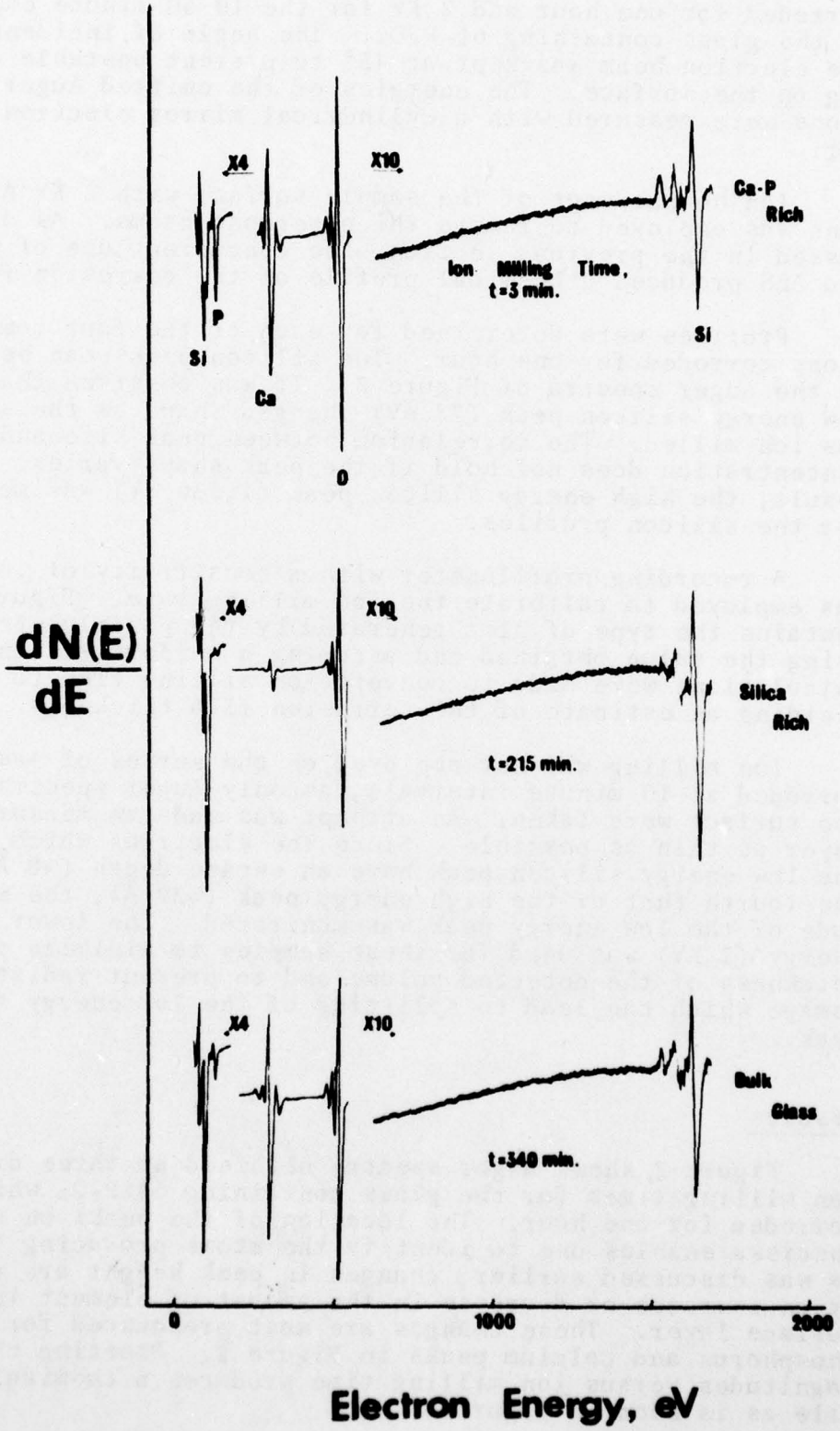

Figure 2. Typical Auger spectra for three depths of ion milling of a 45S-6% P_2O_5 bioglass corroded one hour at 37°C and pH = 7.4.

Figure 3. Schematic diagram of recording profilometer and the type of depth measurement plot generated by the profilometer.

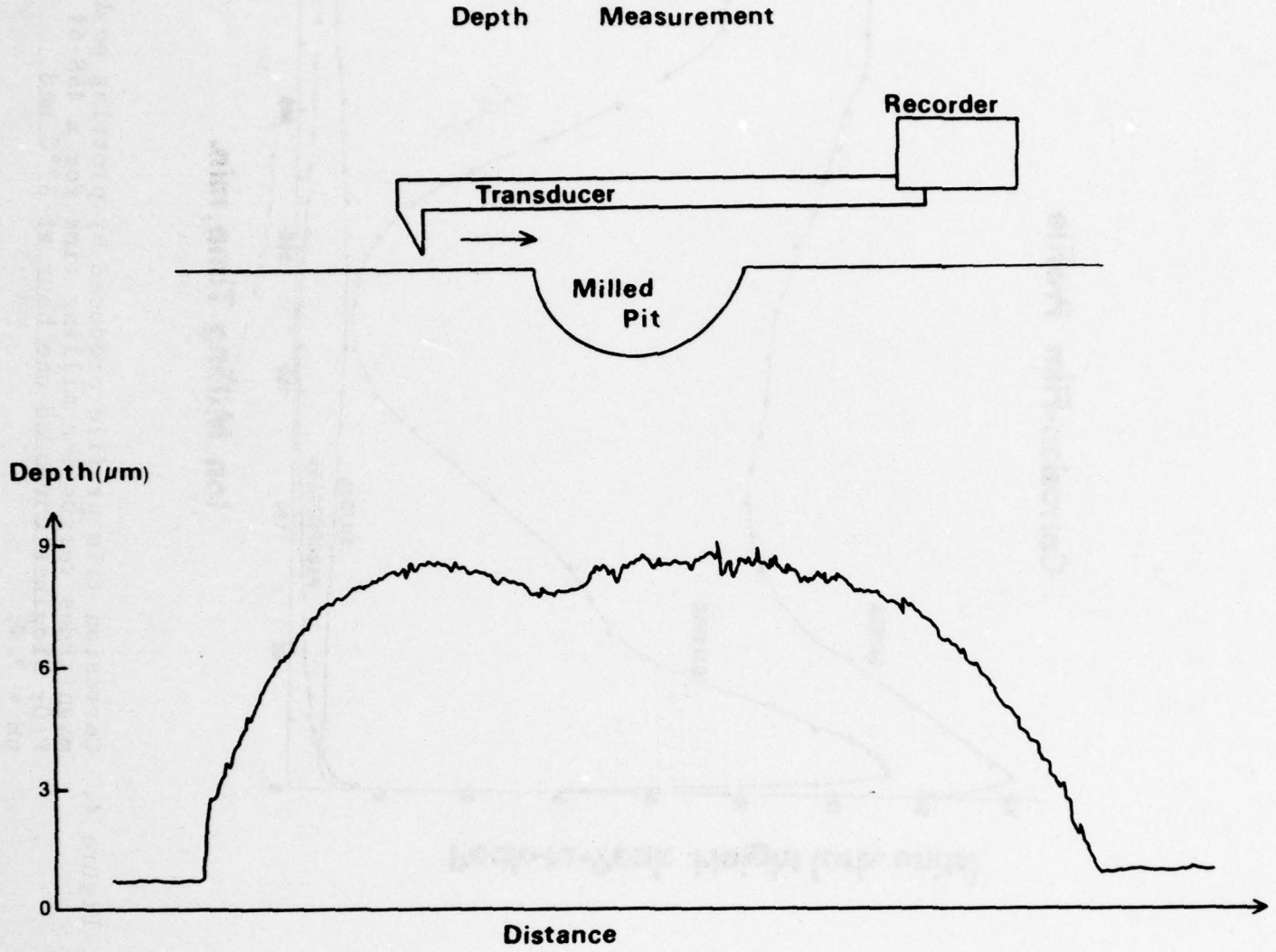

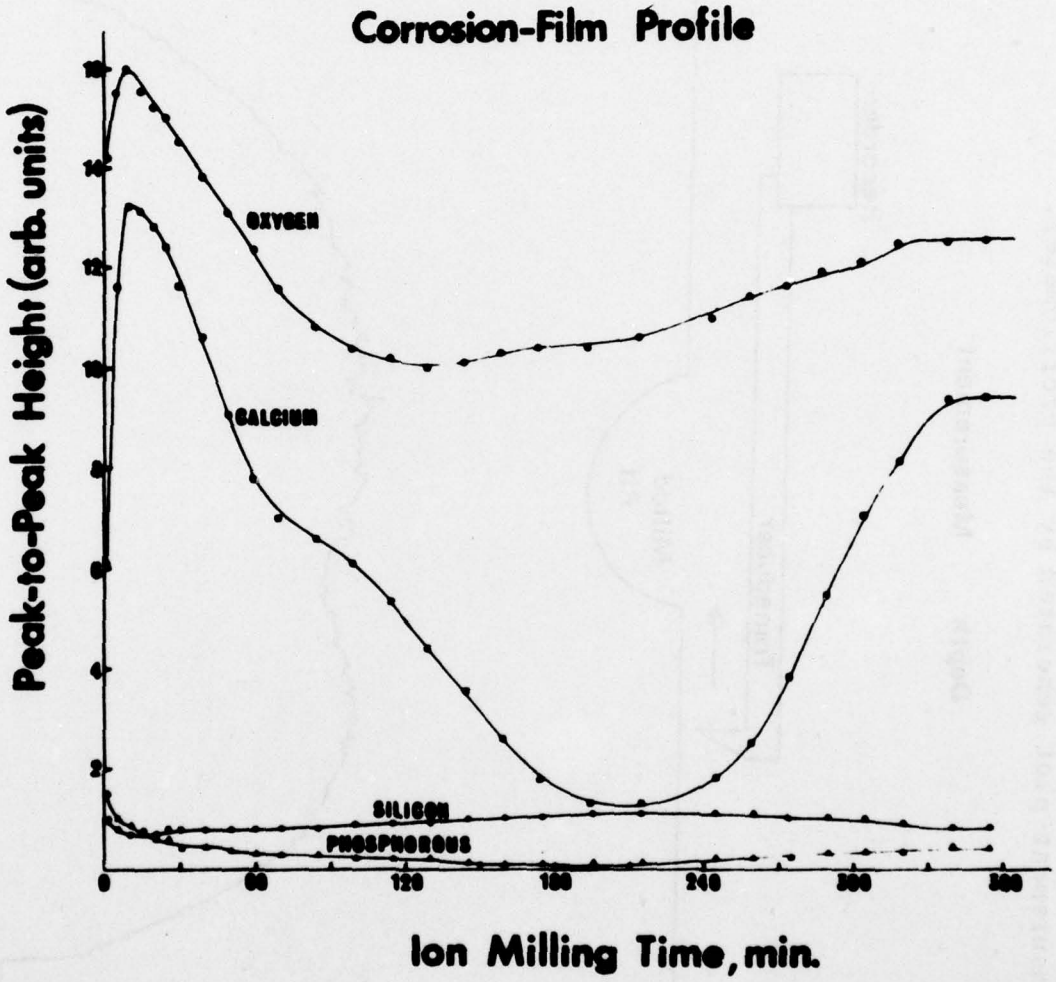

Figure 4. Corrosion film profile produced by plotting peak magnitudes versus ion milling time for a 45S-6% P_2O_5 bioglass corroded one hour at 37°C and pH = 7.4.

Features of importance are the buildup of phosphorus and calcium at the surface, followed by a region in which the oxygen, calcium and phosphorus levels fall off drastically, and finally a buildup in the oxygen, calcium and phosphorus levels to values characteristic of the uncorroded glass. Modifying the raw data with the sensitivity factors and converting ion milling time to depth of milling produces a semi-quantitative chemical profile of the corrosion film. Figure 5 illustrates the results of this process for the glass containing 6% P_2O_5 which was corroded for one hour. When comparing Figures 4 and 5 it is important to note that, although the magnitudes of the elements have been altered with respect to each other, the changes observed with milling time or depth of milling have been maintained. Ion milling through the corrosion films into the bulk glass was achieved only for the glass containing 6% P_2O_5 (Figure 5). The thickness of the silica-rich film is on the order of 2.0-2.5 μm, while the outermost film rich in calcium and phosphorus is only 0.5 μm thick.

Figure 6 is the result of converting atomic percent of surface species to mole percent. This final adjustment of the data can only be applied for the corrosion films, because the sodium has been leached out. Since the bulk glass contains a significant amount of sodium which is not detected with AES, it would be very difficult to accurately compute mole percentages in the region of uncorroded glass.

The absence of sodium which will be seen in all of the chemical profiles is not unexpected. It has been reported by several investigators that leaching of alkali is one of the initial steps in the corrosion of silicate glasses in aqueous solution [4]. In spite of these findings, one factor which had to be considered is the difficulty in detecting the presence of sodium with AES. Previous work [5] has suggested that electrostatic conditions produced by electron bombardment cause the extremely mobile sodium atoms to migrate out of the area of analysis. Another possibility is that the Argon ion milling process preferentially removes the sodium. For these reasons two samples of the glass containing 6% P_2O_5 were examined with Electron Spectroscopy for Chemical Analysis (ESCA). This technique involves bombarding the surface with a beam of x-rays and detecting the ejected photoelectrons. Information on composition and chemical binding can be obtained from this process. By examining a sample which had been corroded for one hour along with an uncorroded sample, the absence of sodium in the corrosion films was shown to be real and not an artifact of AES. Figure 7 compares the sodium, phosphorus and silicon peaks for the uncorroded and corroded samples using ESCA or photoelectron spectroscopy.

Chemical profiles of the glasses containing 0, 3 and 12% P_2O_5 are shown in Figures 8, 9 and 10. They were

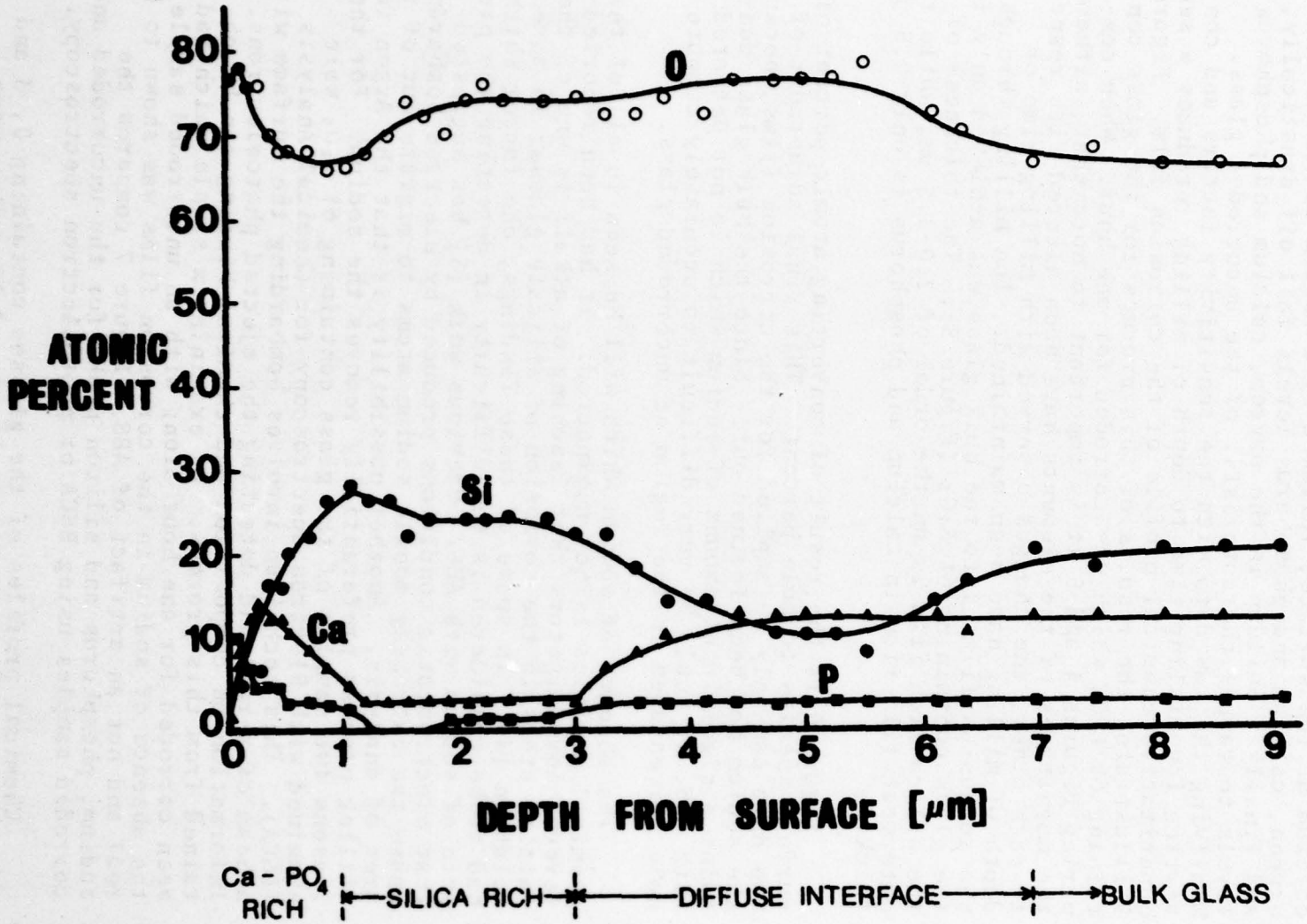

Figure 5. Chemical profile expressed in atomic percent of a 45S-6% P_2O_5 bioglass corroded one hour at 37°C and pH = 7.4.

Figure 6. Chemical profile expressed in mole percent for a 45S-6% P_2O_5 bioglass corroded one hour at 37°C and pH = 7.4.

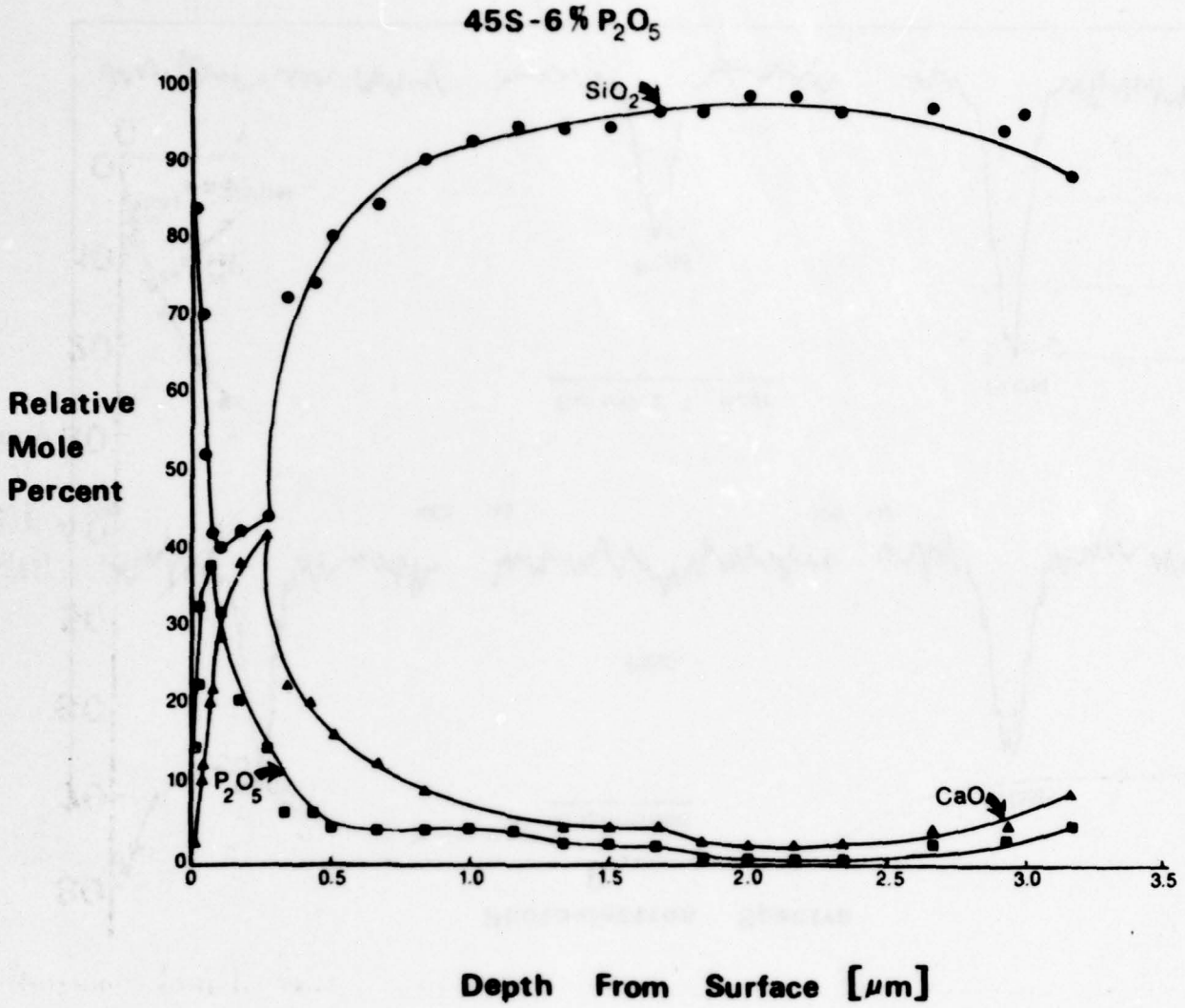

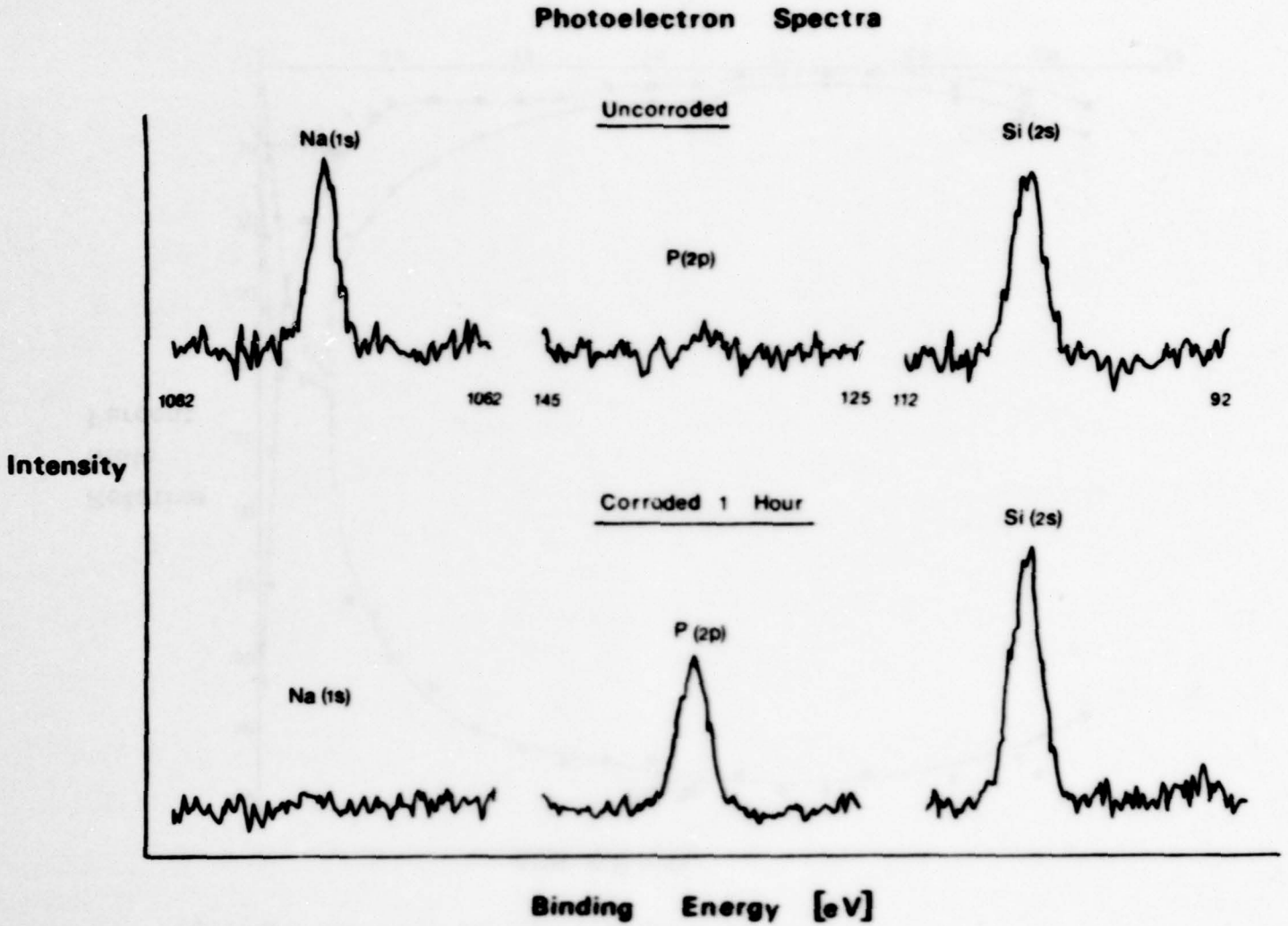

Figure 7. Comparison of photoelectron spectra of a freshly abraded 45S-6% P_2O_5 bioglass with the spectra of a 45S-6% P_2O_5 bioglass corroded for one hour at 37°C and pH = 7.4.

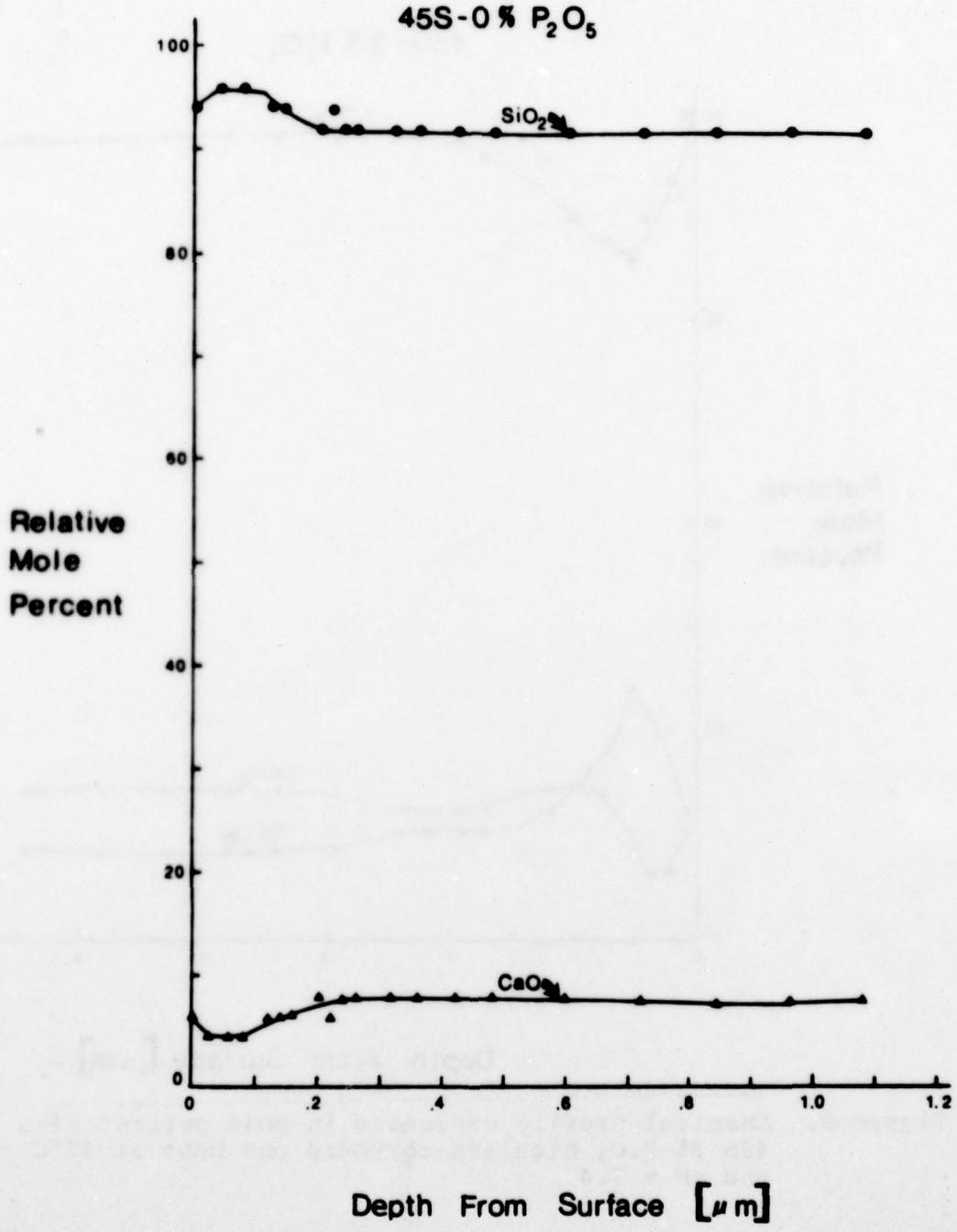

Figure 8. Chemical profile expressed in mole percent of a 45S-0% P_2O_5 bioglass corroded one hour at 37°C and pH = 7.4.

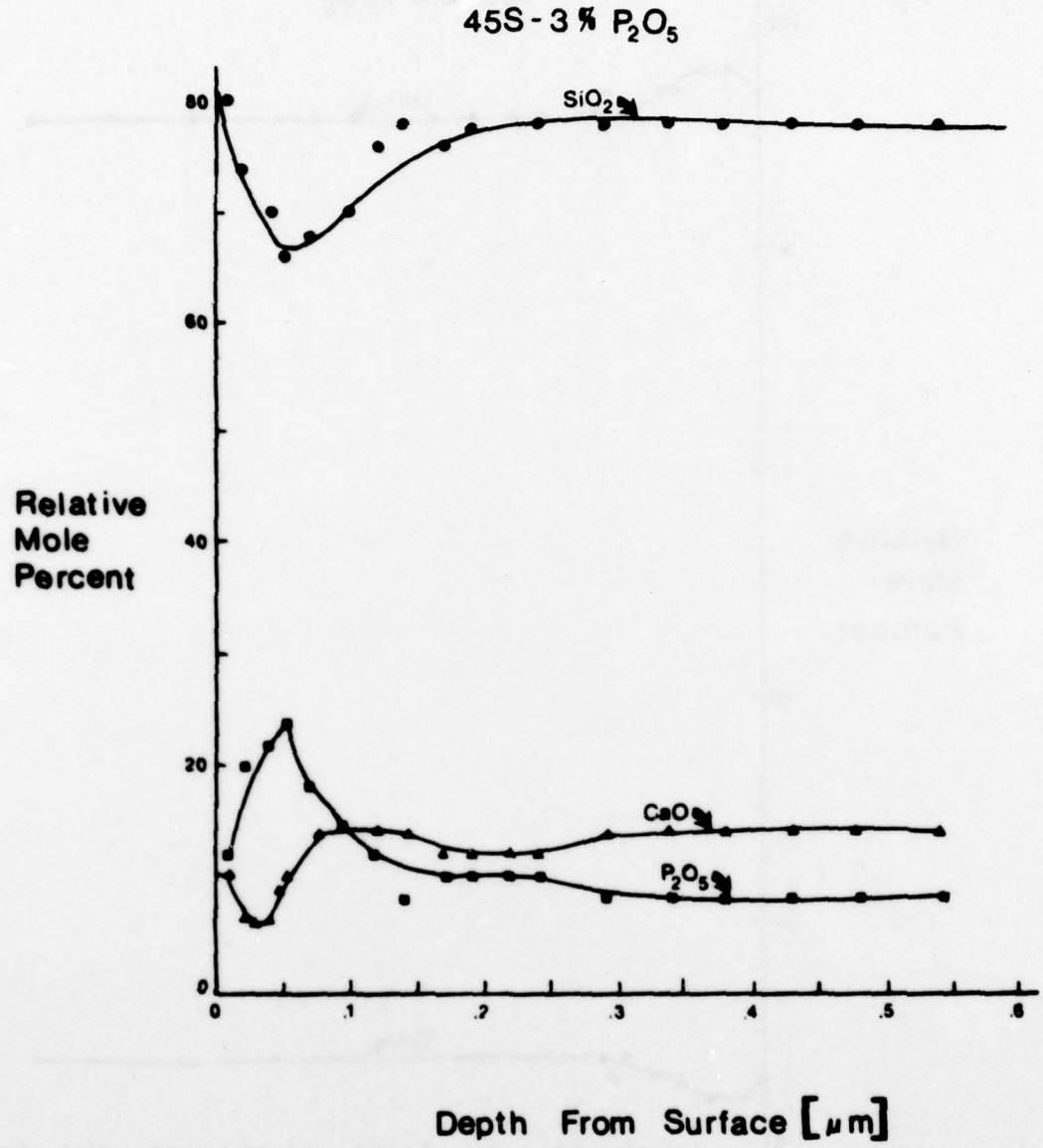

Figure 9. Chemical profile expressed in mole percent of a 45S-3% P_2O_5 bioglass corroded one hour at 37°C and pH = 7.4.

Figure 10. Chemical profile expressed in mole percent of a 45S-12% P_2O_5 bioglass corroded one hour at 37°C and pH = 7.4.

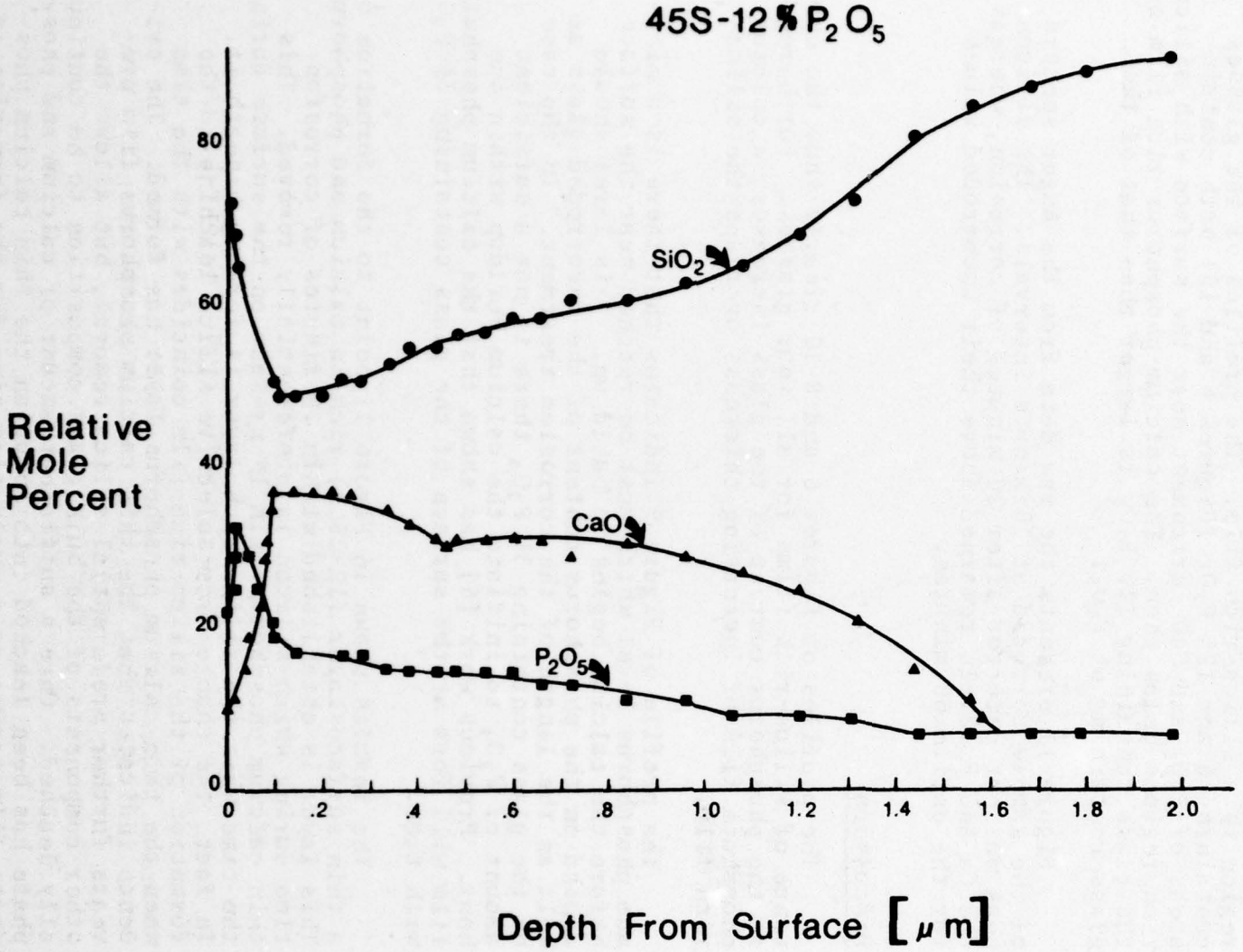

determined by the same technique previously described for the glass containing 6% P_2O_5. Note in Figure 9 that the P_2O_5 level is intensified near the surface but the CaO level remains relatively constant and even drops within .05 μm of the surface. Immediately underlying the phosphorus-enriched region is a silica-rich film. The profiles of the glasses containing 6 and 12% P_2O_5 (Figures 6 and 10) both contain areas of P_2O_5 and CaO enrichment near the surface with silica-rich regions below them. The calcium-phosphorus-rich film of the glass containing 12% P_2O_5 is larger than that of the glass containing 6% P_2O_5.

Figure 11 presents the raw data from the Auger spectra of the sample corroded at 10-minute intervals. The silicon peak was not detected after 20 minutes of corrosion, whereas the Ca and P levels remained above their uncorroded values for the entire 60 minutes.

Discussion

The profiles of Figures 6 and 8-10 clearly show the existence of silica-rich films for all four glasses. Furthermore, as the phosphorus content of the glass increases, a calcium phosphate film of increasing thickness overlaps the silica-rich film.

The profile of Figure 9 indicates that there is a minimum phosphorus level which must be reached near the surface before the calcium begins to build up. This level should depend on the phosphorus content of the uncorroded glass as well as the length of the corrosion treatment. In the case of the glass containing 3% P_2O_5 there is not a sufficient amount of P_2O_5 to initiate the calcium buildup within one hour. Previous work [6] has shown that the calcium phosphate film will form at the surface of the glass containing 3% P_2O_5 with time.

The results shown in Figure 11 point to the formation of a thin surface layer (10-15 Å) rich in calcium and phosphorus. This layer is established within 20 minutes of corrosion time during which silicon is preferentially removed. This thin calcium phosphorus film is present on the surface during the time when the silica-rich layer is forming beneath it. In fact, the change from selective silica leaching to the formation of the silica-rich film coincides with the time when the thin calcium phosphorus layer has formed. The evidence indicates that the thin calcium phosphorus film prevents further preferential silica removal, but allows the other components of the bulk glass composition to be continually leached. Once a sufficient amount of calcium and phosphate has been leached into solution the thin calcium phosphate film serves as a nucleation site for the formation of

Figure 11. Changes in the Auger peak heights of O, Ca, P and Si as a function of corrosion time for a 45S-6% P_2O_5 bioglass.

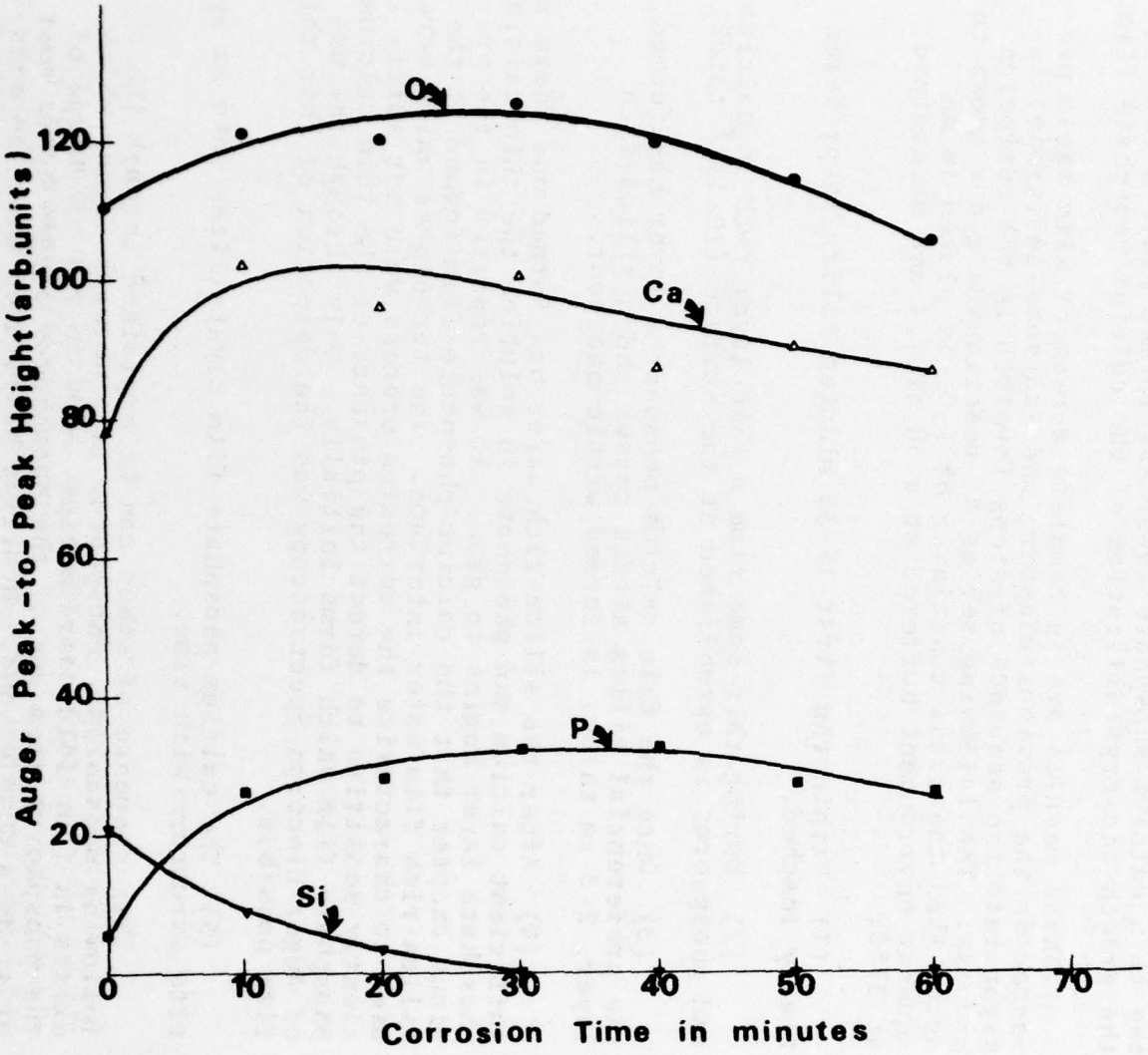

the calcium phosphate layer which eventually crystallized into an apatite structure. One point which is not clear is whether the silica-rich film formation which is produced only after the thin calcium phosphate layer has formed plays a role in the growth and crystallization of the calcium phosphate film.

These results are in complete agreement with those presented in the previous chapter, and add some additional insight into the sequence of steps involved in the corrosion process. The following series of reactions are now known to occur when the glass containing 6% P_2O_5 is placed in an aqueous environment buffered at a pH of 7.4 and maintained at 37°C:

(1) Within the first 15-30 minutes silica is preferentially leached.

(2) During this same time a thin layer rich in calcium and phosphorus is established at the surface (10-15 Å thick).

(3) Once the thin calcium-phosphorus layer has formed, the preferential silica attack ceases and a silica-rich layer, 2-3 μm thick, is formed within one hour.

(4) After the silica-rich layer has formed and there is sufficient calcium and phosphate in solution the thin calcium phosphate layer begins to grow. It was reported in the previous chapter that the calcium phosphate film formed at the silica-rich film-water interface. The techniques which were used to characterize the corrosion process were not sufficiently sensitive to detect the presence of the thin calcium phosphate film which forms initially. Only through the use of Auger Electron Spectroscopy was the detection of this thin film possible.

(5) The calcium phosphate film crystallizes into an apatite structure with time.

This sequence of steps can be explained through the following mechanism. Phosphorus is a network former which exists in four-fold coordination. Due to the +5 charge of the phosphorus atom one of the phosphorus oxygen bonds must exist as a double bond. McMillan has stated that the existence of the double bond in the phosphorus tetrahedra leads to conditions which promote separation of the phosphate groups from the silica network. Furthermore, he states that it would be probable for the P_2O_5 to be associated with alkali or alkaline earth oxides present in the glass composition [6]. Tomozawa has reported that P_2O_5 additions to sodium silicate and lithium silicate glasses promote phase separation by widening the immiscibility boundary and accelerating the kinetics [7]. The influence on the immiscibility boundary is related to the relative magnitude of the cationic

AD-A048 630 FLORIDA UNIV GAINESVILLE DEPT OF MATERIALS SCIENCE --ETC F/G 6/5
AN INVESTIGATION OF BONDING MECHANISMS AT THE INTERFACE OF A PR--ETC(U)
SEP 74 L L HENCH, H A PASCHALL, W C ALLEN DADA17-70-C-0001

UNCLASSIFIED NL

2 OF 2
AD A048630

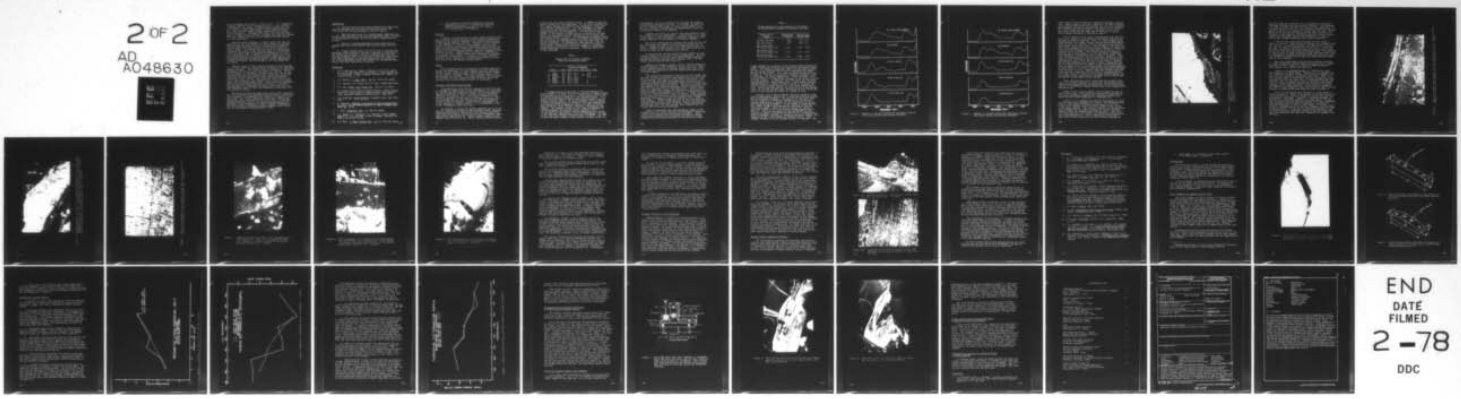

END
DATE FILMED
2-78
DDC

field strength with respect to that of Si^{+4}. P^{+5}, which has a larger cationic field strength [$Z/a^2(P) = 1.91$, $Z/a^2(Si) = 1.58$] than Si, was shown to promote phase separation while Ti^{+4} and Zr^{+4}, which have smaller field strengths than Si, were both found to suppress phase separation in the soda silica system [7]. Although this effect was only substantiated for simple binary systems, Tomozawa felt that the chances for this relation to hold in more complex silicate glasses were quite possible.

Based on these findings, it seems likely that the P_2O_5 additions to the soda-lime-silica glass promote a tendency towards phase separation and, in the process, disrupt the silicate phase by tying up some of the calcium from the ternary phase. This would have the effect of reducing the corrosion resistance of the silicate phase as calcium additions have been shown to increase the durability of soda silicate glasses [8]. Evidence for phase separation of the glass containing 6% P_2O_5 was presented by Hench et al. [9]. A scanning electron micrograph showed a second phase which existed as droplets, and was thought to be the phosphorus-rich phase.

The net result of this situation would be that the soda silica phase would be preferentially attacked by the alkaline aqueous solution. This effect would be enhanced as additional phosphorus tied up an increasing amount of calcium. As the silicate phase is attacked, a surface layer rich in calcium and phosphate would be produced which would then shield the remaining silicate phase from further network breakdown. Diffusion of Ca^{+2} and Na^{+1} into solution would still be possible, thus leading to the formation of a silica-rich layer under the calcium phosphate layer. When sufficient phosphate and calcium have been released into solution, a reaction between these two components and water would cause the calcium phosphate layer to grow and eventually crystallize into the apatite structure.

Reactions of this type have been cited in the literature. Weyl has postulated that phosphate opacification in soda-lime-silica glasses is produced by the formation of apatite crystals [10]. The crystal formation occurs when calcium and phosphorus react with water in the glass melt. It was also reported that the reaction of calcium and phosphorus with moisture in the atmosphere can lead to apatite formation at the glass surface, producing surface roughness and brittleness of the phosphate opacified glass [10].

Conclusions

1. Chemical profiles have been measured with Auger Electron Spectroscopy and ion beam milling which define the silica-rich and calcium phosphate corrosion layers.

2. When the bioglasses are corroded under identical conditions, the thickness of the calcium phosphate layer increases as the phosphorus content of the bulk glass composition increases.

3. There is a minimum phosphorus level which must be reached near the surface before the calcium begins to build up.

4. A thin surface layer (~10-15 Å) rich in calcium and phosphate forms during the initial 15 minutes of corrosion of the 45S-6% P_2O_5 bioglass. The data indicate that the thin calcium phosphate layer initiates the formation of the silica-rich layer and serves as the nucleation site for growth of the calcium phosphate layer once sufficient calcium and phosphorus have been leached into solution.

References

1. A.E. Clark and L.L. Hench, "Effects of P^{+5}, B^{+3}, and F^- on the Surface Chemistry of Bioglass," Annual Report #4, U.S. Army Med. R and D Command, Contract No. DADA-17-70-C-0001 (1973), p. 37.

2. L.A. Harris, J. Appl. Phys., 39 [3], 1419-1431 (1968).

3. C.G. Pantano, G.Y. Onoda and D.B. Dove, unpublished data.

4. C.R. Das, Trans. Ind. Ceram. Soc., 24 [1], 12 (1965).

5. G.Y. Onoda, First Annual Progress Report, "Glass Surface Chemistry: Application of Auger Electron Spectroscopy," Glass Container Industry Research Corp., July 1974.

6. P.W. McMillan, Glass Ceramics, Academic Press, New York, 1964.

7. M. Tomozawa, Advances in Nucleation and Crystallization in Glass, Special Publication No. 5, Amer. Ceramic Soc., 1971, pp. 41-50.

8. J. Enss, Glasstech. Ber., 5, 449-474 (1928).

9. L.L. Hench, T.K. Greenlee, Jr., and W.C. Allen. Annual Report #1, U.S. Army Med. R and D Command, Contract No. DADA-17-70-C-0001 (1970).

10. W.A. Weyl, J. Amer. Ceramic Soc., 24 [7], 221-225 (1941).

D. The Influence of Surface Chemistry on Implant Interface Histology: A Theoretical Basis for Implant Materials Selection, by A.E. Clark, L. L. Hench and H. A. Paschall

Abstract

A theory is proposed that an ideal implant material must have a dynamic surface chemistry that induces histological changes at the implant interface which would normally occur if the implant were not present. Evidence for the validity of this theory is a series of bone-implant studies which result in stable interfacial osteogenesis under specific implant surface chemistry conditions. Insufficient or excess surface ion concentrations produce negative osteogenesis and fixation results. Implantation of osteogenic implants in soft tissues also produce undesirable histological responses as proposed in the theory. A variety of surface chemical analyses of the implant are reviewed which provide a scientific basis for the implant surface theory.

Theory

The following theory is proposed for implant materials design and selection: An ideal implant material must have a dynamic surface chemistry that induces histological changes at the implant interface which would normally occur if the implant were not present. This paper examines the histological evidence for this theory in hard and soft tissues and describes the surface chemical basis of the theory.

Evidence from Hard Tissue Studies

Long experience with metallic implants in bone has led to the general observation of the development of a non-adherent fibrous capsule around the implant of varying thickness dependent upon type of metal, implant location, geometry, stability of fixation, etc. The surface chemistry of the metallic implants is such that if reactions do occur, both the pH change and the ions leached into the physiological solutions are not normally associated with development of either immature or mature osteoid. As a consequence, interfacial osteogenesis does not occur.

In contrast, a series of studies conducted on Ca, P, Na and SiO_2 containing bioglasses and bioglass-ceramic implants reported previously in this report and elsewhere show that these materials exhibit stable interfacial osteogenesis when appropriate combinations of implant surface chemistry and implant sites are met [1-6]. These studies provide positive

evidence for the theory advanced above. A summary of the evidence includes the following data: (1) The ions released from the implant surface are required for osteogenesis (see Table 1 for implant compositions). (2) Time dependent pH changes occurring at the implant interface are equivalent to the changes necessary for osteogenesis. (3) Ultrastructural changes of the implant surface provide a medium for collagen fibril and mucopolysaccharide bonding with an inorganic gel and mineralization to occur. (4) Hydroxyapatite precipitation takes place at the implant-osteoid interface simultaneous with the precipitation of hydroxyapatite crystals away from the implant interface. (5) Mechanical loads applied to the bioglass-ceramic implant-bone interface, either by chipping, microtoming or torsional fracture of segmental replacements, always break away from the interface. Fracture lines stop at the interface.

Table 1

Composition of Bioglass Implants
Used for Developing Theory

		Weight Percentage					
	Code #	SiO_2	Na_2O	CaO	CaF_2	P_2O_5	B_2O_3
1.	45S5	45	24.5	24.5		6.0	
2.	45S5F	43	23	12	16	6.0	
3.	$45B_5S5$	40	24.5	24.5		6.0	5.0
4.	$45S\infty$	45	30.5	24.5			
5.	45S10	45	27.5	24.5		3	
6.	45S2.5	45	18.5	24.5		12	

If compositional alterations of the bone-bonding bioglass-ceramics are made, the surface chemistry dynamics change as discussed in sections B and C. These changes lead to the following evidence in support of the proposed theory: (1) A slower reacting implant surface when placed midshaft in old femoral cortical bone in rat (slow metabolic rate) produced a fibrous encapsulation; an implant of the same composition when placed in the metaphyseal region of young rat tibiae (high metabolic rate) induced interfacial osteogenesis and bonding. (2) Implants placed in the young rat metaphyseal region accompany the adjacent bone as growth occurs. (3) Altering the interfacial pH-time dependence by a factor of 100 does not significantly alter the osteogenesis as long as the interface becomes alkaline within 5-6 weeks. (4) The silica-rich layer formed on the bioglass surfaces serves as

an induction site for osteoblasts to lay down the organic intercellular substance of bone. (5) Implant surfaces that are too reactive and release a surplus of phosphate ions result in ectopic calcification of neighboring tissues and histological attack of the implant.

Evidence for points (4) and (5) has been obtained from a new series of in-vivo experiments. Compositions 1, 4, 5 and 6 (see Table 1) were selected to study the influence of phosphorus additions on the behavior of bioglass implants.

One series containing the glasses with 0 and 6% P_2O_5 was gas sterilized and soaked in conditioning solution for 72 hours. Samples of each of these two compositions were subjected to IRRS and SEM analysis after gas sterilization, 24, 48 and 72 hours in the conditioning solution.

A second series was gas sterilized and soaked in conditioning solution for 72 hours before implantation. The conditioning solution contains Eagles MEM (Minimum Essential Medium) and Earles balanced salt solution, 10% fetal calf serum, and 10% newborn calf serum [7].

Samples of bioglass 5 mm by 5 mm by 1 mm were placed in defects products in the metaphysis of the tibia just distal to the epyphyseal plate of Sprague Dawley male rats. The limbs were not immobilized and the animals were sacrificed at 3 and 8 weeks.

The tibiae were dissected clean of all soft tissues and the area of bone surrounding the bioglass was cut into 1 mm thick sections with bone on either side of the glass. The slices of bone and glass were immediately placed in cold cacodylate buffered gluteraldehyde, fixed for two hours and then washed with fresh cold buffer. The tissue sections were then placed in 2% osmium tetraoxide collidine buffered at a pH of 7.4 and fixed for an additional hour. After a final wash with additional buffer, the blocks were dehydrated in graded alcohols and embedded in Epon 812. Sections were prepared on a Porter-Blum MT-2 ultra microtome. Thick sections (1 m) were cut with glass knives, stained with Richardson's methylene blue azure II stain and examined with a light microscope. A diamond knife was used to cut thin sections (600 Å thick). Prior to TEM analysis the thin sections were stained with saturated fresh alcoholic uranyl acetate and lead citrate [8]. All TEM sections were examined with an Hitachi HU 11C electron microscope.

Table 2 illustrates the time dependent change in the surface ratios of Si/Ca and Ca/P for the glasses containing 0 and 6% P_2O_5 during the conditioning treatment. These ratios were obtained with a scanning electron microscope equipped with an energy dispersive x-ray analysis system.

Table 2

Energy Dispersive X-ray Analysis of the Effect of Conditioning Treatment on Bioglass Surfaces

Condition of Sample	45S-0% P_2O_5 Si/Ca	45S-6% P_2O_5 Si/Ca	45S-6% P_2O_5 Ca/P
Freshly abraded	.910	.912	6.2
Gas sterilized	.912	.912	6.1
Gas sterilized + 24 hrs in cond. sol.	2.03	1.43	2.38
Gas sterilized + 24 hrs in cond. sol.	2.41	1.75	1.97
Gas sterilized + 72 hrs in cond. sol.	2.40	0.80	1.89

X-rays produced as a result of the electron beam striking the sample surface are detected and identified according to their energy. As different atoms have their own discrete energies, the resulting spectrum can be used to determine the atoms present on the surface. For a more detailed discussion refer to page 35. The gas sterilization treatment produces little or no change for either composition. After 24 hours in the solution there is a significant increase in the ratio of Si/Ca for both glasses. In addition, the Ca/P ratio for the glass containing 6% P_2O_5 drops drastically. These trends continue through 48 hours. Between 48 and 72 hours of exposure the ratio of Si/Ca remains constant for the glass containing 0% P_2O_5. During the same period, the ratio of Si/Ca has dropped from 1.75 to 0.80 for the glass containing 6% P_2O_5, while the ratio of Ca/P continued to drop to a value of 1.89.

Figures 1 and 2 show infrared reflection spectra of the glasses containing 0 and 6% P_2O_5 at selected intervals during the conditioning treatment. The spectra of the glass with 0% P_2O_5 (Figure 1) reveal the formation of a silica-rich surface layer which is present at the conclusion of the 72-hour conditioning treatment. Little change is noted between the freshly abraded spectrum and the spectrum of the gas sterilized sample. After 24 hours in solution, there is selective attack of the silicon-nonbridging oxygen peak at 840 cm^{-1}. The silicon-oxygen-silicon stretching (S) and rocking (R) peaks, located at 955 and 500 cm^{-1}, respectively, begin to sharpen, increase in intensity and shift towards the location of the S and R peaks of vitreous silica. These changes continue to occur through 48 hours of exposure. The

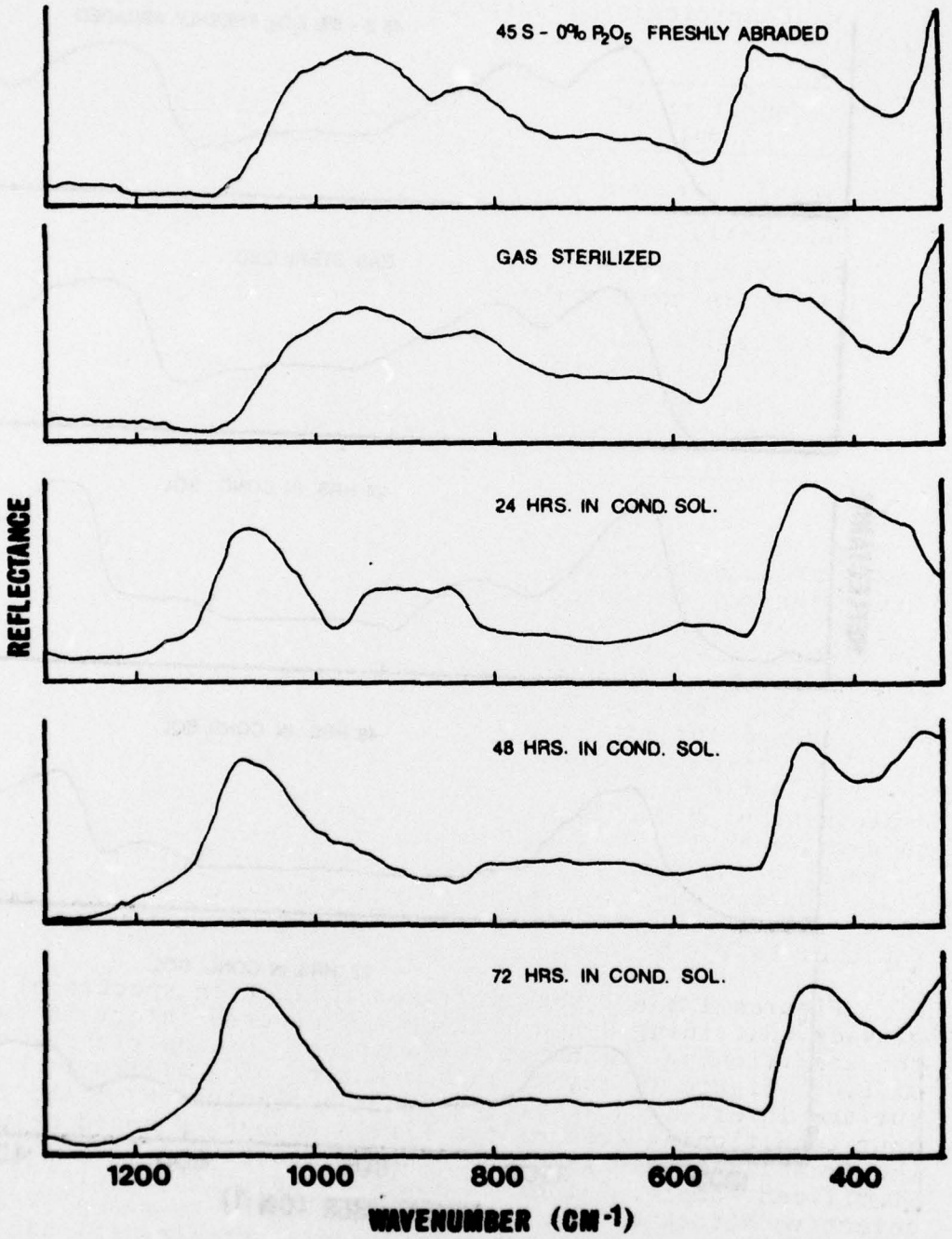

Figure 1. Changes in infrared reflection spectrum of 45S-0% P_2O_5 glass during conditioning treatment.

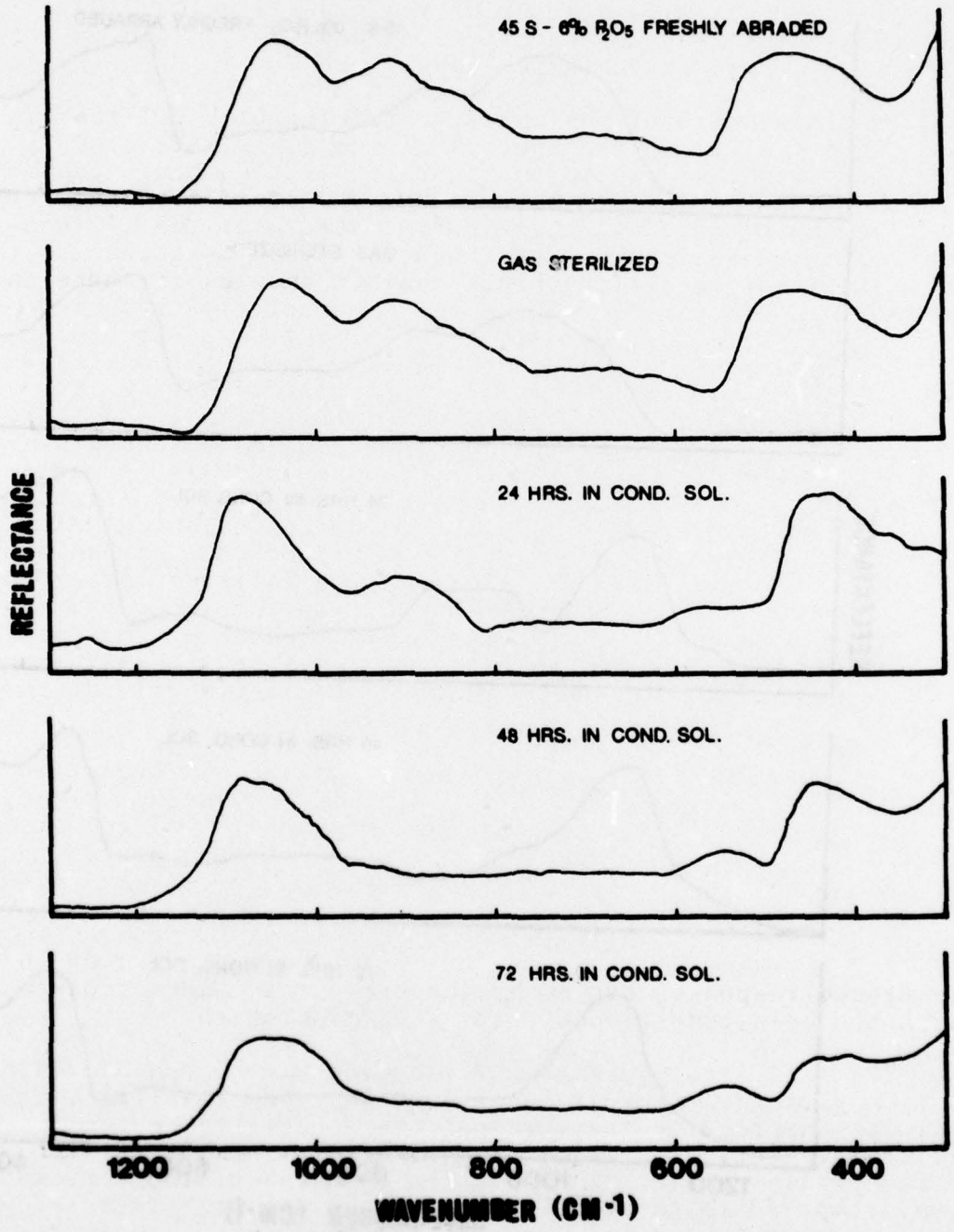

Figure 2. Changes in infrared reflection spectrum of 45S-6% P_2O_5 glass during conditioning treatment.

curve after 72 hours exhibits no additional changes, indicating a stable condition has been achieved. The data obtained with infrared reflection spectroscopy and the x-ray system of the scanning electron microscope both point to the formation of a silica-rich surface layer on the glass with 0% P_2O_5. This glass exhibited the same type of behavior in the in-vitro studies presented in sections B and C.

The IR spectra of the glass containing 6% P_2O_5 (see Figure 2) are similar to the spectra of the glass with 0% P_2O_5 through 24 hours of exposure. That is, little change can be noted between the freshly abraded and gas sterilized spectra. After 24 hours in solution, selective attack of the silicon-nonbridging oxygen peak occurs, and the peaks associated with the silicon-oxygen-silicon bonds exhibit changes in shape and location which indicate the concentration of silica is increasing on the surface. The 48-hour spectrum of Figure 2 contains the S and R peaks of silica but their intensities have dropped to values below their level at 24 hours. This trend continues with the 72-hour spectrum. Behavior of this type was also observed in the in-vitro studies on the glass containing 6% P_2O_5. After the silica-rich layer is formed, the calcium phosphate layer begins to grow. Apparently the rate of these reactions is slower in the conditioning solution and there is not a sufficient amount of calcium phosphate on the surface at 72 hours to produce the infrared reflection spectrum seen in-vitro. However, the data obtained with the x-ray analysis shows the ratio of Ca/P is becoming smaller with time, while the ratio of Si/Ca drops significantly from its 48-hour level, indicating an increase in the calcium and phosphorus concentration on the surface.

These observations clearly show that the surface structure of a bioglass implant is drastically influenced by the conditioning treatment and interpretation of the histological results of conditioned samples should take these changes into consideration.

Small pieces of glass implant were attached to bone in almost every case, but a distinct variation was observed in the tissue responses evoked by the different compositions which had been conditioned prior to implantation.

Figure 3 is a transmission electron micrograph of a 45S-0% P_2O_5 glass-bone interface at 3 weeks. The material which exhibits the regular fracture pattern appears to be the silica-rich corrosion film (CF) which forms on the surface of the glass implant. The relative softness of the corrosion layer compared to the glass produces the uniform fracture pattern, with long nonbranching fracture lines. The corrosion film contains a tear which was probably produced during the sectioning process. Close examination reveals that a thin layer of the corrosion film (CF) remains attached to

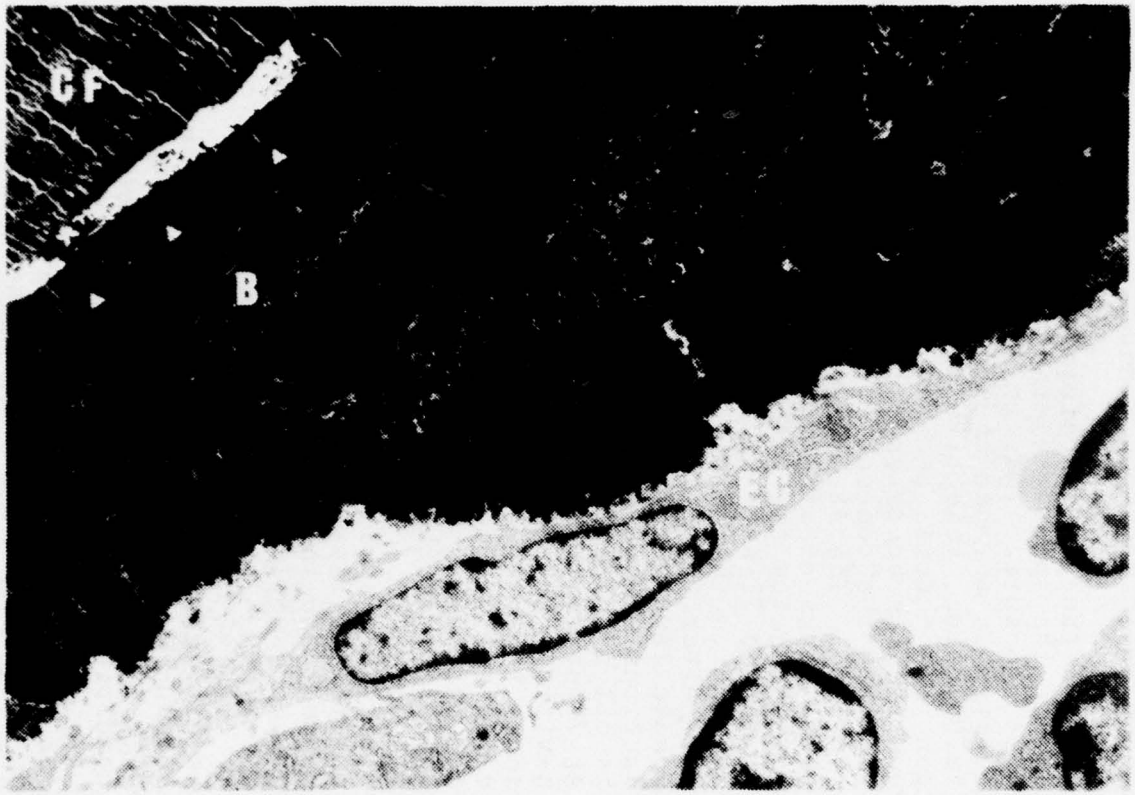

Figure 3. Electron micrograph of junction between 45S-0% glass and bone three weeks after implantation in rat tibia. The corrosion film (CF) is tightly bound to bone (B) along the interface designated by arrows (↑). (8,500X)

bone (B) along the interface (I), indicating the corrosion film-bone interface has considerable strength. The elongated cell (EC) in close proximity with bone has the appearance of a normal endosteal cell on a resting bone surface and does not appear to be actively engaged in laying down new bone. Examination of thick sections containing the glass with 0% P_2O_5 revealed a small number of viable osteocytes present in newly formed bone and bone surfaces characterized by a lack of active bone formation and very few active osteoblasts.

A 45S-3% P_2O_5 glass-bone interface at three weeks is shown in Figure 4. Small pieces of implant are attached along the surface. It should be pointed out that before sections are cut, the glass is chipped out of the block. If this was not done it would be very difficult to cut sections as glass knives are used and they would constantly break. The presence of small pieces of glass attached to bone indicates that there is considerable strength associated with the glass-bone interface because fracture occurs within the glass implant rather than at the interface.

The mineralized bone adjacent to the implant interface of Figure 4 contains several osteocytes and an area of unmineralized osteoid. There is a layer of plump osteoblasts which appear to be laying down new bone.

Figure 5 is a photomicrograph of a 45S-6% P_2O_5 glass-bone interface at three weeks. Large pieces of bioglass (G) are intimately attached to bone (B) and several normal osteocytes (O) are present in the mineralized area. There is a well-defined layer of osteoblasts actively engaged in laying down new bone (OF) and this front is separated from the mineralized area by a transition zone of partially mineralized osteoid. These features indicate that induction of normal osteogenesis has been achieved. An electron micrograph of the same section (Figure 6) shows the corrosion layer directly attached to mineralized bone along the wavy interface I.

A 45S-12% P_2O_5 glass-bone interface at three weeks is shown in Figure 7. There is an absence of activity along the ossification front with no evidence of osteoid and only one osteoblast in the area. Figure 8 is a photomicrograph of a 45S-12% P_2O_5 glass-bone interfcce at eight weeks. An important feature to note is that the implant G has been separated from the bone B by an interval containing a capillary C. Electron microscopy of this section (Figure 9) reveals intercellular crystallization (X) has been induced along the edges of the capillary. It can also be observed that part of the corrosion film (CF) remained attached to the bone when the interval containing the capillary separated the implant from the bone.

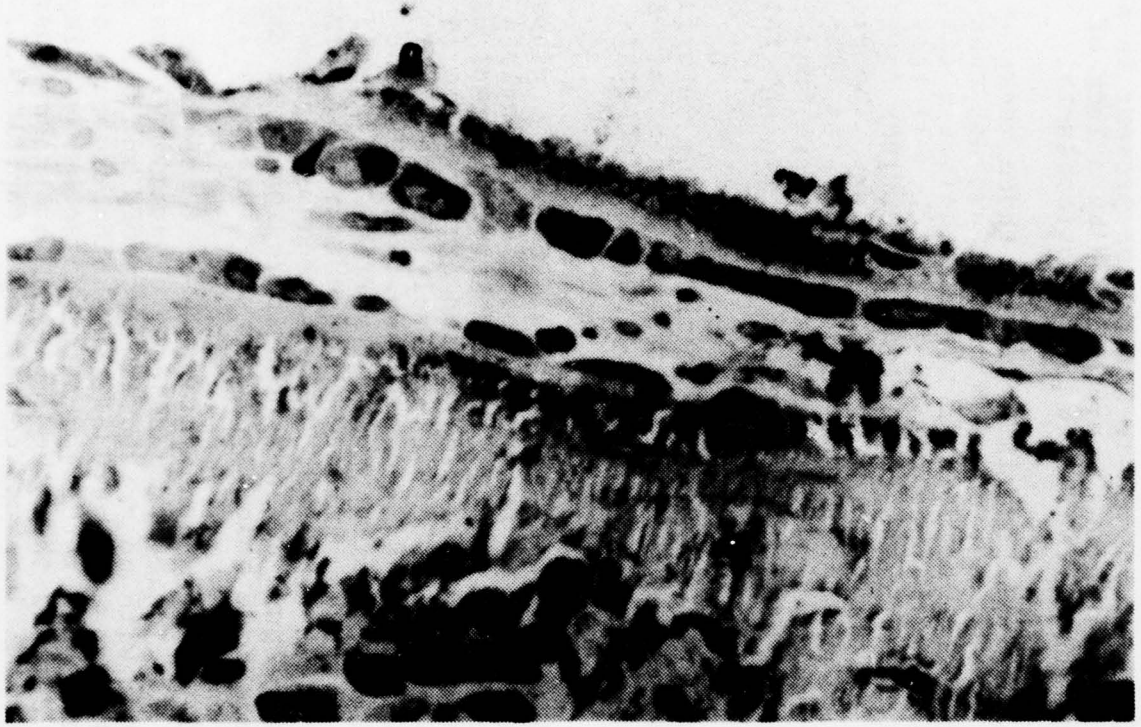

Figure 4. Light microscopy three weeks after implantation of a 45S-3% P_2O_5 glass. Remnants of the glass implant (G) are attached to bone. (800X)

Figure 5. Photomicrograph of a 45S-6% P_2O_5 glass-bone interface three weeks after implantation in rat tibia. Large pieces of bioglass (G) are intimately attached to bone (B). New bone contains several osteocytes (O) and a layer of osteoblasts laying down new bone (OF). (1,800X)

Figure 6. Electron micrograph of the junction between the corrosion film of a 45S-6% P_2O_5 glass (CF) and mineralized bone (B). (17,600X)

Figure 7. Light microscopy three weeks after implantation of a 45S-12% glass. Glass (G) is attached to bone (B). There is an absence of activity along the new bone surface (OF). (1,800X)

Figure 8. Photomicrograph of a 45S-12% P_2O_5 glass-bone interface eight weeks after implantation. Glass implant (G) has been separated from bone (B) by an interval containing a capillary (C). (1,800X)

Figure 9. Electron microscopy of capillary in Figure 8. Note intercellular crystallization (X) along edges of capillary. (44,200X)

Referring to Figure 8, note the unhealthy appearance of the osteocytes (O). They have withdrawn from their lacunar walls and the nuclei are pyknotic. There is also an absence of new bone formation at the bone surface.

The in-vivo results of this study show that direct attachment of glass to bone is achieved within three weeks for the four compositions studied.

The in-vitro studies in sections B and C establish that silica-rich corrosion films form on the surface of the bioglasses in a simulated physiologic environment. Furthermore, the in-vitro results of this chapter show that the conditioning treatment produces the same response.

Carlisle has reported that silicon-rich regions are associated with active mineralization sites in young mice and rats and, once mineralization has gone to completion, the silicon content drops [9]. Recent in-vitro investigations by Hench and Paschall [5] have shown that 45S-6% P_2O_5 glass implants are bonded to bone by an amorphous cement-like layer, probably comprised of SiO_2, CaO, and P_2O_5, which serves as the active site for collagen attachment followed by mineralization.

In view of the findings of this study as well as those in the literature, it seems likely that the silica-rich layer serves as an induction site for osteoblasts to lay down the organic intercellular substance of bone. This substance contains collagen and mucopolysaccharides. Normally, mineralization would begin to occur as soon as the organic intercellular substance was secreted by the osteoblasts. The exact mechanism of mineralization is not completely defined; however, the concentration of Ca and PO_4 ions in the area is thought to play an important role [10].

The phosphorus content of the bioglasses may be the important parameter which influences mineralization. The buildup of calcium and phosphorus which occurs on the surface of the silica-rich films could provide a source of ions for mineralization. The results obtained indicate that, as the phosphorus content of the glass increases from 0 through 6% P_2O_5, the appearance of the total ossification process becomes increasingly healthy. In the case of the glass containing 6% P_2O_5, the resulting situation is one of normal ossification.

The results obtained with the glass containing 12% P_2O_5 suggest that there is an optimum phosphorus content which should not be exceeded. The ectopic crystallization seen in Figure 9 might well have been induced by an excessive amount of phosphorus. Matthews et al. have reported that the addition of phosphates to a fixative, followed by incubation, will result in apatite crystal formation [11]. Furthermore,

they reported that release of phosphate from cells which led to the formation of an amorphous calcium phosphate was prompted as a response to administered doses of thyrocalcitonin.

In the case of a bioglass, a specific enzyme would not be necessary to release large amounts of calcium and phosphorus as the response of the bioglass surface to body fluids would accomplish the same end. If the calcium and phosphorus released from the glass when combined with calcium and phosphorus present in the body fluids resulted in a critical supersaturation, apatite crystal formation would result.

Based upon the evidence obtained, it can be concluded that the optimal response is elicited by a composition which has the ability to form a silica-rich corrosion film and provide an adequate but not excessive supply of ions to be incorporated in the mineralization process. The glass composition containing 6% P_2O_5 (45S5) appears to be the best candidate based upon the relatively short implantation times of this study.

As added evidence for the importance of implant surface chemistry on osteogenesis, a series of uncrystallized, partially crystallized, and nearly fully crystallized 45S5 implants were compared as rat femoral implants. Equivalent osteogenesis and interfacial bonding was observed for all three microstructures and crystallographic states. In-vitro analyses showed nearly equivalent surface chemical behavior due to the presence of a residual glassy phase left after crystallization.

Evidence from Soft Tissue Responses

Whenever muscle is injured or foreign material is implanted into muscle, healing occurs by formation of a collagenous scar of fibrous incapsulation of the implant without direct attachment to the implant. Bone induction in muscle has not been successful, although autogenous bone grafts implanted in muscle are revascularized and new bone is formed within the graft. Therefore, an ideal implant for muscle or other soft tissues which behave in the same fashion, i.e., tendon, ligaments, or skin, would be one which induces a collagenous scar with direct attachment to the implant. With these facts in mind, several possibilities of the type of response to the implants in muscle would be: (1) induction of bone formation around the implant thus securely anchoring it to the muscle; (2) fibrous tissue incapsulation of the implant without attachment; (3) fibrous tissue encapsulation with direct collagen bonding to the implant; (4) incapsulation and bursa formation about the implant; or (5) tissue rejection with acute and chronic inflammatory response with sterile abcess formation and extrusion of the implant.

Recognizing the above possible physiological reactions to an implant, a study was done to determine the histological response of muscle to various compositions of bioglass-ceramic implants [12]. Small pieces of each material that exhibit variable surface reactivity (Table 1) measuring 1 cm x 1 cm x 0.1 cm were implanted under asceptic techniques in the lateral thigh muscles of male Sprague-Dawley rats. The animals were sacrificed at 3, 6 and 16 weeks. The bioglass and surrounding muscle were removed as a block and fixed in cold cacodylate buffered (pH 7.4) gluteraldehyde, dehydrated in graded alcohols and Propylene oxide and embedded in Epon 812. The blocks were sectioned for light and electron microscopy.

All of the compositions evoked a similar tissue response which varied quantitatively according to the surface reactivity of the material. At three weeks, there was a resolving inflammatory reaction with early fibrous incapsulation of the implants. Figure 10a is a photomicrograph of a 45S5 glass-muscle interface at three weeks. Several layers of elongated fibroblasts (F) are separating the glass implant (I) from the muscle tissue (MT). An electron micrograph of the glass cell interface (Figure 10b) reveals a single layer of macrophage-like cells (MC) between the glass implant (I) and the fibroblasts (F). These cells have attacked and are altering the implant surface. There is a band 3 or 4 cell layers thick where cells have ingested bioglass (IB) within cisternae.

At six weeks, there was a synovial membrane identifiable about all implants. At 16 weeks, there was evidence of continued attack of the implants by the synovial cells and phagocytosis of the ceramic particles. The less surface reactive materials showed the slowest development of attack. These findings demonstrate that although certain bioglass-ceramic compositions (45S5, $45B_5S5$, and 45S5F) fulfill the criteria of an ideal implant material for bone, in that they induce normal bone formation with direct attachment to the implant, they do not fulfill the criteria of an ideal implant material in soft tissues. The reactive surfaces of the materials release into the micro environment surrounding the implant Ca and P ions which ordinarily are not found in muscle in any significant quantities. Therefore, the materials evoke an inflammatory reaction which continues into a form of rejection. A similar form of rejection for the same reasons has been found in equivalent implants in porcine tendon.

Dynamic Surface Chemistry Evidence

The histological reactions of bioglasses and bioglass-ceramics are significantly influenced by composition as indicated in both hard and soft tissue responses. Therefore, it is important to define the roles of the individual ionic species in the surface chemical reactions of these materials in order to establish a surface chemical theory of response.

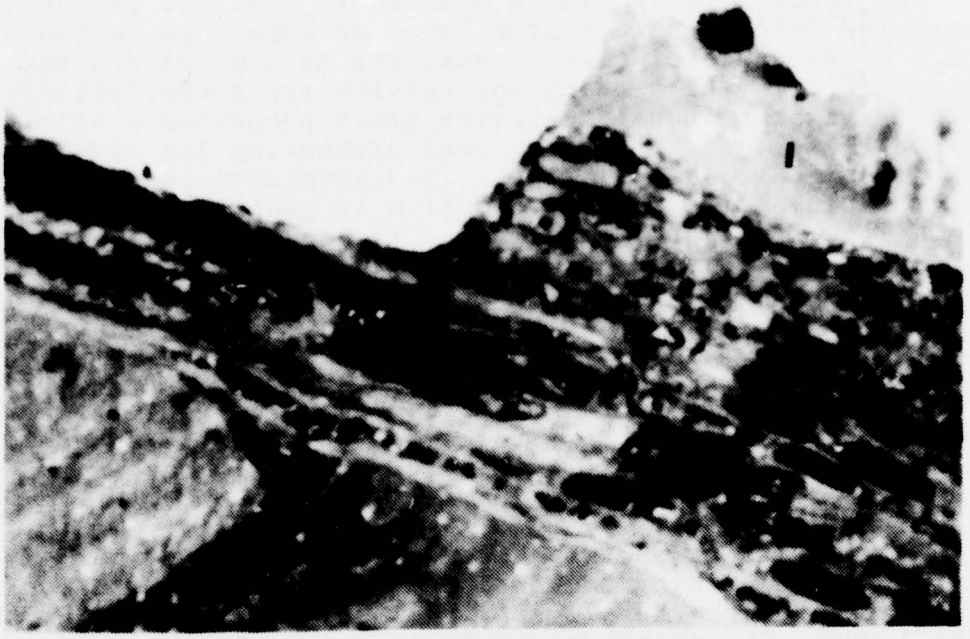

Figure 10a. Photomicrograph of a 45S5 bioglass-muscle interface at three weeks. (1,670X)

Figure 10b. Transmission electron micrograph of the area adjacent to the implant surface of Figure 10a. (47,500X)

The results of section B have shown that the glasses investigated develop a corrosion layer or layers in response to attack by an aqueous solution buffered at a pH of 7.4 and maintained at 37°C. Sodium and calcium are preferentially leached from the soda-lime-silica glass producing a silica film which serves as a buffer zone protecting the remaining bulk glass from aqueous attack. As phosphorus is added to the glass composition, a second film is generated at the silica-rich film-water interface. The second film is an amorphous calcium phosphate compound which crystallizes to an apatite structure with time. Increasing the phosphorus content of the glass reduces the time required for the calcium phosphate film to form. Partial substitution of B_2O_3 for SiO_2 leads to weakening of the silicate network and acceleration of the initial dissolution process. Fluorine additions significantly enhance the resistance of the glass to aqueous attack, probably by substituting for hydroxyl ions in the apatite structure of the corrosion film.

The results of section C confirm the observations of section B by providing chemical profiles of the corrosion films which define the silica-rich layer and the calcium phosphate layer. The thickness of the calcium phosphate layer was found to increase as the phosphorus content of the bulk composition increased when glasses were corroded under identical conditions.

Additional results in section C point to the existence of a thin surface layer (10-15 Å) rich in calcium and phosphorus which forms during the initial 15 minutes of corrosion. The observed sequence of events indicates that the thin calcium phosphate layer initiates the formation of the silica-rich layer and serves as the nucleation site for growth of the calcium phosphate layer once sufficient calcium and phosphorus have been leached into solution.

The consequence of the sequence of surface chemical reactions described above is osteogenesis. Sodium ion release from the surface eventually overrides the effect of acidic enzymes associated with would healing and bone repair and permits a local alkaline pH to be maintained. Osteoblasts differentiate in the implant vicinity. The silica-rich gel and amorphous calcium phosphate layer produced on the implant surface incorporates collagen fibrils and mucopolysaccharides generated by the osteoblasts. Crystallization of the calcium phosphate layer proceeds simultaneous with mineralization within the collagen fibrils resulting in a cojointly crystallized bone-implant junction.

In soft tissues high calcium and phosphorus ion concentrations are not desired and an inflammatory reaction is evoked which develops into a form of rejection.

References

1. L.L. Hench, R.J. Splinter, W.C. Allen and T.K. Greenlee, Jr., J. Biomed. Res. Symposium, No. 2, Interscience, New York, 1972, pp. 117-143.

2. L.L. Hench, T.K. Greenlee, Jr., and W.C. Allen, "An Investigation of Bonding Mechanisms at the Interface of a Prosthetic Material," Reports #1, #2, #3, August 1970, 1971 and 1972, U.S. Army Med. R and D Contract No. DADA-17-70-C-0001.

3. T.K. Greenlee, Jr., C.A. Beckham, A.R. Crebo and J.C. Malmborg, J. Biomed. Mat. Res., 6, 244 (1972).

4. C.A. Beckham, T.K. Greenlee, Jr., and A.R. Crebo, J. Calcified Tissue Res., 8, 2 (1971).

5. L.L. Hench and H.A. Paschall, "Histo-Chemical Responses at a Biomaterials Interface," to be published in J. Biomed. Mat. Res., Symposium "Prostheses and Tissue: The Interface Problem," Clemson University, 1973.

6. L.L. Hench and H.A. Paschall, "Direct Chemical Bond of Bioactive Glass-Ceramic Materials to Bone and Muscle," in J. Biomed. Mat. Res., Symposium "Materials Design Considerations for the Attachment of Prostheses to the Musculo-Skeletal System," Clemson University, 1972.

7. H. Eagle, Science, 130, 432 (1959).

8. D. Kay, Techniques for Electron Microscopy, Charles and Thomas, Springfield, Ill., 1961.

9. E.M. Carlisle, Science, 167, 279-280 (January 16, 1970).

10. A.W. Ham, Histology, 6th Ed., J.B. Lippincott, 1969, p. 394.

11. J.L. Matthews, J.H. Martin, E.J. Collins, J.W. Kennedy III and E.I. Powell, Jr., Calcium Parathyroid Hormone and the Calcitonins, Proceedings of the Fourth Parathyroid Conference, Excerpta Medica, Amsterdam, 1972.

12. H.A. Paschall, J. McVey and M. Rodabush, "Soft Tissue Response to Bioglass Implants," Orthopaedic Res. Society, Jan. 15, 1974, Dallas, Texas (to be submitted for publication).

E. Development of a Resorbable Bone Plate System, by D. Burney and G. Piotrowski

Introduction

The objective of Phase I of the resorbable bone plate project was to "test the suitability of the existing bioglass and bioglass-ceramic materials as plates, using metal screw fasteners." A plate was designed for application to a fractured dog femur. The plate design was subsequently revised to improve its strength during the implantation procedure. Several dogs have been implanted successfully with sintered composite plates (Figure 1).

Initial attempts at implantation were unsuccessful due to failure of the plates during installation. An extensive in-vitro study revealed that several steps in the manufacture were causing problems. These have been remedied, resulting in the successful implantations.

Early Attempts to Implant Canine Plates

The first attempts to utilize plates to repair fractures of canine femurs were spectacular failures. A group of 12 plates (see Figure 2) were fabricated, 6 from triple strength 45S5C (with 0.01% Pt), and 6 from the BA6 composite, as indicated in Phase I of the July 11, 1973, proposal (compositions 2 and 5, Table III). Four plates of each group were tested in-vitro, following ASTM standard F382* as much as possible, for bend strength. The 45S5 plates required an average bending moment, in air, of 17.3 N·m (153 in-lb) to fracture, while the BA6 plates could withstand a moment of 20.3 N·m (180 in-lb). These strengths are about one half of the strength of an intact canine femur. The strengths exhibited proved to be misleading, as the plates fractured readily while the plates were being screwed to the bone during implantation. Both compositions suffered the same fate, but the very low strength reported by the surgeon could not be demonstrated in the laboratory.

Extreme difficulties in the fabrication of the 45S5C (0.01% Pt) plates were encountered, with success rates of less than 50%. Thus it was decided to abandon use of that composition temporarily, until a sintered plate could be demonstrated to be usable.

---

*Recommended Practice for the Static Mechanical Testing of Bone Plates, Annual Book of ASTM Standard, Part 46.

Figure 1. Post-operative x-ray of a fractured dog femur repaired by a bioglass-alumina composite plate. Wire sutures appear as artifacts in the x-ray.

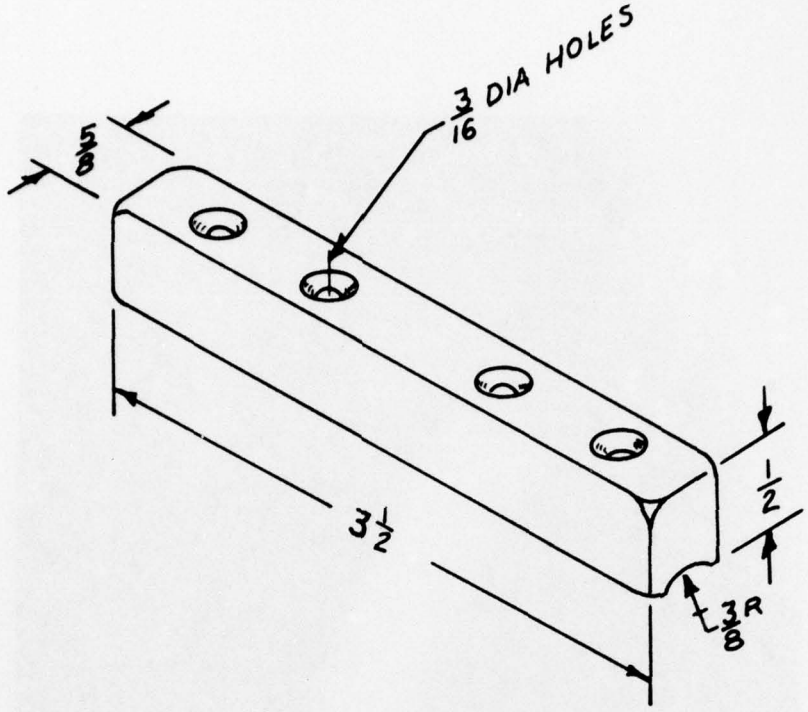

Figure 2. Original design configuration of the plates used for in-vivo trials for repair of canine femoral fractures.

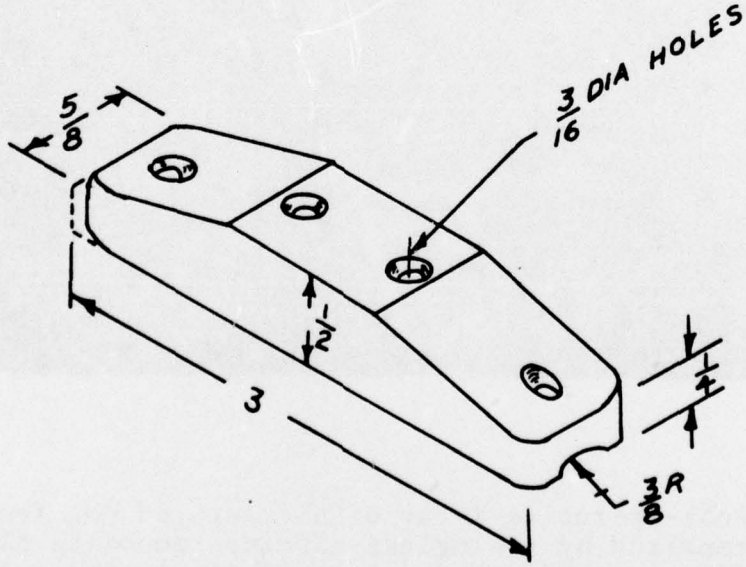

Figure 3. Modified plate design with ends redesigned to be less susceptible to failure due to screws being tightened down against it.

In light of the fact that failures during implantation occurred frequently at the tapered ends of the plate, the plate design was changed to that of Figure 3. Except as noted, all subsequent in-vitro tests were performed with specimens of the configuration of Figure 3.

Preliminary Failure Analysis

A systematic study of the strength of sintered composite bone plates was initiated to establish the cause of the low strength *in situ*. Two types of mechanical tests were performed.

A four point loading test (ASTM F382) was used to ascertain the strength of the plate in bending. The strength of the material in the plate was assessed using the SCADS computer program [1]. A second test involved tightening a screw down on the plate. The torque required to produce fracture was monitored and recorded. In both of these tests the fabrication procedure was analyzed by varying sintering temperatures and compaction force. The degradation in saline for short times was also examined.

a. Ten plates were used to establish a baseline set of data for bending strength. These plates required bending moments of 12.4 N·m (110 in-lb) for fracture. The nominal fracture stress was computed to be 60.7 MPa (8,800 psi).

b. For plates fabricated identically except for the compaction force during the pressing stage, the strength was found to increase linearly with compaction force (Figure 4). At the higher forces internal defects called laminations were formed by the transverse contraction of the die as the compaction force is removed. This problem was overcome by the construction of a stiffer die, which allows the higher compaction forces to be used during fabrication.

c. After pressing, the plates are fired to cause the particles to fuse into a single mass. The bending strength was found to be nonlinear with firing temperature (Figure 5). The large scatter can be attributed to surface condition of the pre-machined specimens.

d. A group of plates was fabricated without holes to study the effect of exposure to saline on the strength. The group was divided into three batches. One batch was tested dry, one was immersed in saline for 30 minutes prior to testing, and one was soaked in saline for 24 hours. No significant differences were found for both the bending moment and the fracture stress. The bending moment at failure was 25.4 N·m (225 in-lb), while the fracture stress was about 77.2 MPa (11,200 psi).

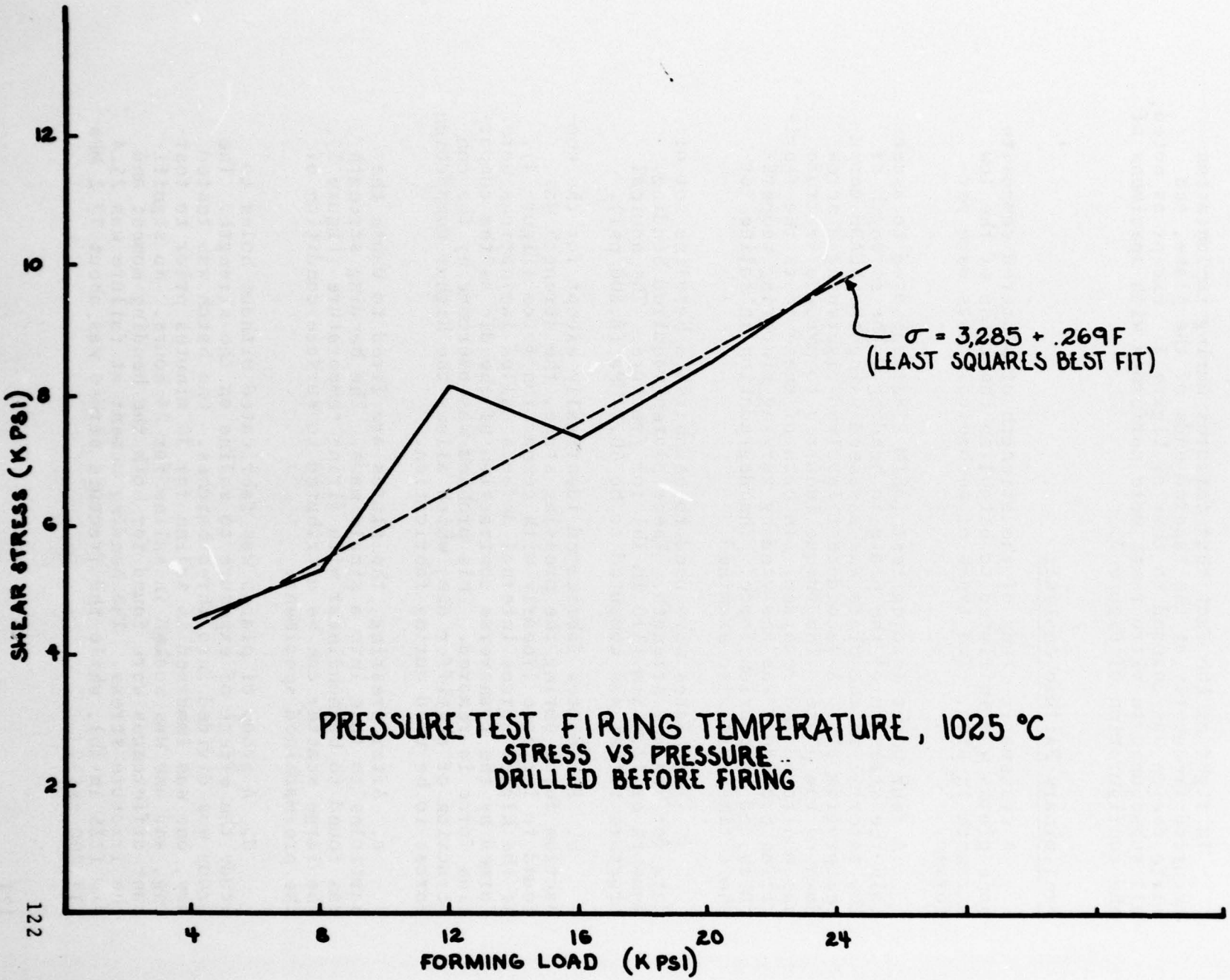

Figure 4. Influence of forming load on strength of plates.

Figure 5. Influence of firing temperature on strength of plates.

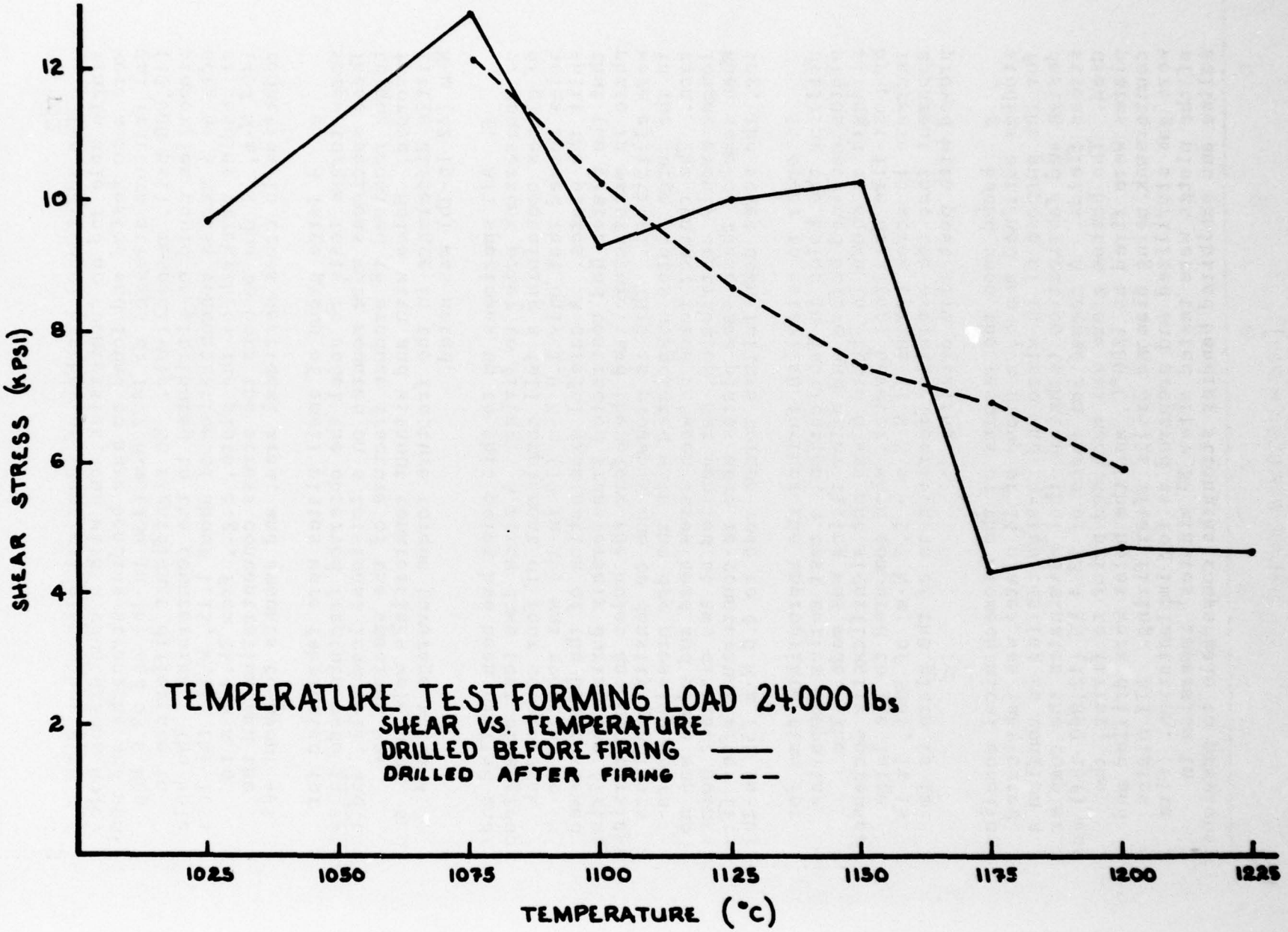

Two additional batches of identical plates but with a single hole and no countersink, and with a countersunk hole, were also tested and found to have bending strengths and nominal fracture stresses of 14.7 N·m (130 in-lb) and 68.9 MPa (10,000 psi), respectively. No significant difference in properties could be attributed to the countersink. The hole acts as a stress concentration of about 1.15, while the loss of bending strength of the plate, e.g., from 25.4 N·m to 14.7 N·m, is due to both the stress concentration and the reduction in cross sectional area, and amounts to about 40%.

e. A large group of small plates were fabricated for screw torque tests to model the observed fracture mode in situ. These specimens were mounted on a torsional load cell, and the torque required to produce fracture of the specimen was recorded. Holes with and without countersinks were used, and little difference in the fracture torque (average value 4.7 N·m (42 in-lb) was noted.

f. All specimens up to this point had been drilled and/or countersunk prior to firing. A screw down test of a group of plates containing a full complement of four countersunk holes showed that only 1.9 N·m (17 in-lb) was required to split the plates. A careful examination of the holes showed that the plates had contracted transversely during the firing phase in manufacture, and therefore the holes and countersinks were elliptical. This is probably due to density gradients in the large plates associated with the dry pressing operation. The contact force between screw head and plate was no longer evenly distributed, but applied at two distinct points. When some of these same plates were re-countersunk after firing, the screw down failure torque rose to 4.0 N·m (35 in-lb).

In order to establish further the appropriate time for drilling the holes in fabrication, a test series comparing plates machined before and after firing was made. The strength as shown in Figure 6 was not significantly decreased by post-fire drilling; however, when compared to the large increase in screw torque (1.9 N·m → 5.7 N·m) of 300%, it is apparent that the overall effectiveness of the plate is improved with post-fire drilling.

g. Based upon the results of the biomechanical modeling studies outlined above, a group of 14 plates was fabricated for the purpose of in-vitro and in-vivo testing to confirm a design and fabrication technique that eliminates the complex stress fields. A compaction force of 53.4 kN (12,000 lbf) was used. The bottom grove was machined prior to firing, the plates were fired at 1200°C, and the holes were drilled and countersunk using diamond drills after firing. All plates were gas sterilized and prepared as for implantation. Five of the plates were tested after 30 minutes' immersion in saline and exhibited bending strengths comparable to previous

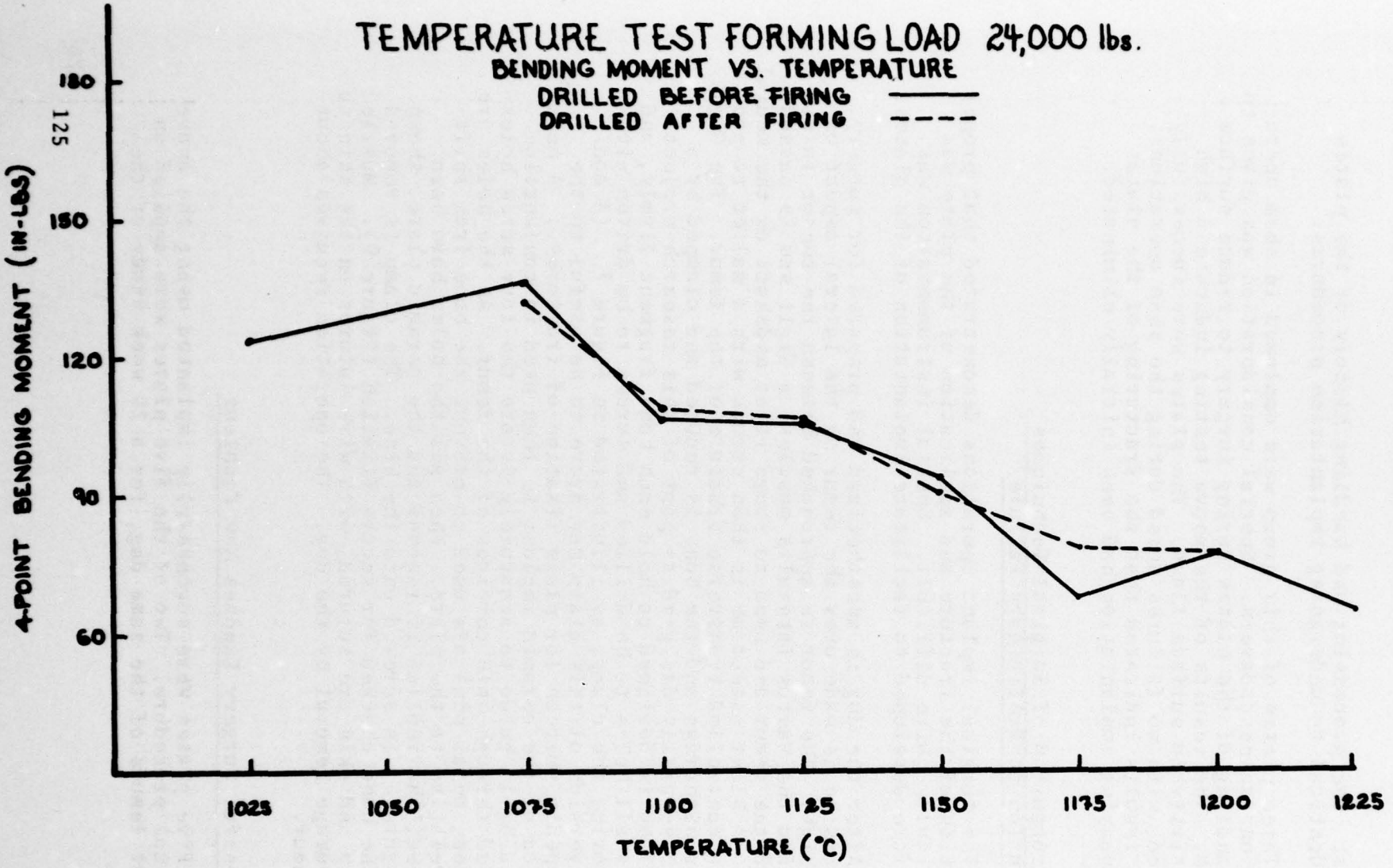

Figure 6. Effect of drilling before and after firing on strength of plates.

values. The processing and handling history of the plates was identical to undergoing implantation procedures.

Three plates of this group were employed in sham operations on canine cadavers. Special consideration was given to the handling of the plates during surgery to reduce surface damage. The results of the above testing indicate a high sensitivity to surface flaws. The plates were successfully applied, with no failures noted during the sham operations. These results indicated that the fracturing of the plates accompanying implantation had been initially eliminated.

Re-structuring of Surgical Techniques a Solution to Preliminary Failure

The surgical implant operations demonstrated that proper reduction of the fracture and application of the plate was technically quite difficult. Special instrumentation was therefore developed to facilitate implantation of the plates.

After the dog is anesthetized and prepared for surgery, an incision is made over the femur on the lateral aspect of the thigh. The femur is approached between the tensor fascia lata and the vastus lateralis muscles, a Gigli saw is passed around the femur and used to score it at midshaft on the medial side. A blunt osteotome is then struck with a mallet to produce a controlled transverse fracture of the femur. The Gigli saw is withdrawn and the bone is reduced and clamped by a device specially designed as part of this research project. The clamp is designed to hold each bone fragment firmly, and allows all holes to be drilled and screws to be driven without moving the clamp, as illustrated in Figure 7. (A modified version of this clamp may prove to be useful to the orthopedic surgeon for plate fixation of fractures.) A metal replica of the ceramic implant is then used in conjunction with a drill guide to accurately locate the four screw holes drilled through both cortices of the femur. As the holes are drilled, metal pins are used to prevent the bone from shifting relative to the plate. When all the holes have been drilled, the replica is removed and the ceramic plate, shown in Figure 8, is screwed onto the bone. The clamp is removed and the bone checked for secure fixation (Figure 9). Muscle, fascia and skin are sutured, with wire sutures on the skin to discourage removal by the dog. The operation requires about one hour.

Successful Surgery Exposes New Problems

Five plates were successfully implanted using the above surgical procedure. Two of the five plates were applied on intact femurs of the same dog, for a 20 week study of the

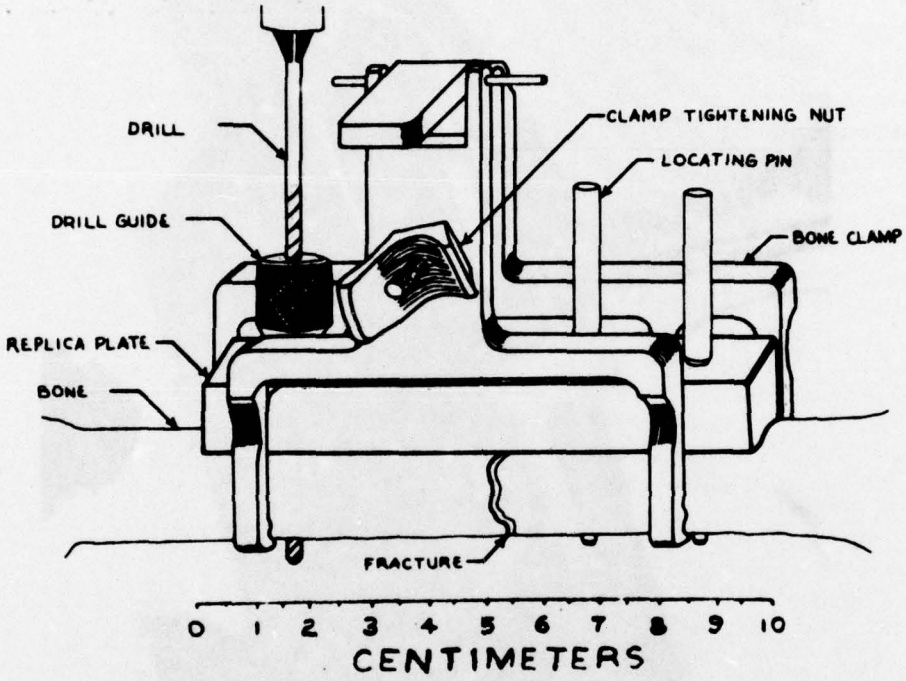

Figure 7. The clamp holds both bone fragments in alignment while the four screw holes are drilled, using the metal replica plate as a template. The locating pins are inserted into the drilled holes to prevent shifting of the plate during the subsequent drilling.

Figure 8. Once all the holes have been drilled, the ceramic plate is substituted for the replica plate, and the screws inserted.

Figure 9. After all screws are tight the clamp is removed and the quality of the fixation checked.

biocompatibility of the plate geometry (Figure 3). The other three implants were applied on fractured femurs of the dogs. The plates remained stable for nine, five and four days. The three failures may be attributed to static fatigue, which is proportionate to ultimate strength, or high contact stresses induced by femur geometry. Experience with the fatigue phenomena has created the need for developing a higher strength glass by further studies in the variations of the fabrication procedures.

The first hurdle of successful implantation has been overcome with the previously described procedure. However, post-operative plate stability is not maintained and a thorough study to improve resistance to static fatigue has necessitated a temporary halt to plate manufacture and a concentrated effort to manufacture a large quantity of small test discs.

A More Sophisticated Fabrication Study is Needed to Solve New Problems

Canine plate manufacture was temporarily discontinued to allow time for an extensive study of fabrication variables using 1-1/8" dia. x 1/8" circular discs for ease of manufacture. Stress is tested using a biaxial flexural test rig [2,3]. The parameters for study are firing temperature, firing time, alumina variations, forming pressures, and nucleation of frit. Once an optimized procedure is found, variations on the sintering techniques are proposed in hopes of a further increase in strength. Variations of particle size recompressed composite material, nucleation and crystallization of the sintered discs, etc., will be tried. Results from these studies will be utilized in the next quarter for continuation of canine plate fabrication and implantation studies.

A Theoretical Approach to Optimize Design of Plate Geometry

A computer study, using the SCADS program, has been initiated to investigate the effect of changes in the cross sectional configuration of the plate on its strength. The first phase of this study is nearly complete, and should lead to in-vitro verification of an improved plate design. This work will be carried over into the next year.

References

1. G. Piotrowski and G.I. Kellman, "A Stress Calculator for Arbitrarily Drawn Sections--The SCADS Computer Program," Report No. 4, p. 96, 1973.

DISTRIBUTION LIST

Commanding General U.S. Army Medical Research and Development Command ATTN: MEDDH-SI Washington, D.C. 20314	4
Defense Documentation Center ATTN: DDCIR Cameron Station Alexandria, Virginia 22314	12
Commanding Officer U.S. Army Combat Development Command Medical Service Agency Brooke Army Medical Center Fort Sam Houston, Texas 78231	1
National Institute of Dental Research Dental Materials Science Bethesda, Maryland 20014	1
NASA Materials Science Division Washington, D.C. 20546	1
Army Research Office - Durham Metallurgy and Ceramics Division Durham, North Carolina	1
National Institute of Health Division of Orthopaedics Bethesda, Maryland	1
Defense Ceramic Information Center Battelle Memorial Institute 505 King Avenue Columbus, Ohio 43201	1
National Institute of Health National Institute of General Medical Sciences Bethesda, Maryland 20014	1
Colonel Simon Civjan, DC Chief, Division of Dental Materials U.S. Army Institute of Dental Research Washington, D.C. 20012	1

CURITY CLASSIFICATION OF THIS PAGE (When Date Entered)

REPORT DOCUMENTATION PAGE

READ INSTRUCTIONS BEFORE COMPLETING FORM

REPORT NUMBER	2. GOVT ACCESSION NO.
3. RECIPIENT'S CATALOG NUMBER	
TITLE (and Subtitle)	5. TYPE OF REPORT & PERIOD COVERED
An Investigation of Bonding Mechanisms at the Interface of a Prosthetic Material	Annual Report Sep 1, 1973 - Aug 31, 1974
	6. PERFORMING ORG. REPORT NUMBER
7. AUTHOR(s) Larry L. Hench, George Piotrowski, William C. Allen, Homer A. Paschall	8. CONTRACT OR GRANT NUMBER(s) DADA17-70-C-0001
9. PERFORMING ORGANIZATION NAME AND ADDRESS University of Florida, Department of Materials Science and Engineering, Gainesville, Florida 32611	10. PROGRAM ELEMENT, PROJECT, TASK AREA & WORK UNIT NUMBERS
11. CONTROLLING OFFICE NAME AND ADDRESS US Army Medical Research and Development Command, Washington, DC 20314	12. REPORT DATE September 1974
	13. NUMBER OF PAGES 131
14. MONITORING AGENCY NAME & ADDRESS(if different from Controlling Office)	15. SECURITY CLASS. (of this report)
	15a. DECLASSIFICATION/DOWNGRADING SCHEDULE

16. DISTRIBUTION STATEMENT (of this Report)

Approved for public release; distribution unlimited.

17. DISTRIBUTION STATEMENT (of the abstract entered in Block 20, if different from Report)

18. SUPPLEMENTARY NOTES

19. KEY WORDS (Continue on reverse side if necessary and identify by block number)

Bioceramics	Transmission electron microscopy	Bone growth
Glass	Scanning electron microscopy	Glass-ceramics
Orthopaedics	Auger electron spectroscopy	Microstructure
Hydroxyapatite	Infrared reflection spectroscopy	Solubility
Collagen	Bone	Surface chemistry (contd)

20. ABSTRACT (Continue on reverse side if necessary and identify by block number)

The influence of phosphorus, boron and fluorine additions on the surface chemical reactivity of a soda-lime-silica glass has been investigated. Several techniques, including infrared reflection spectroscopy, ion solution analysis, scanning electron microscopy, energy dispersive x-ray analysis, x-ray diffraction, Auger electron spectroscopy and ion beam milling, have been employed to develop insight into the morphological and chemical changes which occur on glass surfaces corroded in a simulated physiologic environment.

(continued)

DD FORM 1 JAN 73 1473 EDITION OF 1 NOV 65 IS OBSOLETE

SECURITY CLASSIFICATION OF THIS PAGE (When Date Entered)

408 174

19. (continued)

Selective leaching
p^H
Nucleation
Crystallization
Interfacial bonding
Mechanical strength
Proteins
Epitaxy
Crystals
Kinetics
Histology
Stress analysis
Implant
Surfaces
Biomechanics
Cancellous bone
Flame spray
Femur
Segmental bone replacement
Rats
Monkeys
Strain measurement
Computer calculations
Torsional strength
Stainless steel
Fatigue strength
Paired bones

20. (continued)

The resulting corrosion layers and the influence of phosphorus, boron and fluorine on their compositions and rates of formation are defined. Surface ion concentration profiles determined with Auger spectroscopy and ion beam milling detail the structural alterations produced by aqueous attack. A mechanism is postulated which explains the sequence of events leading to the formation of the multiple-layer corrosion structures. Having defined the surface chemical behavior of the glasses in an invitro environment, an effort is made to relate these observations to the response elicited when identical glasses are implanted in laboratory animals. Stable interfacial fixation results when specific surface chemistry conditions are satisfied. Insufficient or excess surface ion concentrations produce negative osteogenesis and fixation results. Based upon the invivo observations, a theory is proposed that an ideal implant material must have a dynamic surface chemistry that induces histological changes at the implant surface which would normally occur if the implant were not present. Progress in the development of a mechanically suitable resorbable bone plate for bioglass-ceramics is reviewed. A long series of invitro and invivo fabrication and design experiments have been conducted to produce plates which will not fracture during implantation. Several successful implantations have resulted.